ELECTROCHEMICAL DISCHARGE MACHINING : MECHANISM AND A SCHEME FOR ENHANCING MATERIAL REMOVAL CAPACITY

A Thesis Submitted
In Partial Fulfilment of the Requirements
for the Degree of
DOCTOR OF PHILOSOPHY

by

INDRAJIT BASAK

to the

DEPARTMENT OF MECHANICAL ENGINEERING
INDIAN INSTITUTE OF TECHNOLOGY KANPUR

December, 1991

CERTIFICATE

Certified that this work entitled **"ELECTROCHEMICAL DISCHARGE MACHINING : MECHANISM AND A SCHEME FOR ENHANCING MATERIAL REMOVAL CAPACITY"** has been carried out by Indrajit Basak under my supervision and has not been submitted elsewhere for a degree.

Amitabha Ghosh
Professor
Department of Mechanical Engineering
Indian Institute of Technology
KANPUR - 208016
INDIA

December, 1991

SYNOPSIS

The electrical discharge in the electrochemical system has been proved to be a powerful means for machining materials in the field of the nonconventional machining techniques. Both, electrically conducting and nonconducting materials can be machined by such electrical discharge. The phenomenon of this type of discharge is known as electrochemical discharge (ECD). The technique of machining electrically nonconducting materials with the help of ECD is termed as electrochemical discharge machining (ECDM). Though the mechanism of the material removal in ECDM has been identified to some extent, the mechanism of ECD is still not well understood.. Perhaps due to this reason no theoretical model either for the ECD phenomenon or for ECDM has been developed.

The objectives of the present work include (i) the identification of the mechanism of electrochemical discharge, (ii) the development of a simplified, idealistic theoretical model of electrochemical discharge capable of predicting the minimum required voltage and the corresponding current to initiate the discharge and (iii) the development of a simplified quantitative model of material removal in ECDM. The material removal rate (MRR) in ECDM is characteristically low. Therefore, investigation into the possibility of enhancing the MRR in ECDM is also included

in the objectives of the present work.

A series of investigating experiments were conducted to gather adequate information on the characteristics of the processes of ECD and ECDM. Based on these information and on the observations made by the previous researchers the theoratical models were developed. The processes of ECD and ECDM being quite complex, some idealizing assumptions were necessary to reduce the problem to a tractable one.

The model of ECD is based on the switching phenomenon. The switching action between the tool electrode and the electrolyte takes place due to the blanketing of the tool electrode by a layer of gas. Both the water vapour generated due to the interface heating and the hydrogen gas from the electrochemical reactions participate in blanketing the electrode surface.

In the model of ECDM, the thermal effect of the discharge on the workpiece material is considered as the only factor for the material removal. The inductance is added as an extra circuit parameter. The MRR increases significantly, when the total circuit inductance is increased. The applied voltage was found to be the most important parameter governing the MRR.

Verification of the models were done by comparing the results obtained from the verifying experiments with those predicted by the models. The results obtained by the previous researchers were also used for the verification of the ECDM model. Only cathode tools were employed to eliminate tool dissolution

and the consequent change in tool size. Though smooth D.C. supply was used for the verification of ECD model, experiments to verify the ECDM model were conducted with 100Hz full wave rectified D.C. This was done to eleminate the unwanted effect of capacitive discharge from the filter capacitors. The voltage-current characteristics for the smooth and the rectified D.C. were studied and it was found that the critical voltages and the corresponding currents are nearly equal. Both the characteristics are also similar upto the point of discharge onset. But,the characteristics differ at the discharging condition. In this region the current values differ in magnitude.However,this difference can be considered as constant. Therefore,it is expected that the material removal rates should differ only by a constant for smooth and rectified D.C. supply . Different sizes of solid cylindrical steel tool, ranging from 0.08 cm to 0.195 cm in diameter, and the aqueous electrolytes of NaOH, KOH, NaCl and KCl were used to conduct the ECD experiments. Only glass workpiece was used for the experiments on ECDM as the time constraint made the use of other nonconducting materials beyond the scope of the present work.

Comparing the natures of the characteristics obtained experimentally with those predicted theoretically by the model it may be logical to conclude that the suggested mechanisms represent the actual process with a reasonable degree of reliability. The theoretically predicted values match quite well with the experimental results.

The thesis has been arranged in the following way. An overview of the nonconventional machining techniques is given in the beginning of Chapter 1. This chapter also presents the basic information about the ECD phenomenon and ECDM, including a survey of the past research in the area. Chapter 2 contains the experimental investigations of the ECD phenomenon and ECDM. The general characteristics of ECD and ECDM obtained from the experiments are presented in this chapter. In Chapter 3 the idealistic model of the ECD is developed and verified. The model of ECDM is developed and verified in Chapter 4. A technique to increase the process capability of ECDM is also discussed in this chapter. Chapter 5 contains the discussion on the results and the scope for the future work. The thesis ends with the concluding remarks in Chapter 6.

ACKNOWLEDGEMENT

The author expresses his unbound gratitude to Dr. A. Ghosh of Mechanical Engineering Department, IIT-KANPUR for suggesting the problem and his inspiring guidance throughout the course of the work.

I am also grateful to Dr. M.K. Muju of Mechanical Engineering Department, Dr. R.N. Biswas of Electrical Engineer Department, Dr.A.P. Shukla of Physics Department and Dr. P.K. Guptabhaya of Chemistry Department for their valuable suggestions during the course of the work.

The author is thankful to the Staff of the Manufacturing Science Laboratory for their help in making the experimental setups and consistent cooperation.

Mr. Vivek Shukla did the typing of the thesis. Mr. S.S. Kushwah, Mr. G.K. Shukla and Mr. A.K. Ganguli have drawn the sketches. I am grateful to them all.

I extend my thanks to the administration of Regional Engineering College, Durgapur and Ministry of Human Resource Development, Government of India for sponsoring me to pursue Ph.D. study under the Quality Improvement Programme.

The encouragement rendered by my parents and the help and cooperation extended by my wife and my little son at every stage of the programme enabled me to complete the research work.

Lastly, I must not forget about my friends in IIT-Kanpur, whose company made my stay at Kanpur a pleasent and memorable one. There are many other left, whose direct or indirect involvement has helped me to complete this research work smoothly. I thank them all.

Indrajit Basak

Dedicated
to my
parents

CONTENTS

LIST OF FIGURES

PHOTOGRAPHIC PLATES

NOMENCLATURE

a – radius of discharge channel.

A_e – equivalent active area of electrode.

C – capacitance.

D – diameter of the bubble.

D_d – diameter of the bubble at the time of detachment from the electrode surface.

d – diameter of tool electrode.

E – switching e.m.f. or back e.m.f.

f – frequency of bubble generation.

I – current.

J – current density.

K_2 – coefficient for determining R_{2C} ($\Omega\ cm^2\ mole^{-0.5}$).

K_3 – coefficient for determining R_{3C} ($\Omega\ cm^2\ mole^{-1.0}$).

k – thermal conductivity of work piece material.

$k_{1,2..}$ – constants (used in chapter 3).

L – inductance.

l – length of tool electrode dipped in electrolyte.

l_i – imaginary extension of tool electrode.

l_e – equivalent length of tool electrode, ($l+l_i$).

M – mole fraction.

m_1 – no of moles of solvent.

m_2 – no of moles of solute.

N – number of nucleation sites of bubbles.

n – indice to denote the regime of bubble growth.

Q – energy.

R – resistance.

T – temperature.

t – time.

u – volume of material removed per spark.

V – voltage.

v – total volume of gas.

v_1 – volume of H_2 gas.

v_2 – volume of water vapour.

α – thermal diffusivity.

β – fraction of heat utilised in vapour formation.

γ – coefficient of Faradic H_2 generation ($cm^3 A^{-1} sec^{-1}$).

δ – coefficient of vapour generation ($cm^3 watt^{-1} sec^{-1}$).

ε – electrochemical equivalent.

λ – indice on mole fraction.

ν – frequency of discharge.

ρ – density.

subscript:

c – value at critical condition.

m – maximum value.

o – applied value.

other symbols:

$(\dot{})$ – time derivative.

$(\bar{})$ – quantity per unit area.

abbreviations:

ECD - electrochemical discharge.

ECDM - electrochemical discharge machining.

MRR - material removal rate.

RMS - root mean square.

wt% - percentage composition by weight.

CHAPTER 1

INTRODUCTION

1.1 Electrically Assisted Nonconventional Machining

More and more challenging problems are being faced by the scientists and technologists in the field of manufacturing with the advancement of technology. A number of factors necessiated the development of nonconventional or nontraditional machining processes. The primary ones are (i) new materials with low machinability, (ii) dimensional and geometerical accuracy requirement not achievable by conventional processes and (iii) a desirable production rate and economy in difficult situations. The development of such nonconventional machining techniques started in the early 1930s and gained momentum after the second world war. A major challenging problem during this period was the machining of high strength and temperature resistant (HSTR) alloys. Since 1950 the developments in the field of electronics and semiconductor technology has also provided adequate motivation for the development of special manufacturing techniques. However, the ultimate boost to the research and developmental activities in the field of nonconventional manufacturing processes was given by the beginning of the space age.

The nonconventional machining processes vary quite

widely in their basic features, mechanics of the process and the type of energy used. A group of such unconventional machining techniques are dependent on electrical energy. Though the mechanics of material removal in these processes are different, they can be grouped under a common heading `electrically assisted nonconventional machining processes. The more common processes belonging to this group are (i) electrochemical machining (ECM), (ii) electric discharge machining (EDM), (iii) electron beam machining (EBM) and (iv) plasma arc machining (PAM). From the point of view of material removal characteristics, the achievable accuracy and shape capabilities, the first two, i.e., ECM and EDM have the maximum potential. Unfortunately, these processes have a major limitation in the fact that only electrically conducting work materials can be machined. To overcome this a hybrid process has been conceived in the early ' 70s in which the phenomenon of electrochemical discharge (ECD) is employed for the removal of material. Use of electrochemical discharge while machining electrically conducting work material has also been attempted leading to a number of interesting results. This hybrid process for electrically conducting material is now termed as "electrochemical arc machining (ECAM)" and that for electrically nonconducting material as "electrochemical discharge machining (ECDM)".

Use of electric power for controlled removal of metal dates back to 1935, when Jacqet noticed the usefulness ' of

electrolysis phenomenon to produce polished surface and subsequently W. Gusself of USSR in 1935 and Burgess of USA in 1941 developed the process to the present day ECM.

The credit of inventing the technique of EDM, should go to the English scientist Pristley and Lazarenko and Lazarenko of USSR. Though Pristley detected the erosive nature of electric spark, Lazarenko and Lazarenko established it as a machining process in 1943. The R-C relaxation circuit developed by them for this purpose was in use for several years.

ECAM and ECDM has a very recent origin in which the ECD phenomenon in used. In 1968, attempts had been made to use this phenomenon for drilling nonconducting materials. In early stages of development both the processes were termed as ECDM. It was treated as a combination of ECM and EDM as it had some common characteristics of both the ECM and EDM. However, the basic feature of these is the ECD phenomenon. Later, ECAM was termed for machining conducting materials and ECDM for non conducting materials.

1.1.1 Electrochemical discharge (ECD) phenomenon

A general electrochemical cell consists of two electrode dipped in an electrolyte (Fig.1.1). Application of external potential between the electrodes causes an electric current through the cell resulting in electrochemical reactions, such as anodic dissolusion, cathodic deposition, electrolysis of the

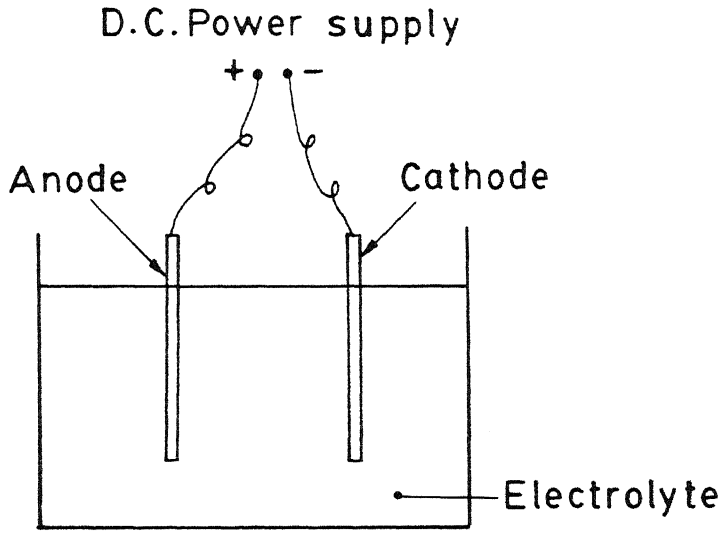

Fig. 1.1 Electrochemical cell

electrolyte etc., depending on the electrode-electrolyte combination. If a suitable electrolyte is choosen and the electrodes are of grossly different sizes, then, beyond a certain value of the applied potential, electric sparks appear at the bottom edge of the smaller electrode and the cell current drops. This phenomenon is known as electrochemical discharge (ECD) phenomenon. The mechanism of ECD, by and large, is not clear, though the observations of this process have established the fact that the discharge takes place due to bubble generation because of electrochemical reaction and thermal processes.

1.1.2 Electrochemical arc machining (ECAM) and electrochemical discharge machining (ECDM).

It will be convenient to understand the process of ECAM and ECDM using a comparative illustration of ECM, EDM, ECAM and ECDM. The typical ranges of the tool size and the work tool gap for these processes are presented in Fig.1.2. Figure 1.3 illustrates the voltage and current density ranges that are used in various electrolyte systems of machining. Usual voltage ranges of ECM is 8 to 20 volts and that for ECAM is 20 to 40 volts. Very high current density is attained by ECAM process upto a value of 800 A/cm^2 and high MRR is obtained, five times compared to ECM and about forty times compared to EDM. The voltage for ECDM is in the range of 30 to 80 volts depending upon the type of workpiece, tool size, electrolyte etc.

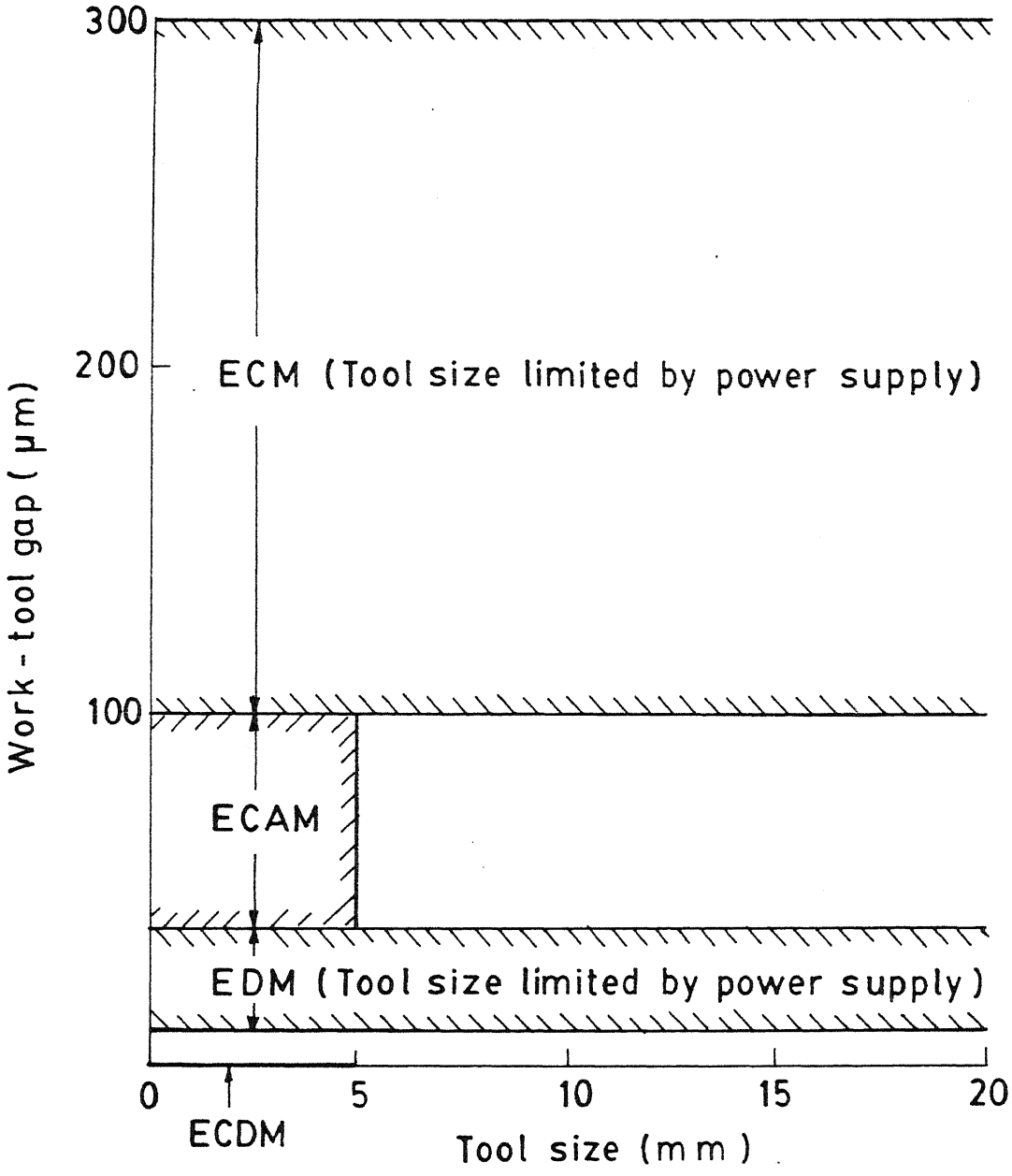

Fig. 1.2 Tool size and work - tool gap in electrically assisted machining processes

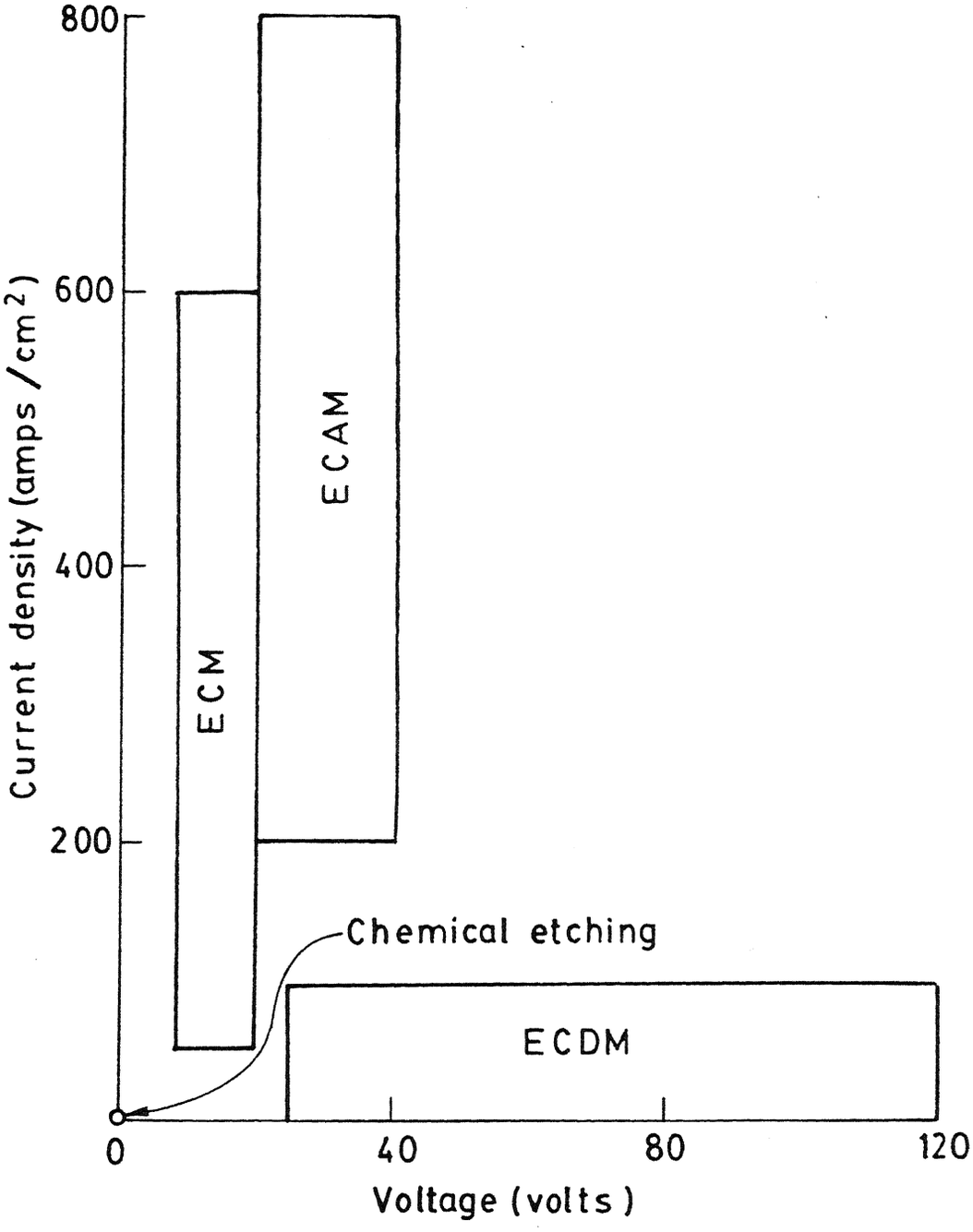

Fig. 1.3 Voltage and current-density ranges of the machining systems using electrolyte solutions

The mechanism of material removal in ECM, EDM and ECAM have been investigated thoroughly and understood reasonably well. In ECM electrochemical anodic dissolution causes material removal and in EDM melting, vaporisation and mechanical shock are responsible for material removal producing a crater. In ECAM both the mechanisms described above are active simultaneously. However, in ECAM it is the arc instead of the sparks which produce the thermal effects.

A major difference between ECAM and ECDM is that, in ECAM discharge takes place between the electrodes, but in ECDM it is between one electrode and the electrolyte. To bring the work surface nearest to the sparking zone in ECDM no gap between the tool electrode and the work is allowed.

1.1.3 Other uses of ECD phenomenon

Apart from machining some other uses of ECD phenomenon have been developed by Allesu [1]. Etching on glass slides has been done by him by using a special type of pen (Fig.1.4). The sharp point or the scribling point is one electrode and the other one is the larger rounded lead. A layer of NaOH solution is used to complete the electrical circuit between these electrodes. From the application point of view this method seems to be quite convenient. Making thermocouple beads is a very cumbersome process using the flame melting method. Allesu [1] developed a unique and simple process where 220V domestic A.C. service line is

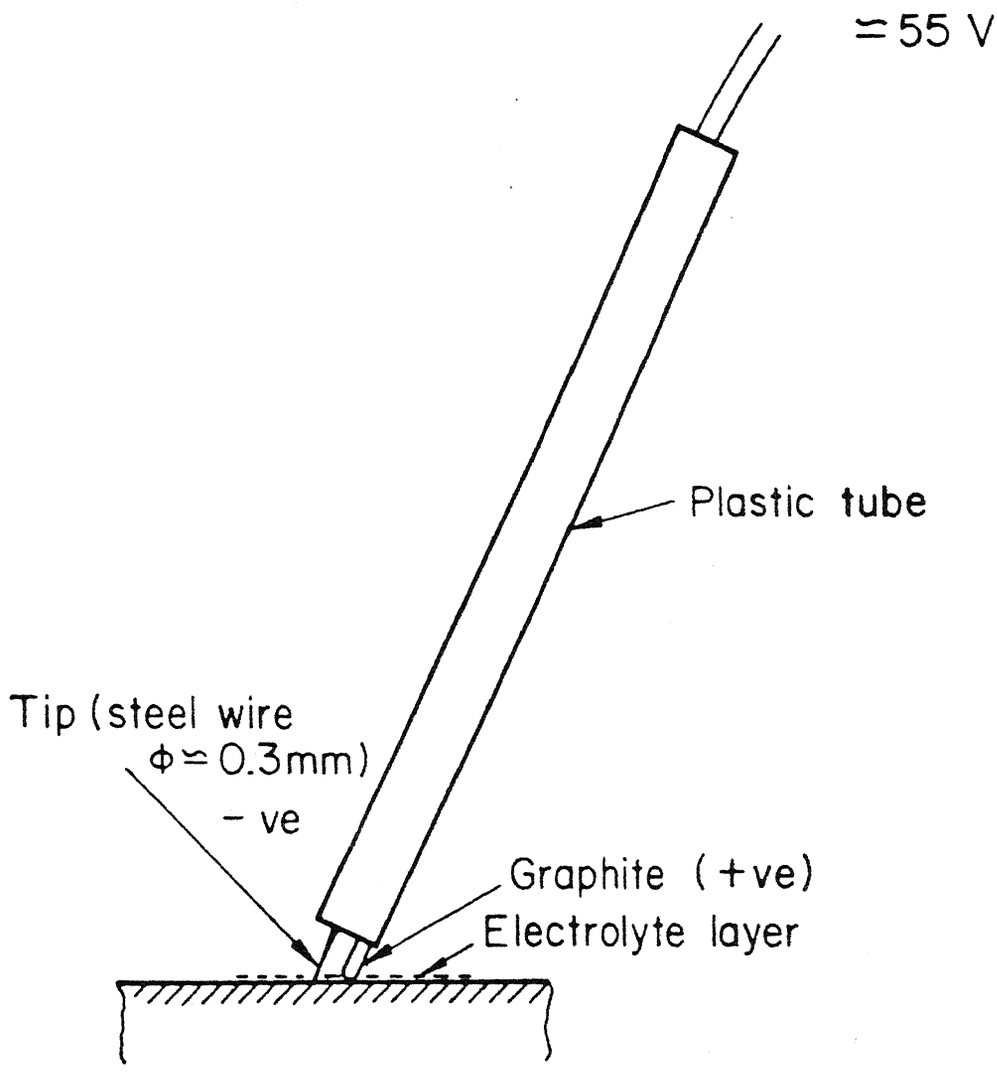

Fig. 1.4 Engraving pen [1]

used directly to make thermocouple beads (Fig.1.5). The twisted junction of the wires are dipped 1mm - 2mm in the electrolyte bath and the supply is switched on. Intense discharge melts the wires and forms the bead and circuit is automatically opened due to loss of contact between the wires and the electrolyte after the bead is formed. The conductivity of this junction was found to be identical with that made by flame method. Judging from the points of view of hazards and time required this method is quite superior to the conventional flame method.

1.2 Survey of Previous Work

Though a good amount of work has been done in the field of ECAM, very limited literature is available in the field of ECDM. This may be due to the less relative importance of ECDM, which failed to generate enough interest among the researchers. The phenomenon of small electric discharges at the anode tip was first reported by Taylor [2] during electrolysis of molten NaCl at high current density and he termed it as `Anode Effect'. Later, Kellog [3] showed that similar phenomenon can occur at the cathode and in aqueous electrolyte also. Electrical discharge between tool and workpiece was also observed during the attempts of enhancing the MRR in ECM by application of higher potential and considered as a detrimental factor as it causes damage to tool and workpiece. Utilising the ECD phenomenon Kurafuji and Suda [4]

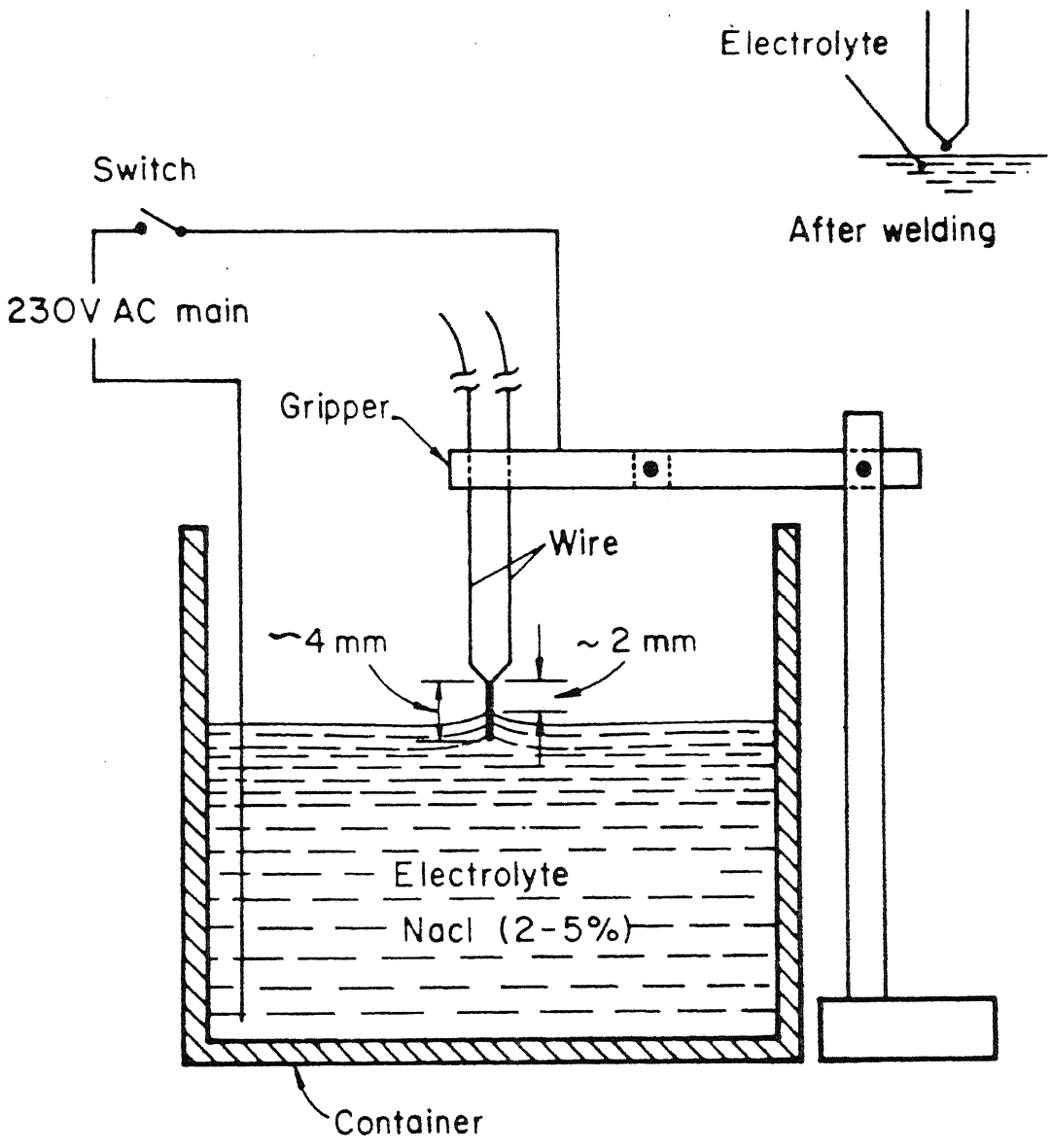

Fig. 1.5 Schematics of micro-welding set-up [1]

drilled holes upto a depth of 0.31 mm in a glass workpiece in 15% (wt/wt) NaOH electrolyte with a cell voltage of 34 volts. Cook et.al [5] conducted experiments with ECD for machining glass and other electrically nonconducting materials and identified the applied voltage, tool polarity, electrolyte temperature and concentration as input parameters, for determining MRR. The corresponding characteristics are given in Figs.1.6 - 1.8. The limited depth characteristic found by them is reproduced in Fig.1.9. They suggested that the possible mechanism of material removal in ECDMcould be due to the thermomechanical, chemical, field effect or due to some other unknown effects. Umesh Kumar [6] carried out experiments with glass and other electrically nonconducting materials using ECD phenomenon. Cook et.al. did the experiments mainly with positive tools but Umesh Kumar had concentrated on negative tool. The results obtained by Umesh Kumar are given in Fig.1.10 - 1.13. He noticed that the discharge vanishes with flowing electrolyte. The mechanism of material removal suggested by him were theromechanical and electrochemical action.

Tsuchiya et.al. [7] used wire electrochemical discharge for machining of glass and ceramics. The cutting technique of wire-EDM combined with the mechanism of ECDM, had been the basis of machining. They used 25Hz rectangular pulse with 80% duty factor. Electrolyte of NaOH and KOH, glass specimen of 1.2 mm thick as workpiece, wire-diameter of 0.2 mm as electrode with

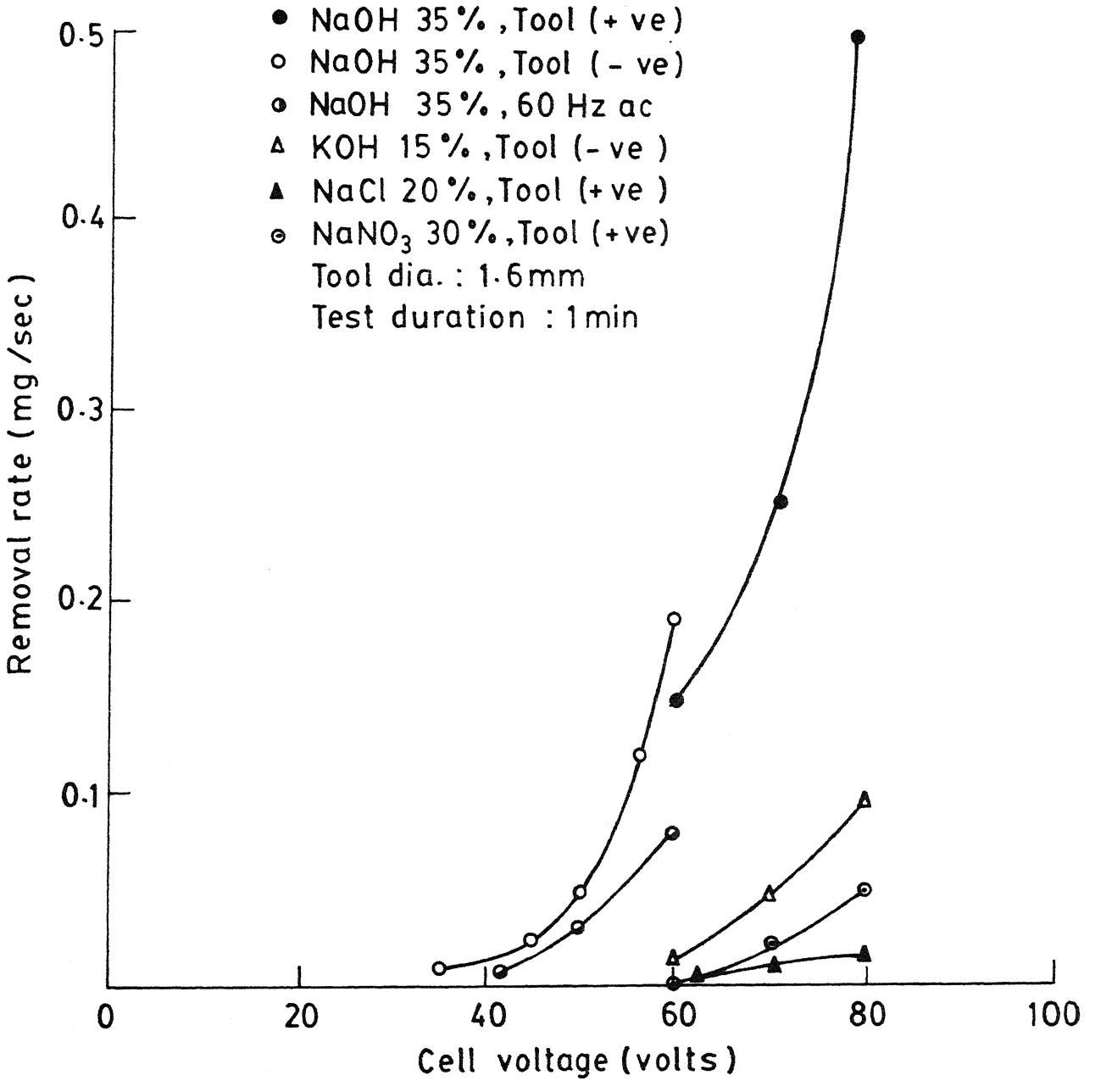

Fig.1·6 Effect of the applied voltage on MRR [5] (workpiece material : glass)

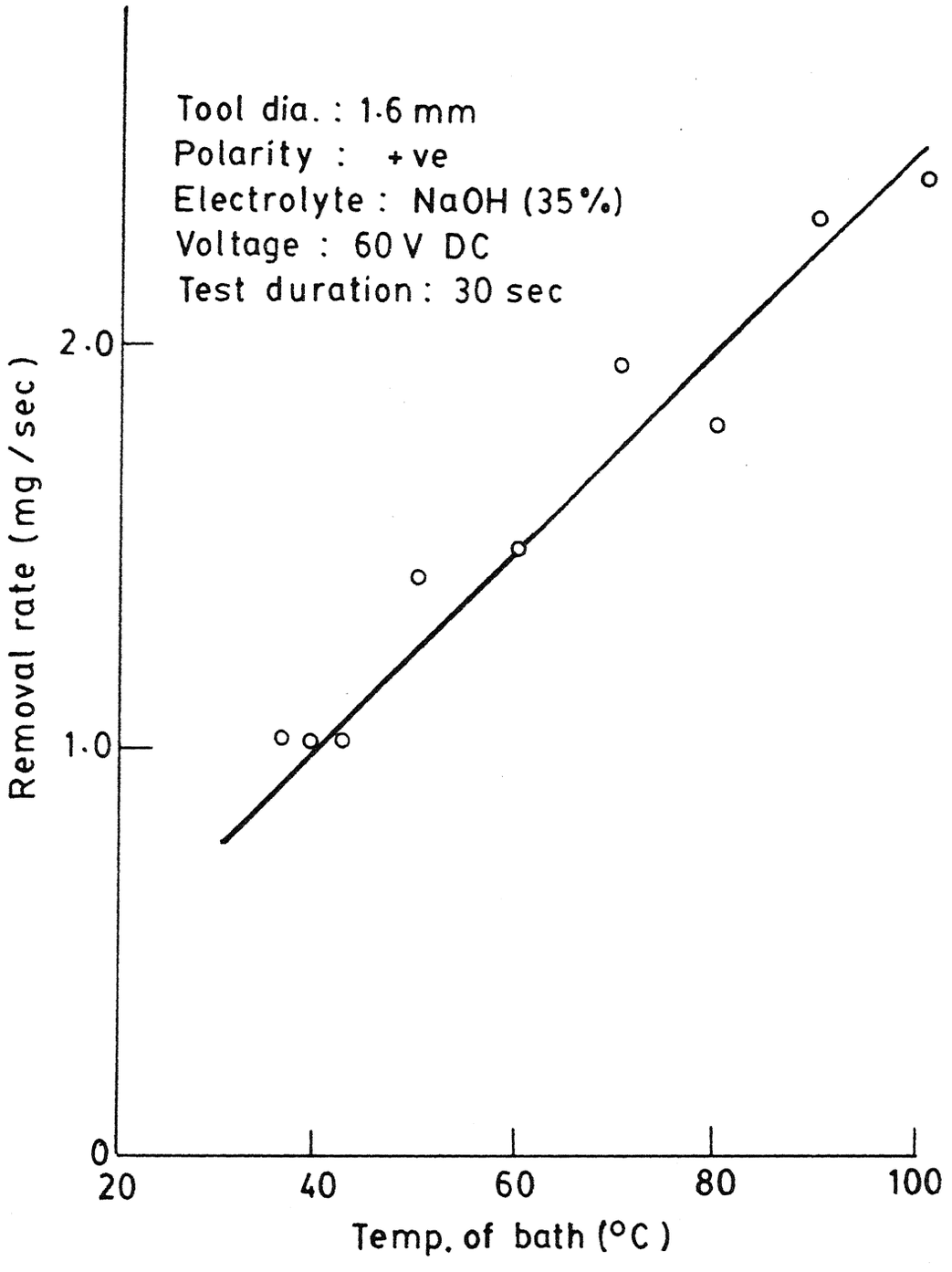

Fig. 1·7 Effect of the electrolyte temperature on removal rate (work material : glass) [5]

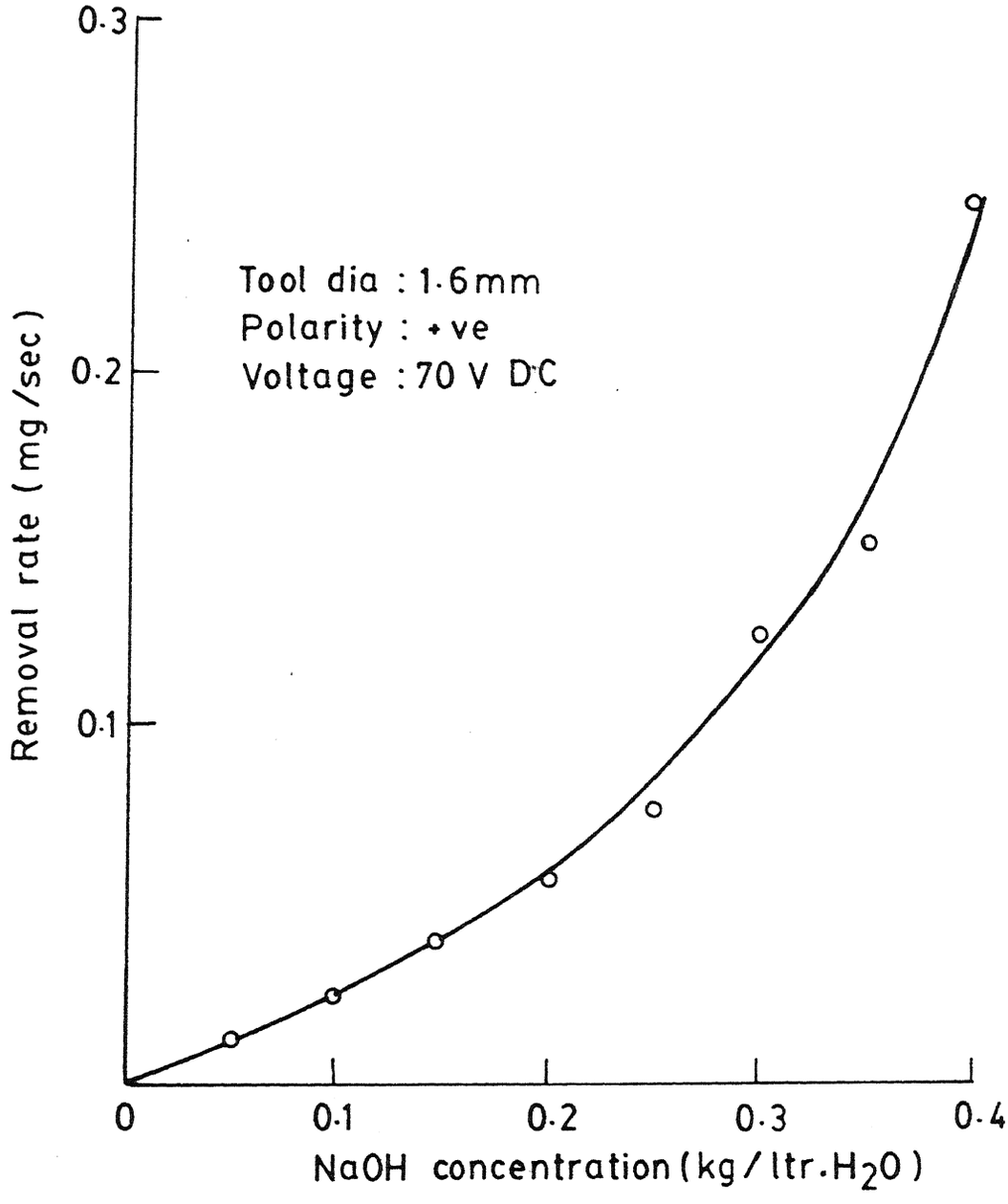

Fig. 1·8 Effect of the electrolyte concentration [5] on removal rate (work material : glass)

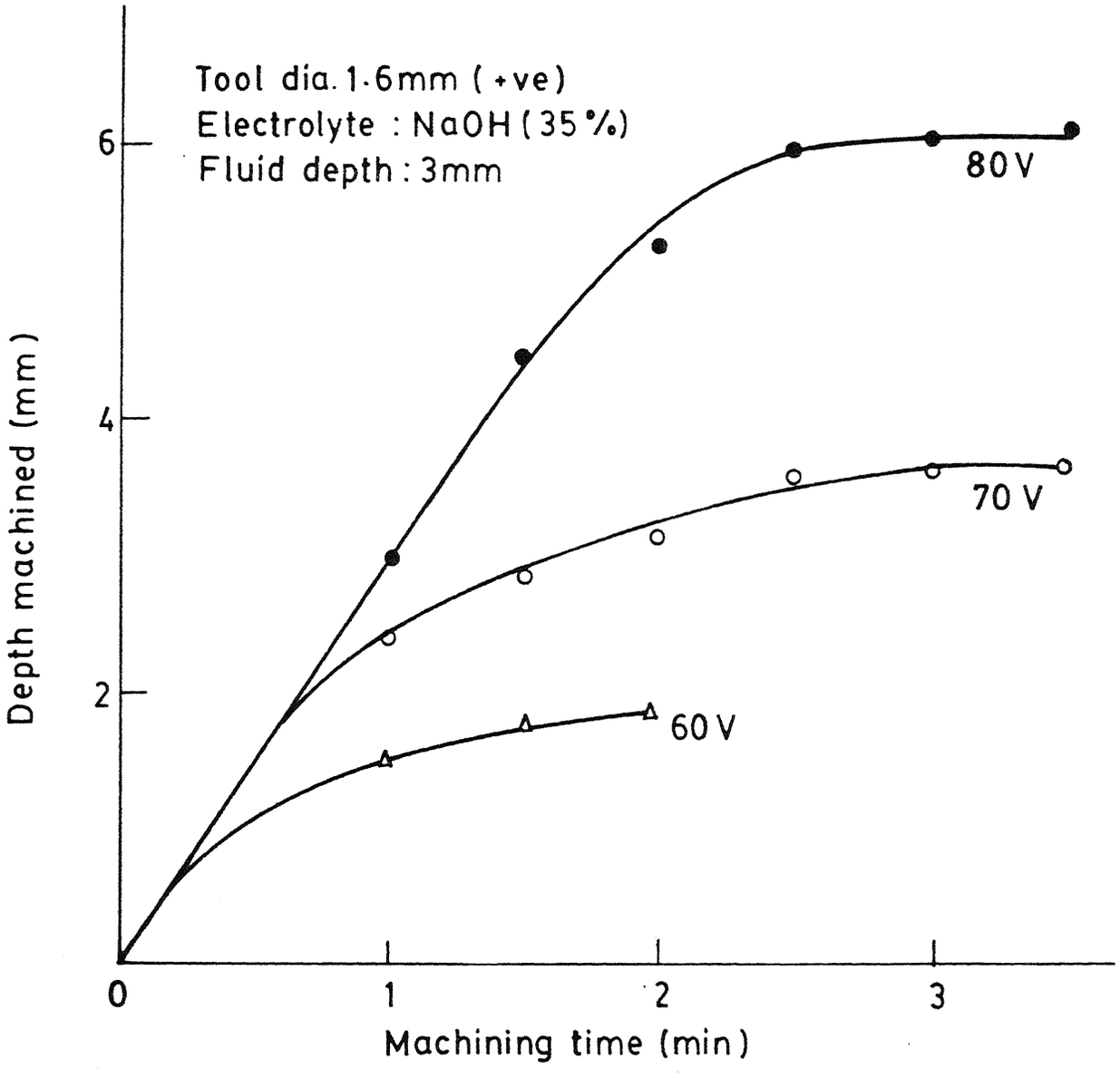

Fig. 1·9 Limited machining depth characteristics (work material : glass) [5]

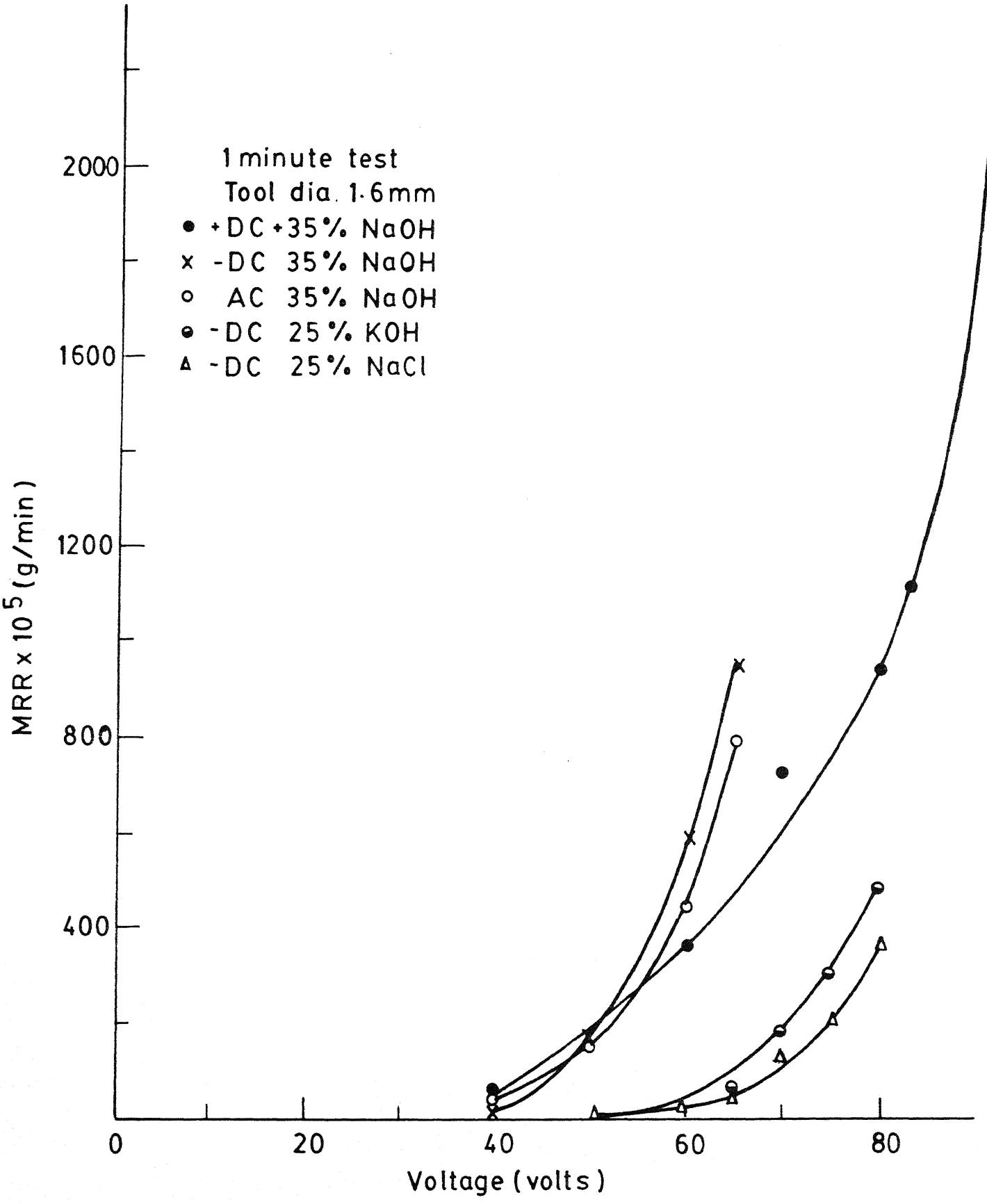

Fig. 1·10 Effect of the machining voltage on material removal rate [6] (work material : glass)

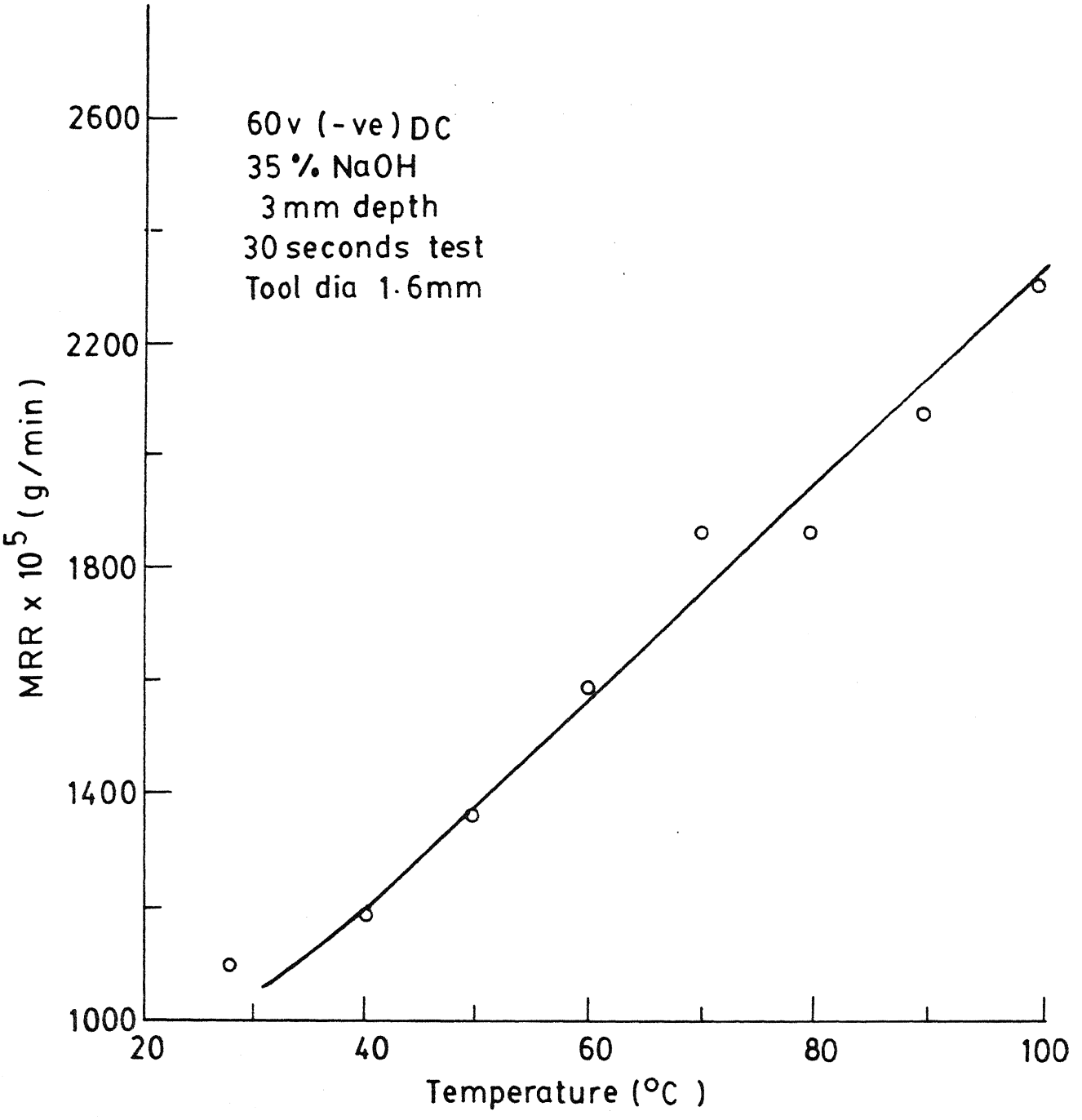

Fig. 1·11 Effect of the temperature of electrolyte on material removal rate (work material: glass)[6]

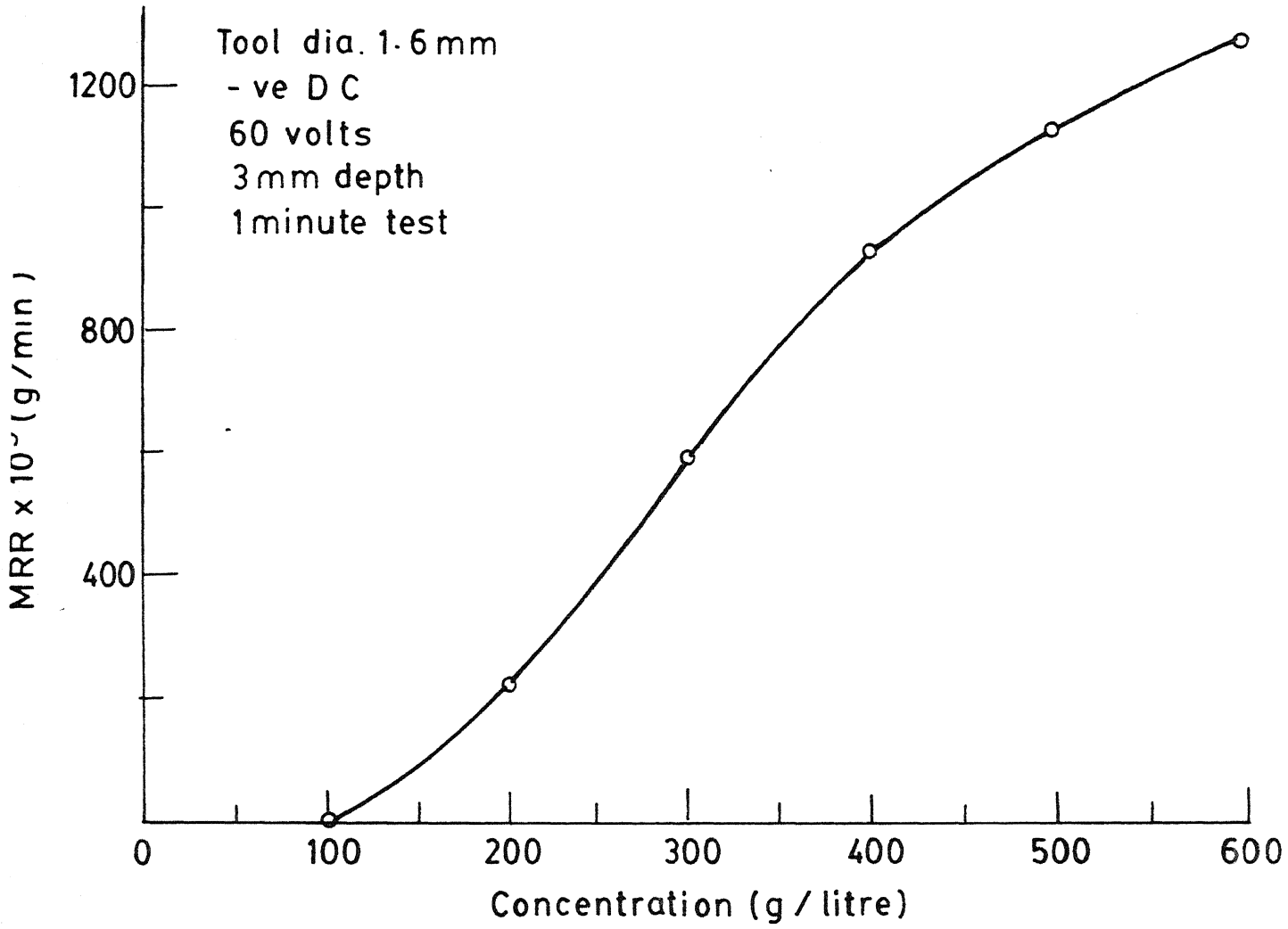

Fig. 1·12 Effect of the concentration of electrolyte (NaOH) on material removal rate (work material: glass)[6]

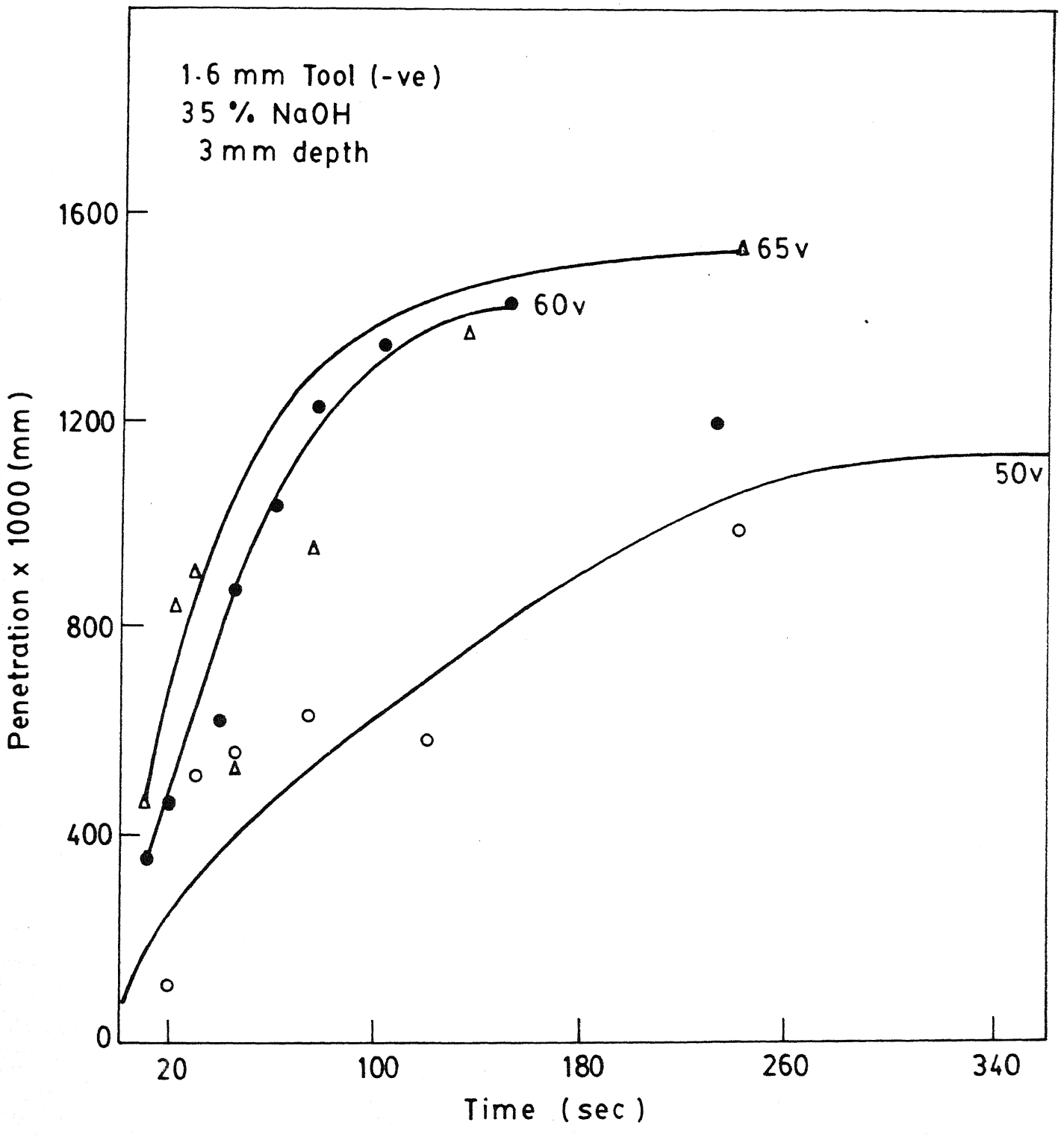

Fig.1·13 Limited depth characteristics [6] (work material: glass)

speed of 60 cm/min was used by them in the experiment.

Recently, Allesu [1] conducted extensive experiments of ECD phenomenon and ECDM. Glass wafer of 0.2 mm thickness was cut along the length using a razor blade. The suggested mechanism of material removal depends on thermal heating, cavitation and electrochemical action. A lot of useful observations, such as the limited depth characteristic, shifting of discharge zone with indentation of tool in work piece and limiting value of applied potential to prevent tool melting, was noticed by him.

Allesu explained the reason for limiting depth characteristic as a result of the loss of potential between the tool electrode and bulk electrolyte with the tool indentation in the workpiece. This is caused by the accumulation of gas bubbles at the point of indentation. He made a configuration such that this type of bubble accumulation did not occur, and he showed that in that configuration the machining rate remains constant (Fig.1.14). Also the discharge zone shifts with the indentation of tool (Fig.1.15) ceasing the machining process. Allesu also examined the effect of the electrolyte flow on the discharge voltage and found that the discharge voltage increases with the electrolyte flow velocity (Fig.1.16). Perhaps, the most useful observation made by him is the distribution of voltage drop in an ECDM both (Fig.1.17) and the sources of the resistances (Fig.1.18). The present author examined the voltage drop characteristics and found only a small variation from the results

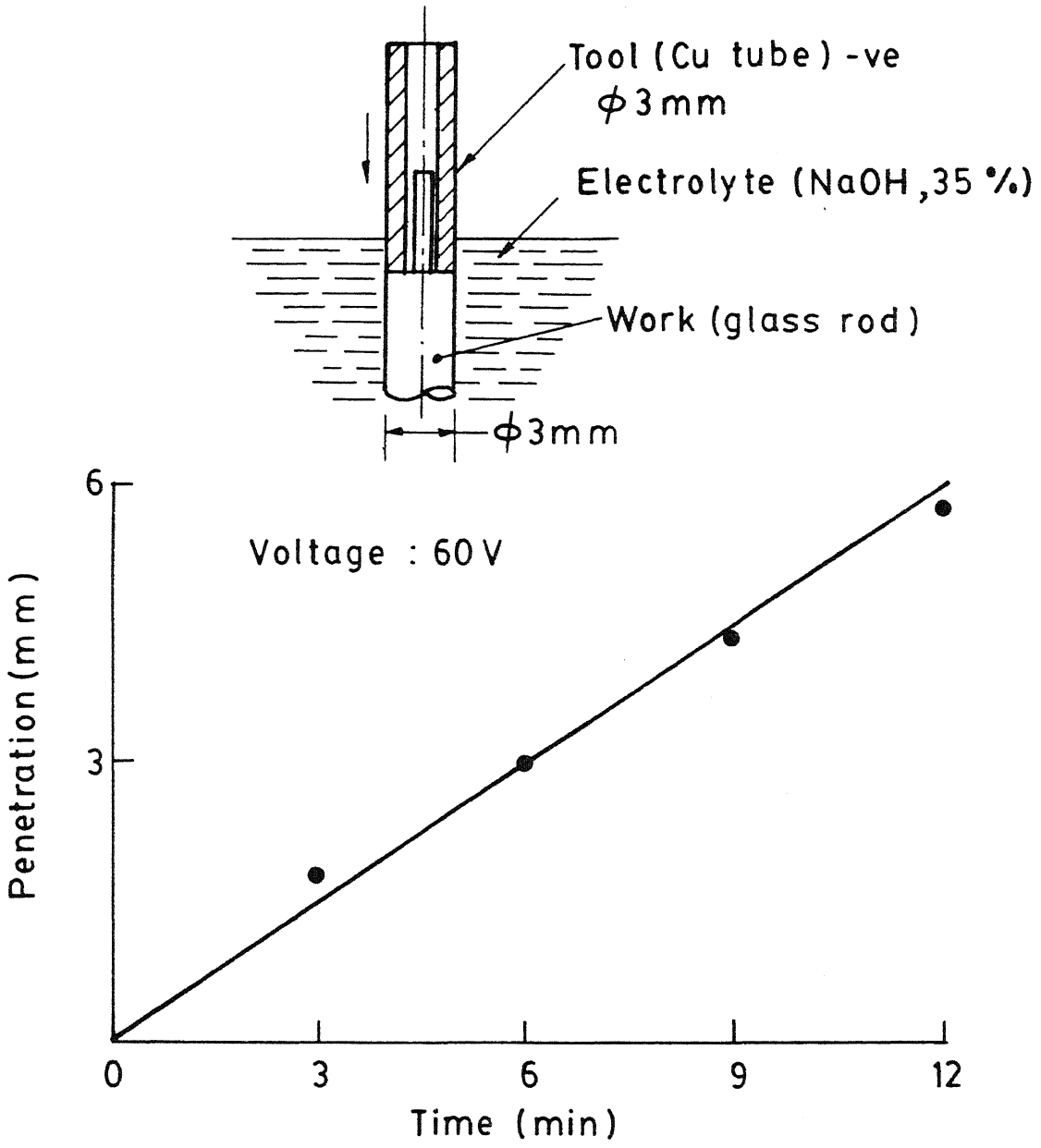

Fig.1-14 Constant rate machining [1]

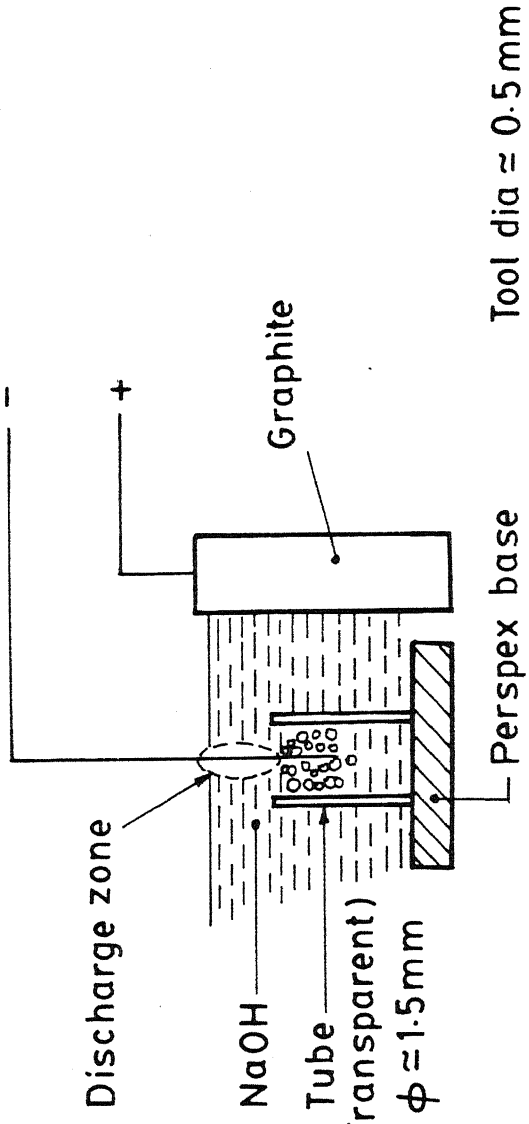

Fig.1.15 Shifting of the discharge zone [1]

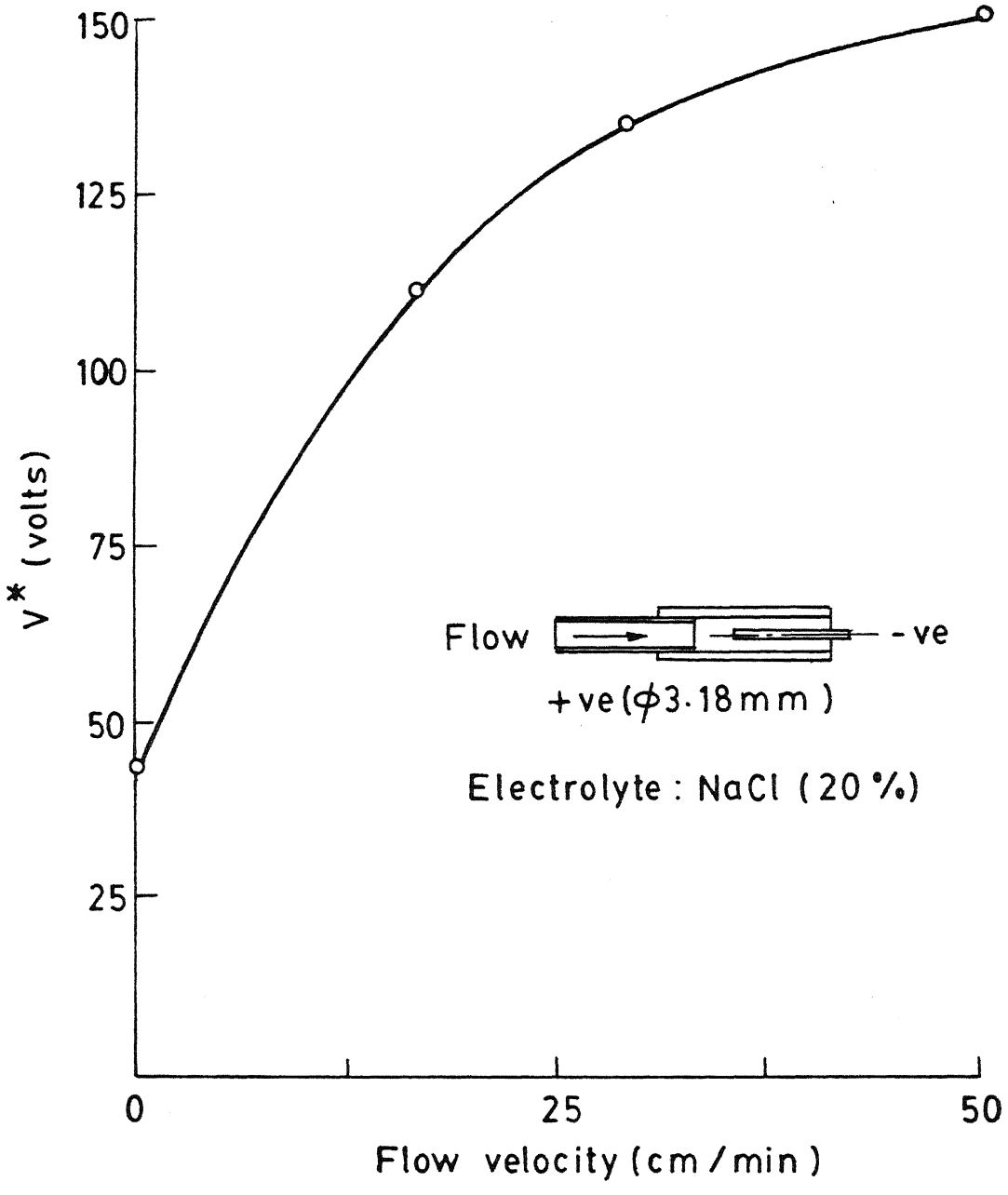

Fig. 1·16 Effect of the electrolyte flow on V^* [1]

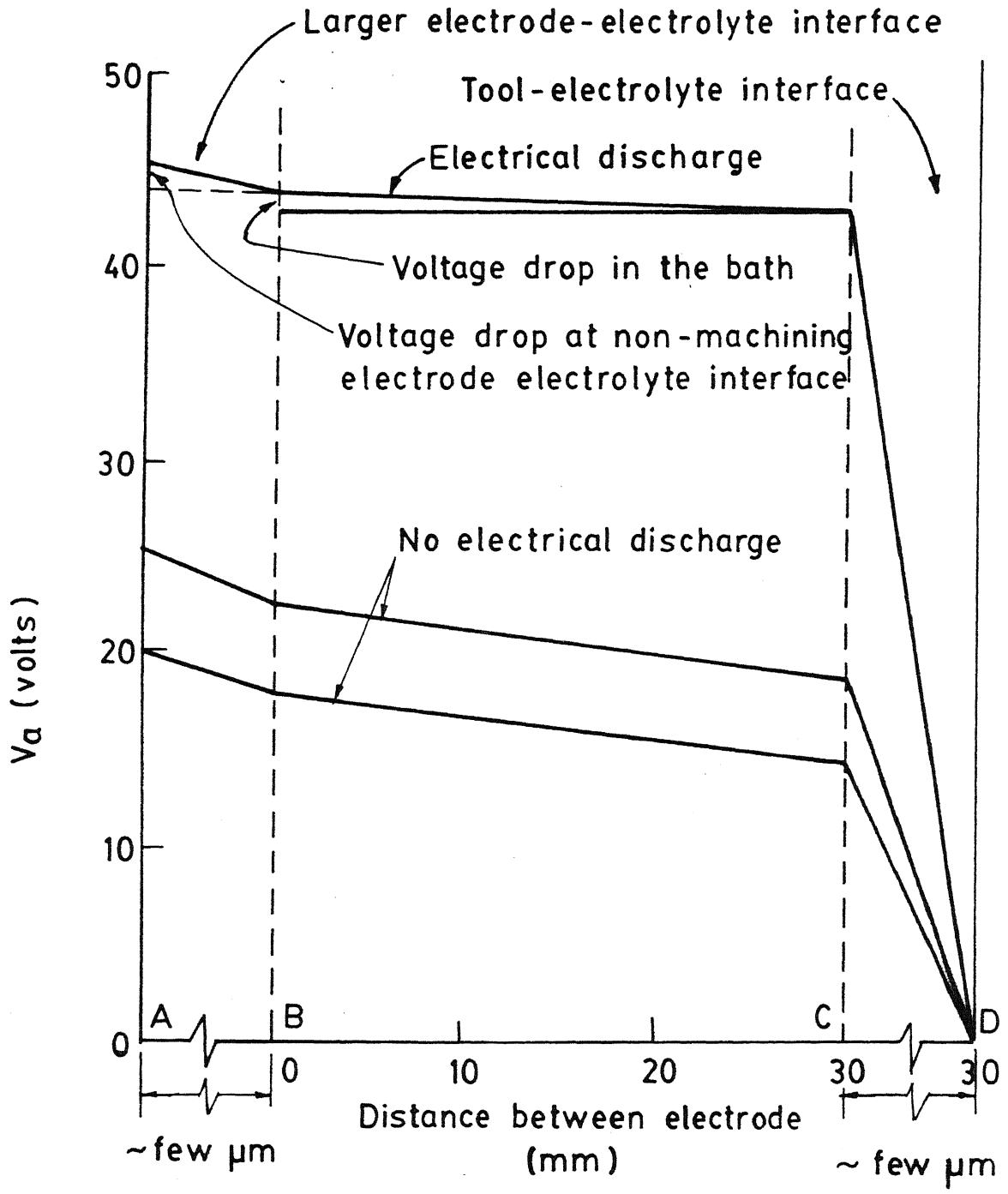

Fig. 1.17 Distribution of voltage drop in an ECDM bath [Electrolyte : NaOH(35%); Tool polarity : -ve ; Power supply : DC] [1]

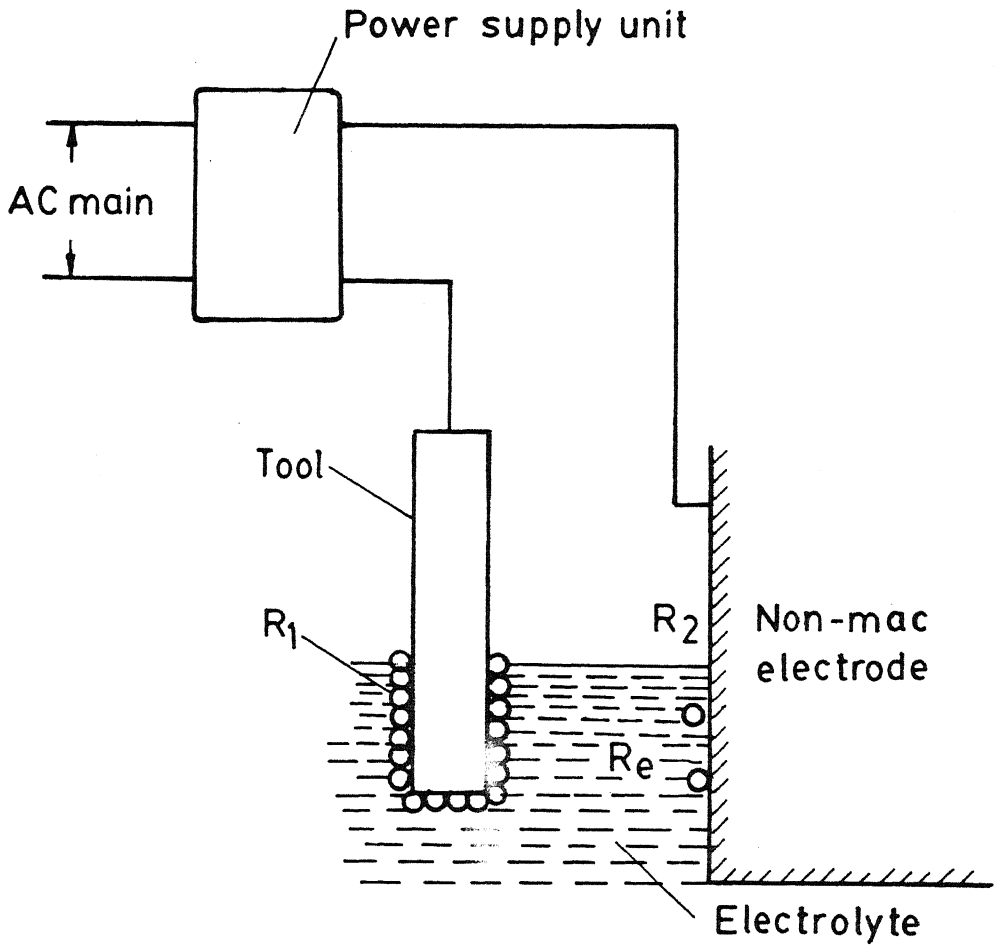

R_e = Electrolyte path resistance

R_1 = Tool - Electrolyte interface resistance

R_2 = Non-machining electrode - electrolyte interface resistance

R_1 Fluctuates depending on voltage

Fig. 1.18 Resistance in ECD (non-conductor machining) configuration [1]

obtained by Allesu.

In the field of ECAM, which was also labelled as ECDM in the early stages, fairly large amount of work has been done and the process is more or less established. Kubota and Tamura [8] reported drilling of steel plates by using ECD in the 1973. In a subsequent report by Kubota [9,10], the process was explained as the combination of ECM and EDM. McGeough and his research team conducted many experiments in the field of ECAM [11-18] and reported very high material removal rate, five times that of ECM and about forty times that of EDM. They examined the process by using single discharge technique and also by high speed photography. The process was analysed both statistically and experimentally and surface finish characteristics were studied. They tried to improve the efficiency of the process by imparting vibration to the tool. A more developed process, wire-ECAM was developed by them.

A few primary work on the machining of composites by ECD have been conducted at IIT Kanpur and reported [19,20].

1.3 Objective and Scope of the Present Work

The literature survey indicates that though the mechanism of material removal in ECDM is identified to some extent, the mechanism of spark initiation at the electrode, i.e., the ECD phenomenon, remains unknown. Furthermore, no attempt has

been made to develop a quantitative model of material removal during ECDM. The main objectives of the present work are as mentioned below:

- To identify the mechanism of the electrochemical discharge phenomenon.
- To develop a simple, realistic and quantitative model capable of predicting the minimum required voltage and corresponding current to initiate sparking for any given condition.
- To develop a simple and idealised quantitative model capable of predicting the MRR in ECDM for any given condition.
- To explore the possibility of enhancing the MRR characteristics of ECDM as it is characteristically a low MRR process. The effect of some extra parameters, associated with the modification of the basic electrical circuit, to enhance MRR will be also investigated.

The secondary objective is to design and develop an appropriate experimental setup to conduct all the investigating as well as final verifying experiments.

The processes of ECD and ECDM are extremely complex involving many interdependent phenomena. Their ranges are widely varied from the field of electrochemistry to the field of boiling phenomenon. It is impossible within the scope of the present work to conduct all the experiments for the required observations. To

make the problem tractable dependency on the observations by the previous researchers of the revelent fields become inevitable. The verifying experiments were conducted with glass workpiece only. The time constraint had made the investigations with other nonconducting materials beyond the scope of the present work.

CHAPTER 2

EXPERIMENTAL INVESTIGATION OF ELECTROCHEMICAL DISCHARGE PHENOMENON AND ELECTROCHEMICAL DISCHARGE MACHINING

2.1 Introduction

To understand the mechanism of the process of electrochemical discharge machining (ECDM), it is essential to have a complete information about the basic features and the general characteristics of the process. Certain amount of information in this direction is available from the published works of the previous researchers in the relevant field. However, to have a comprehensive set of observations resulting from a set of consistent parametric study of the process, it was decided to conduct fresh sets of experiments. These experiments can be divided into two groups. One group of experiments were aimed at investigating the phenomenon of electrochemical discharge (ECD), whereas the other sets of experiments were designed to reveal the basic features of ECDM. For this purpose it was necessary to design a few experimental setups. These setups were also utilised to conduct experiments for verifying the predictions of the theoretical models developed in the subsequent chapters.

2.2 Experimental Setups and Associated Instrumentation

2.2.1 Experimental setup to study ECD phenomenon

To investigate the general characteristics of the ECD phenomenon it was required to design and develop a setup in which the applied voltage, the tool diameter and the tool depth in the electrolyte could be controlled precisely. It was also necessary to read the input voltage, the corresponding current alongwith their wave shapes. The setup is schematically shown in Fig.2.1a. It consisted of a controlled power supply, an electrochemical bath with electrodes, a tool feed mechanism and the required measuring facilities. The whole system was isolated from the A.C. mains by an isolation transformer. The input voltage was controlled by the variac which was subsequently rectified by a bridge rectifier to 100Hz fullwave rectified D.C. There was option to use filter capacitors across the rectifier output terminal to filter the rectified D.C. A capacitor bank of 2000μF was used as the filter. Standard voltmeter and ammeter were employed to read the RMS values of the applied voltage and the corresponding current, respectively. A resistance of 0.1Ω was connected to the circuit and the voltage across the resistor was monitored by one of the channels of a dual channel digital storage oscilloscope [DSS 2011, KIKUSUI,JAPAN]. The voltage waveshape across the resistor represents the current waveshape of the electrochemical circuit. The shape of the supply voltage was monitored by the other channel of the oscilloscope as shown in the figure. This facilitated simultaneous monitoring of the applied voltage and the

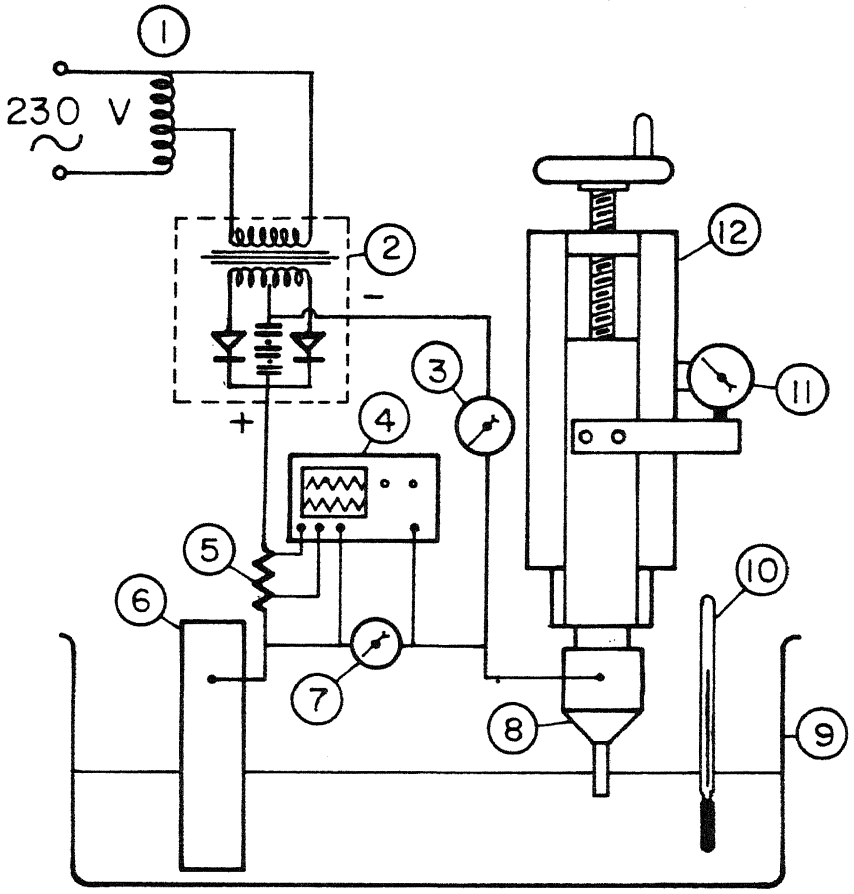

1 Variac
2. D. C. output with isolation transformer
3 R.M.S Ammeter (D.C)
4 Dual channel CRO
5 Low resistance
6 Large electrode
7 R.M.S. Voltmeter (D.C)
8 Tool electrode with holder
9 Electrolyte bath
10 Thermometer
11 Dial gauge
12 Screw feed mechanism

Fig. 2.1a Experimental set-up for E.C.D

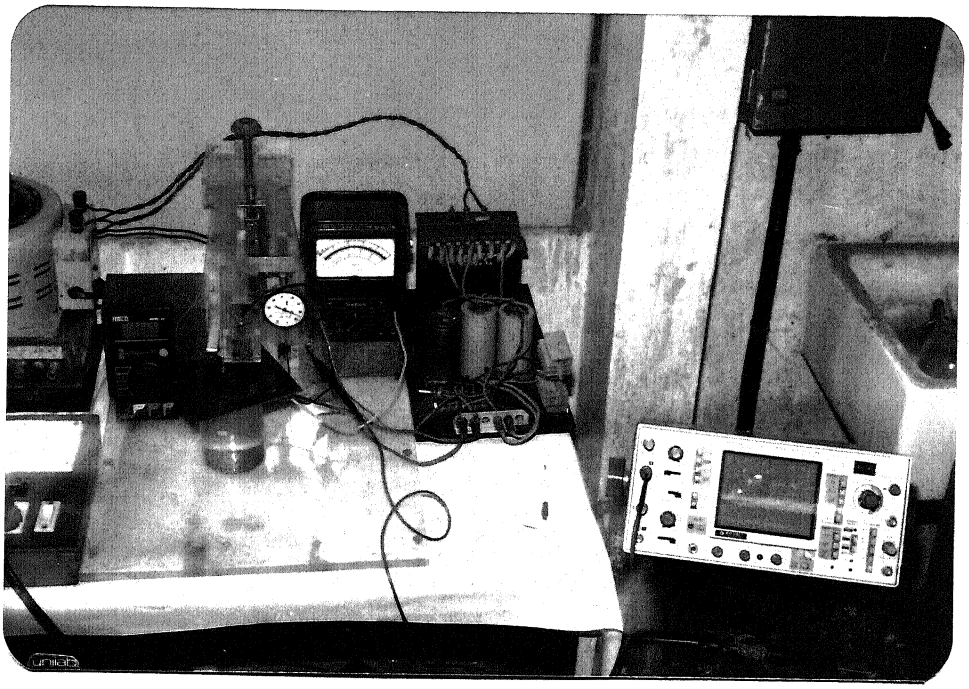

P1. View of ECD Set-up.

P2 Close-up of ECD cell

corresponding current waveshapes. The tool holder was attached to a properly insulated screw-nut feed mechanism and connected to the negative terminal of the power supply unit. Using a dial gauge with this mechanism it was possible to set the depth of the tool electrode in the electrolyte at any predetermined value. A glass beaker of 500ml capacity was used as the electrolyte bath. An electrical heater with on-off control (not shown in the figure) was used to raise the temperature of the electrolyte, whenever required. A mercury bulb thermometer was used to read the electrolyte temperature. 400 ml of electrolyte was used in each experiment. The larger electrode (nonmachining electrode) was made of circular stainless steel bar of 1 cm diameter and was dipped to a fixed depth of 2 cm in the electrolyte. This was connected to the positive terminal of the power supply. In this setup no work piece was used.

2.2.2 Experimental setup for ECDM

In electrochemical discharge machining (ECDM) experiments, it was required to maintain a constant contact between the tool and the workpiece. The beaker which was used as the electrolyte bath in the previous setup was proved to be inconvenient to accommodate the workpiece. Later, in the experiments to verify the proposed ECDM model it was observed that the filter capacitor was causing the unwanted effect of capacitive discharge. So, it was decided to eliminate the filter capacitors and the experiments concerning ECDM conducted only with 100Hz full wave rectified D.C. As it was understood that the discharge was

due to switching phenomenon (discussed later), the author felt that the inductance might be an important parameter in the ECDM performance. This necessiated the addition of an inductance coil. All these modifications required a different setup for the ECDM experiments. The setup for the ECDM experiments is shown in Fig.2.1b. The measuring and monitoring instruments were similar to those of the previous setup. With filter capacitors removed, a variable inductance of range 0-800mH was added to the circuit, to increase the total circuit inductance. A flat glass bath of 1000 ml capacity was used as the electrolyte bath to accommodate the workpiece with the workpiece holder, which was made of perspex. The gravity feed mechanism was employed to maintain the constant contact between the tool and the workpiece. The feed force was adjusted to 50 gm using the counterweights. The penetration of the tool in the workpiece was read with the help of the dial indicator. A constant level of the electrolyte in the bath was maintained so that at any instant of machining the tool depth in electrolyte remains within 0.2 cm. No heating arrangement of electrolyte was made, as all the experiments of ECDM were conducted in room temperature.

2.2.3 Tool material

Preliminary experiments were conducted with different tool materials such as copper, aluminium, platinum and steel. Aluminium tool reacted chemically and dissolved in the alkaline solutions. No other effect of the tool material on the ECD and ECDM characteristics was observed. Therefore, it was decided to

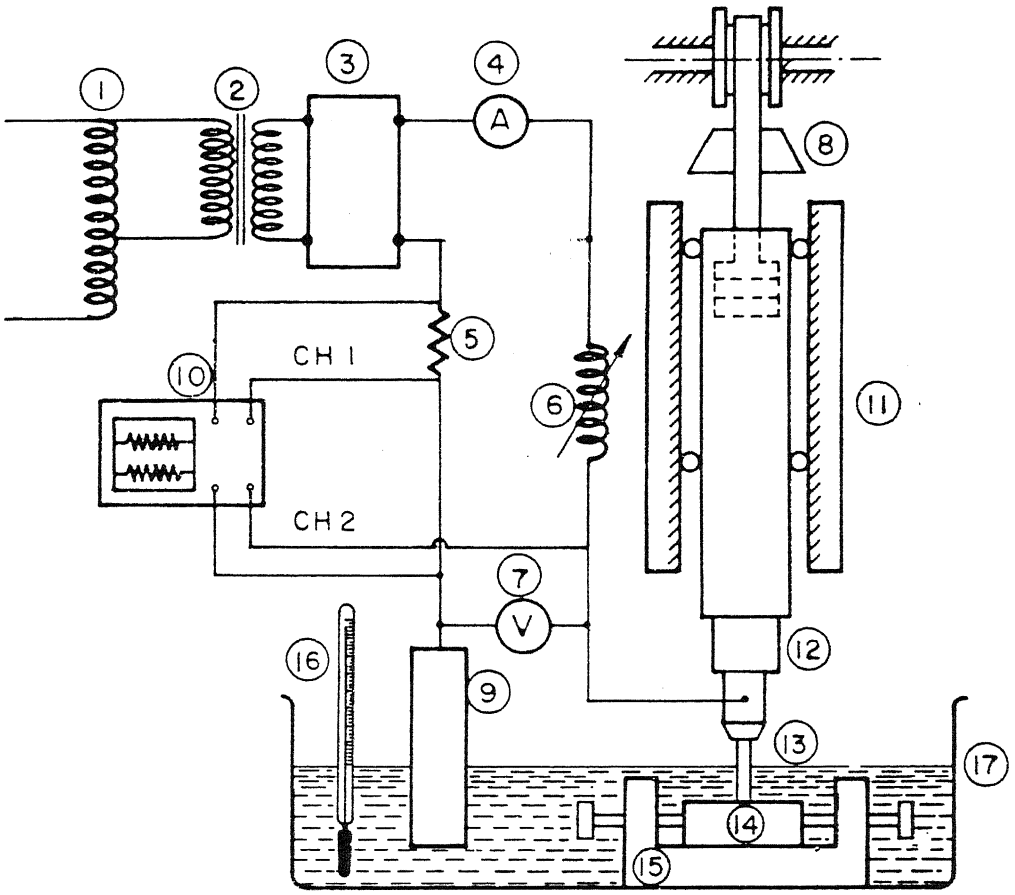

1. Variac
2. Isolation transformer
3. Bridge rectifier
4. R.M.S ammeter (D.C)
5. Resistor, 0.1 Ω
6. Variable inductance
7. RMS voltmeter (D.C)
8. Counter weight
9. Anode (non machining electrode
10. Dual channel storage oscilloscope
11. Gravity feed mechanism
12. Insulated tool holder
13. Tool (cathode)
14. Workpiece
15. W/P holder
16. Thermometer
17. Electrolyte bath

Fig. 2.1b Experimental set-up for E.C.D.M

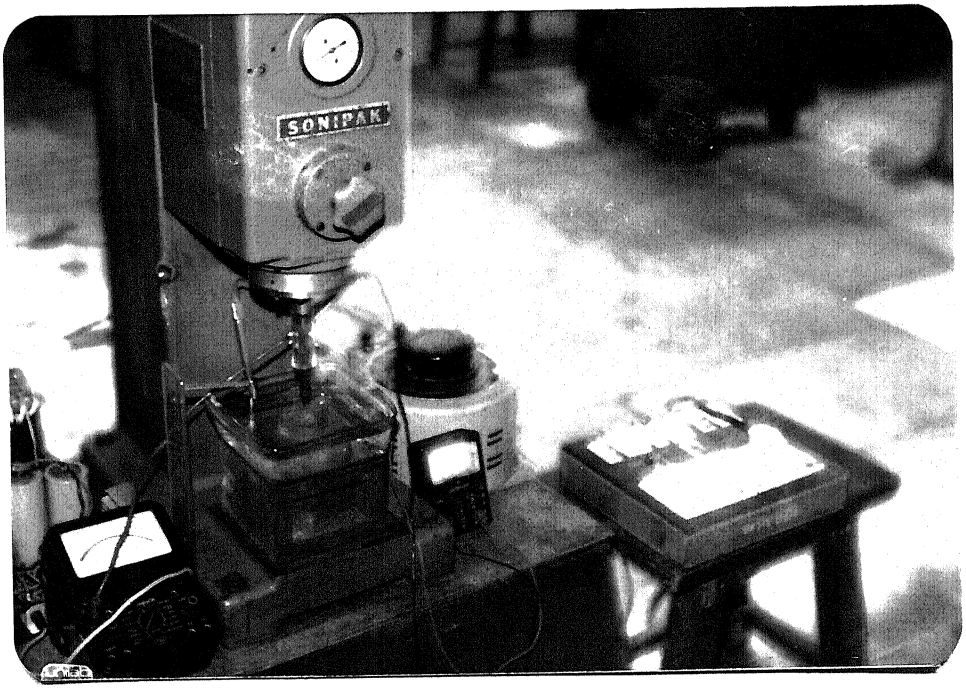

P3. View of ECDM Set-up

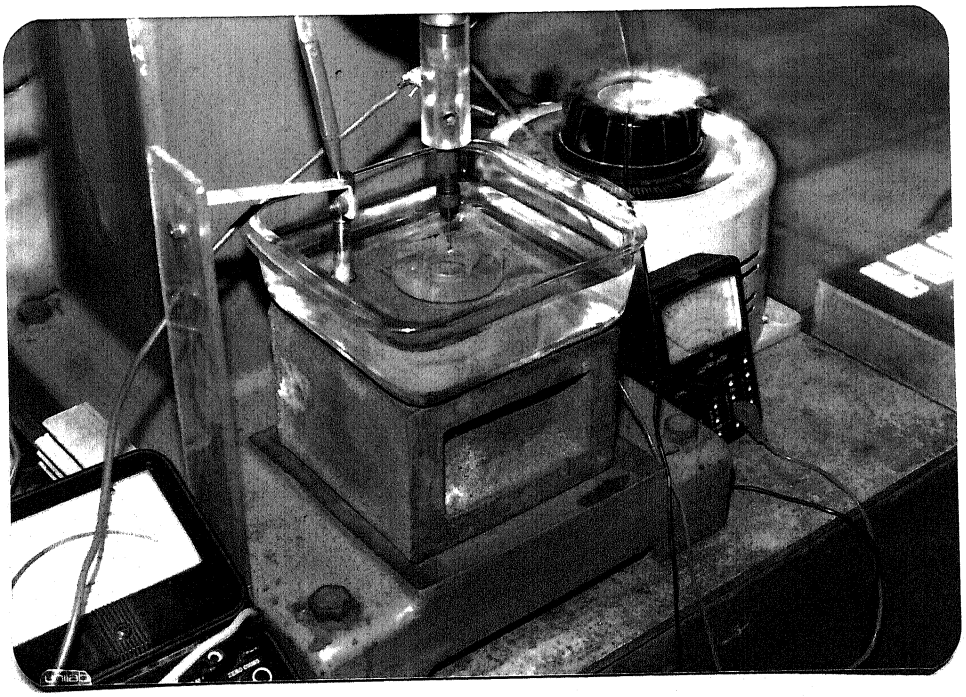

P4. Closeup of electrolyte bath

use steel tool only. The study of the effect of tool geometry was not included in the objectives of the present work and only solid cylindrical tools were used. Tools of diameters 0.08 cm, 0.11 cm, 0.15 cm, 0.16 cm, and 0.195 cm were made from steel wires. The wires were cut to proper sizes and the ends were made orthogonal to the side surfaces. The wires were reduced to the proper diameter with 1/0 emery paper and then polished with 4/0 emery paper for final finish. To eliminate the chance of different bubble nucleation site density for different tools, all the tools were finished to identical surface quality. The tools were used as cathode only to avoid anodic dissolution and the consequent loss of the surface area.

2.2.4 Electrolytes

It was revealed from the literature survey that most of the work has been done with alkaline electrolytes such as NaOH and KOH and neutral electrolyte such as NaCl. To maintain the consistency of the results with those obtained by the previous researchers, the author decided to conduct the experiments with NaOH, KOH and NaCl. However, in the course of experiments, the author felt that the KCl electrolyte could also be tried as well, as it was neutral in nature like NaCl. Aqueous electrolytes of different concentration were prepared by dissolving the appropriate amounts of the respective reagents in water. Due to the electrochemical reactions during experiments the composition of the electrolytes changed. To maintain the quality, the solution was changed after being used for a maximum period of 10

minutes in all the experiments. The concentration was expressed in % wt, which indicates the weight of the reagent dissolved per 100 ml of water to prepare the aqueous electrolyte. The following table shows the numbers of moles of the electrolyte per 100 ml of water, corresponding to the concentration in % wt.

Electrolyte	5%	10%	15%	20%	25%	30%	40%
NaOH	0.125	0.250	0.375	0.500	0.675	0.750	1.000
KOH	0.089	0.178	0.268	0.357	0.446	0.536	0.714
NaCl	0.086	0.171	0.257	0.343	0.429	-	-
KCl	0.067	0.134	0.201	0.268	-	-	-

2.2.5 Workpiece material

Commercial sodalime glass available in the local market was used as workpiece material. The approximate composition of the sodalime glass is, SiO_2 - 72%, CaO - 10%, Na_2O - 14%, MgO - 3.2% and Al_2O_3 - 0.8%. The glass pieces were available in the form of slides of size 6 cm. long, 2 cm wide and 0.18 cm thick. In some experiments the glass wafer with the same composition were used which were 1.8 cm square with a thickness of 0.03 cm. Only glass specimen was used as the workpiece material as the time constraint made the experiments with other materials beyond the scope of the present work.

2.2.6 Determination of material removal

The amount of the material removed was determined by the weight difference method. A mechanical microbalance [MLW, VEB Analytic, Germany] of range 0-100 gm and with an accuracy of 0.01 mg was used for this purpose. The glass specimen was rinsed with tap water thoroughly to remove the layer of the electrolyte. Then it was dried by mild heating to expel any water particle which might be present, particularly at the machined blind holes. These procedure were repeated before taking each weight reading. The difference between the readings taken before and after machining was the amount of the material removed. The average of a sufficient number of such readings were taken to obtain a reliable result. The average material removal rate was obtained by dividing the amount of material removed by the time of machining.

2.3 General Characteristics of Electrochemical Discharge Phenomenon

2.3.1 Voltage - current (V-I) characteristics

The effects of different input parameters on the V-I characteristics of an electrochemical discharge cell are as follows:

(i) Effect of the nature of the power supply: Figure 2.2 shows the V-I characteristics for the smooth and the 100Hz full wave rectified D.C. power supply. There are four distinct regions in the characteristics. In region 1 current increases linearly with the applied voltage. Beyond this region the rate of rise of

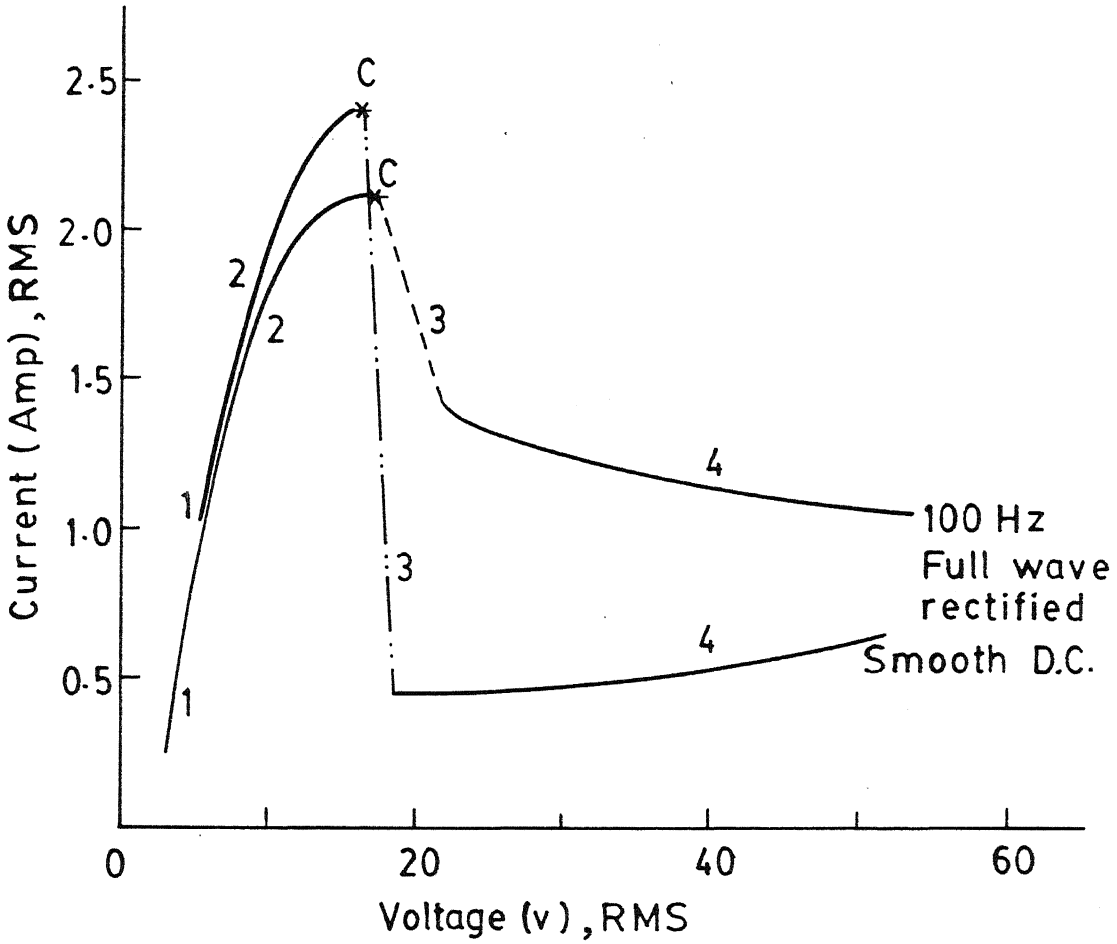

Electrolyte : 40% KOH ; Tool dia : 0·11 cm ;
Depth in electrolyte : 0·2 cm

Fig. 2·2 V-I Characteristic for different type of power supply

the current with the applied voltage falls and finally levels off (region 2). At the end of region 2, small sparks appear at the tool electrode edge (point C), followed by a transition region (region 3), where no particular relationship between the voltage and the current exists. The transition zone ends with a small increment of the applied voltage and marked by a stable discharge at the electrode edge. The current restabilizes at this point, though the magnitude of this current is much smaller than that at the point of initiation of discharge (point C). With further increase of the applied voltage, the rate of change of the current is much slower (region 4) compared to the rate at the predischarge stage. However, the intensity of the discharge increases with the applied voltage. The characteristics for the smooth and rectified D.C. are similar upto the beginning of the region 4. In region 4, for smooth D.C. supply, the current increases slowly, whereas it drops for the rectified D.C. supply. Point C, the corresponding voltage and current are termed as the critical point, critical voltage (V_c) and critical current (I_c), respectively. The nature of the characteristics upto the critical point can be explained in terms of a simple resistive circuit. Beyond this point it is the switching phenomenon which influences the characteristic. In region 1, only the constant path resistance being active, the current is proportional to the applied voltage. The bubble density on the electrode surface increases with the applied voltage and results in increased interface resistance. Due to this the rate of rise of the current in region 2 drops. The discharge at the electrode edge at point C is the outcome of the

switching action between the electrode and the electrolyte. An intermittent and irregular switching action causes the transition at region 3. Regular switching chops off the current at small intervals and as a result the RMS value of the current at the end of the region 3 is considerably low.

(ii) Effect of the electrolyte: The V-I characteristic for different electrolytes is shown in Fig.2.3. It can be noticed that though the pattern of the characteristics is more or less similar the magnitudes of V_c and I_c are different for different electrolytes. This indicates that the electrolyte properties influence the V-I characteristics.

(iii) Effect of tool diameter: The V-I characteristic for different tool diameter is shown in Fig.2.4. The critical current increases proportionally with the tool diameter, without any significant change in the critical voltage. This increase in current is due to the increased surface area of contact between the tool and the electrolyte. The current at the discharging zone (zone 4) is, however, not proportional to the tool diameter. This is the result of the complex switching phenomenon, which is not a simple function of the area of contact between the tool and the electrolyte.

(iv) Effect of the tool depth: Figure 2.5 shows the V-I characteristic for different tool depths. This characteristic is similar to the previous one, as in both the situations the area of contact between the tool and the electrolyte is the guiding feature. However, the critical current is not proportional to the tool depth.

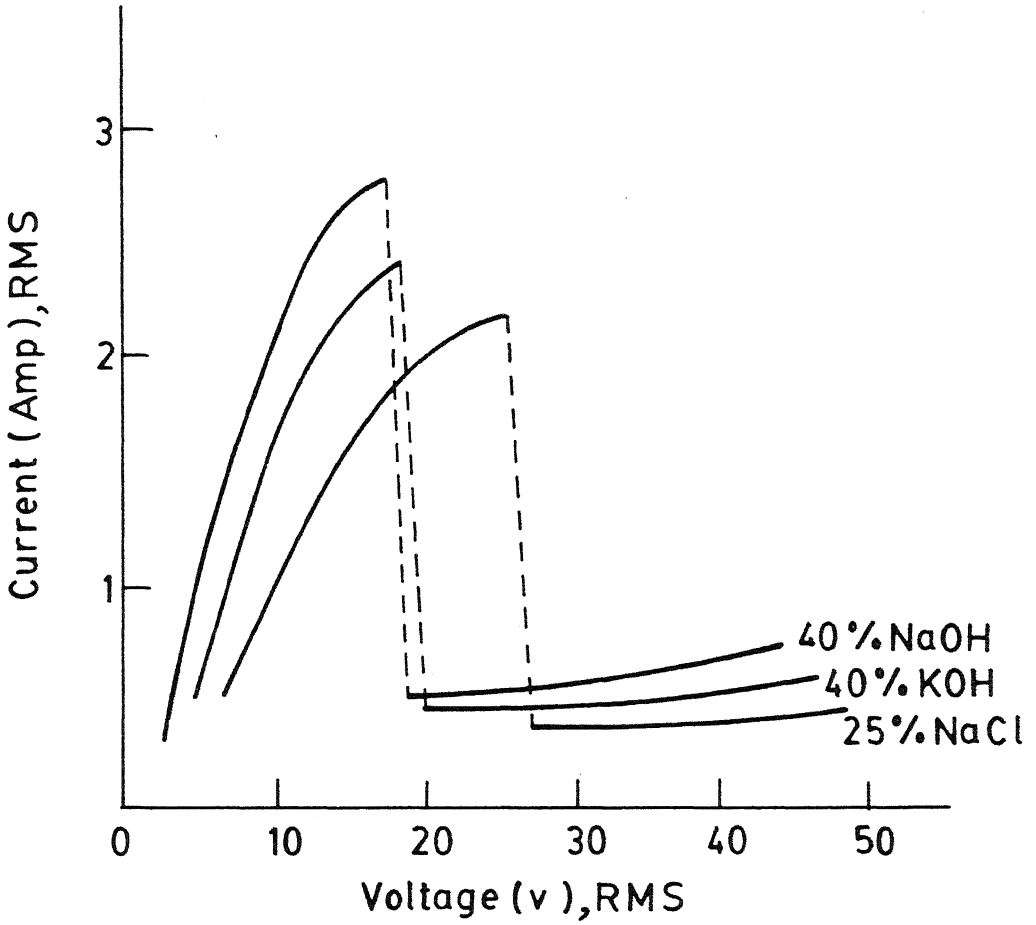

Tool dia : 0·11 cm Tool depth :=0·2 cm
Power supply : Smooth D.C.

Fig. 2·3 V-I Characteristics for different electrolyte

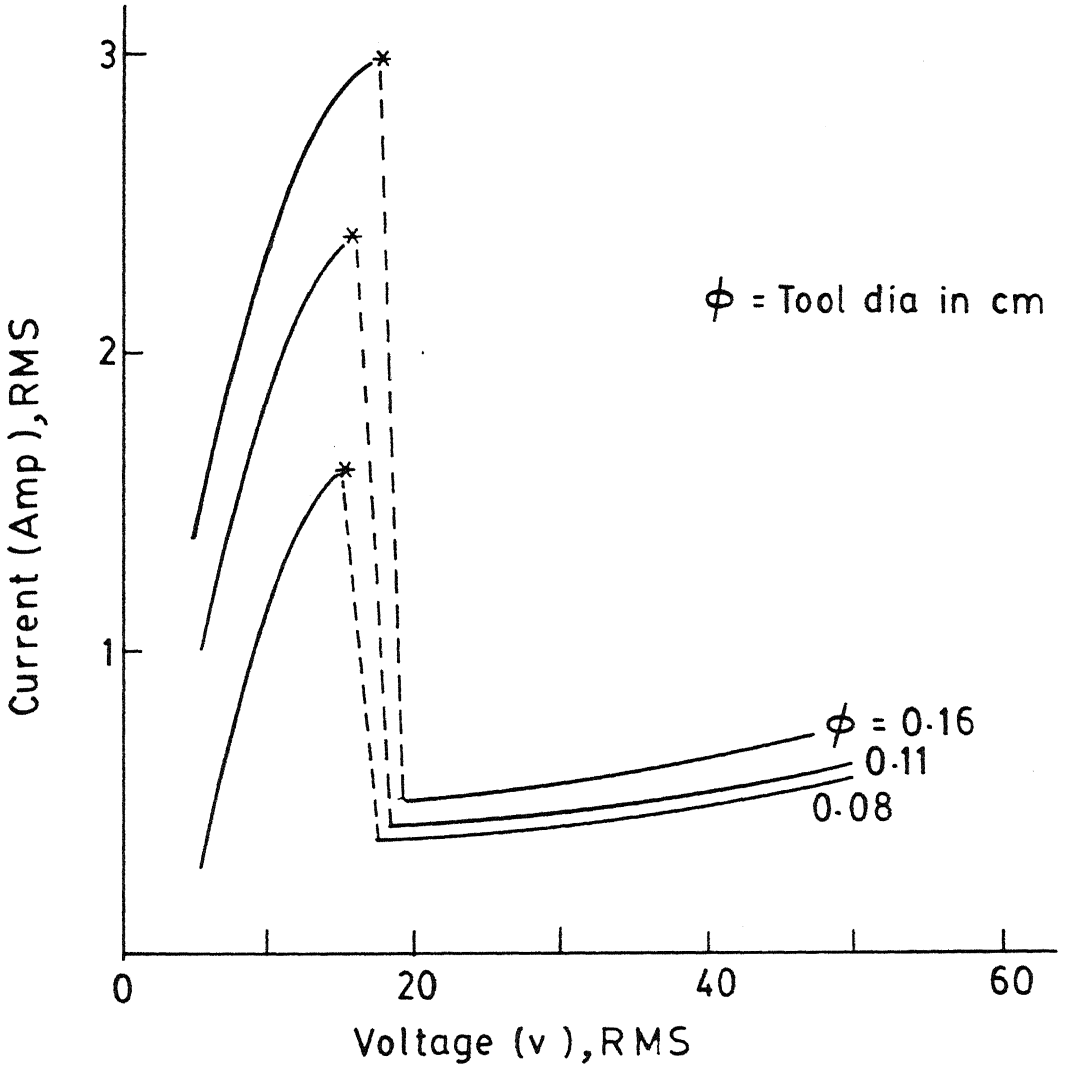

Electrolyte : 40 % KOH ; Power supply : Smooth D.C. ;
Depth in electrolyte : 0·2 cm

Fig. 2.4 V-I Characteristic for different tool diameter

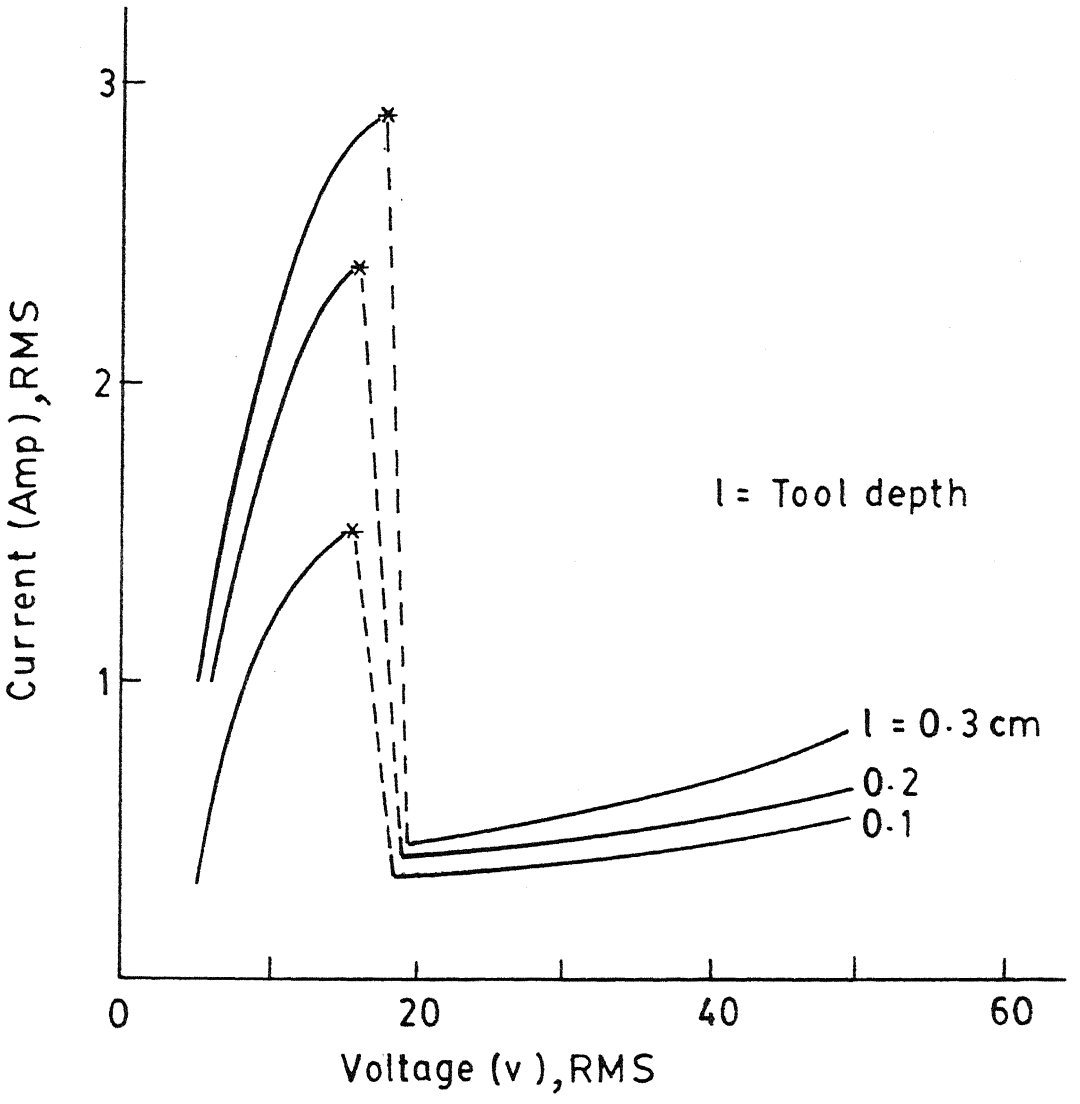

Electrolyte : 40 % KOH ; Tool diameter : 0·11 cm ;
Power supply : Smooth D.C.

Fig. 2·5 V-I Characteristic for different tool depth

(v) Effect of the electrolyte concentration: The V-I characteristic for different concentration of an electrolyte is shown in Fig.2.6. The critical current increases with the electrolyte concentration, but the critical voltage decreases. This is primarily due to the increase of the electrolyte conductivity with the concentration, though there may be some secondary effect of the concentration on the system. The variation of the critical voltage and the critical current with the concentration is shown in Fig.2.7a and 2.7b. It is interesting to note that the power consumption at the critical condition ($= V_c \times I_c$) remains constant and independent of the concentration. This indicates that the thermal heating is a factor to initiate the spark (discharge).

(vi) Effect of the electrolyte temperature: The variation of the critical voltage and the critical current with the electrolyte temperature is shown in Fig.2.8. The critical current drops with the rise of the electrolyte temperature without any change in the critical voltage. Early bubble generation at the electrode surface results in significant interface resistance even with a lower applied voltage. Therefore the rate of rise of current is low. The power consumption at the critical stage decreases with increased electrolyte temperature, as both the heat loss to the electrolyte from the interface and the heat required to raise the electrolyte temperature to the boiling point (at the interface) decrease.

(vii) Effect of the electrode temperature: The discharge takes place due to the vapour blanketing of the electrode. The

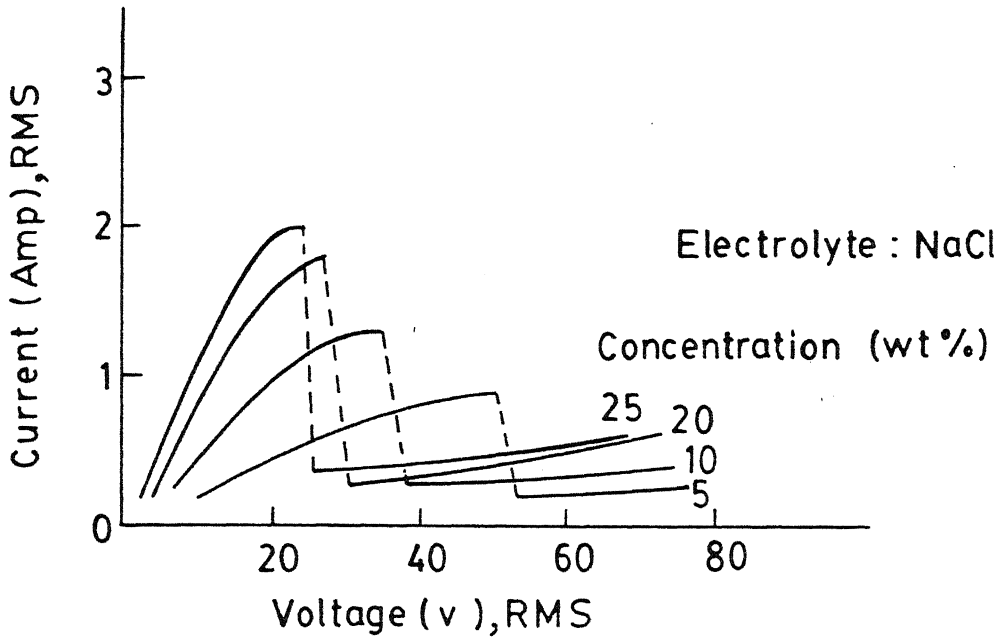

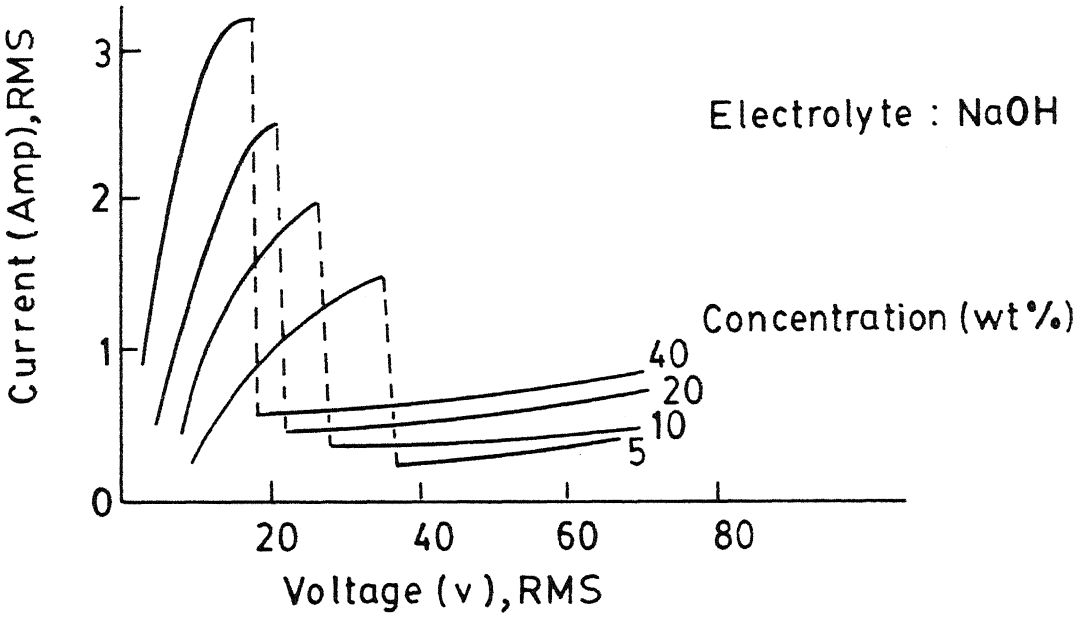

Tool dia = 0·11 cm ; Tool depth = 0·2 cm
Smooth D.C.

Fig. 2·6 V-I Characteristic for different concentration of electrolyte

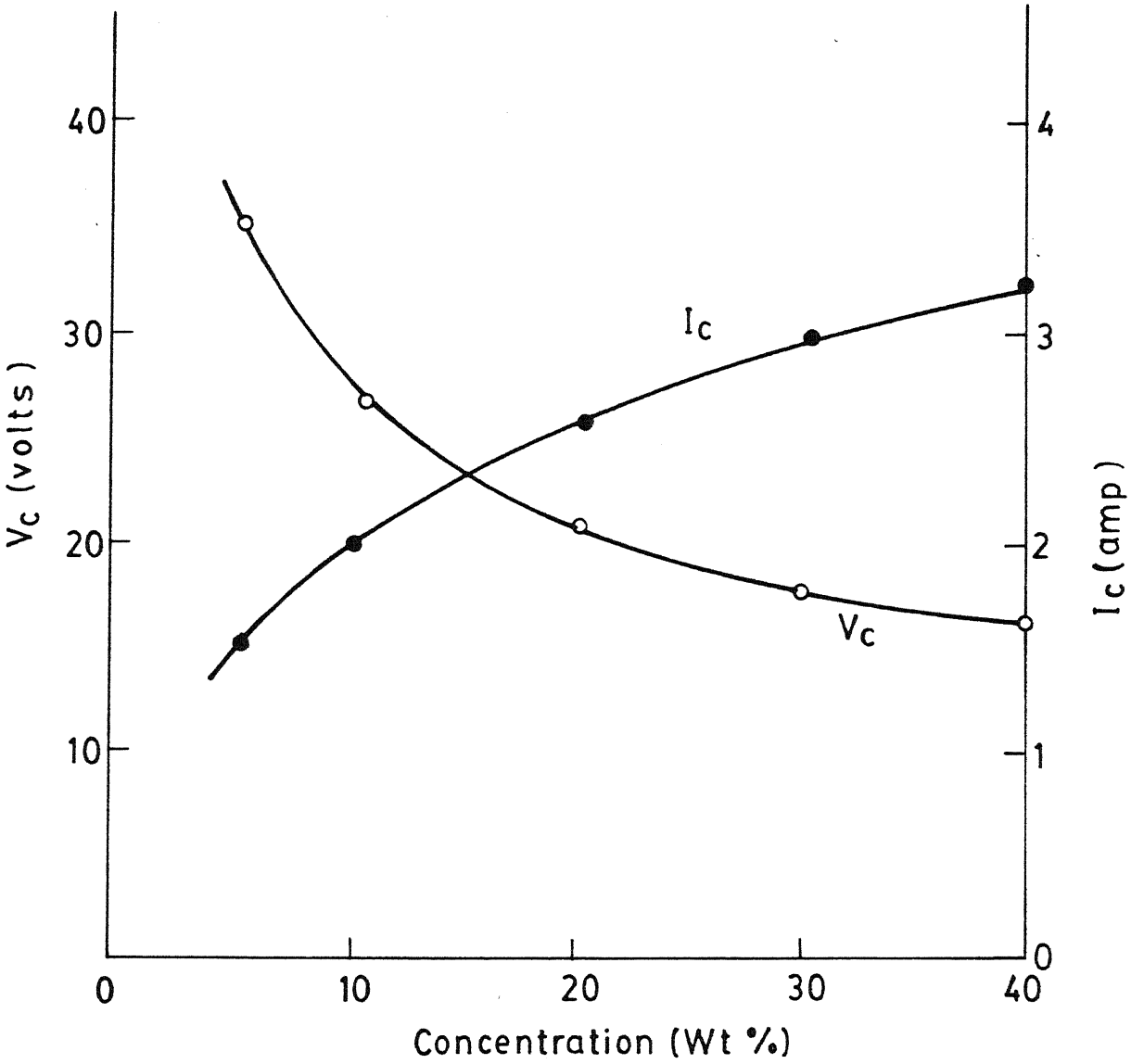

Tool dia = 0·11 cm ; Tool depth = 0·2 cm ;
Electrolyte = NaOH ; Smooth D.C.

Fig. 2·7a Critical voltage and current at different concentration (NaOH)

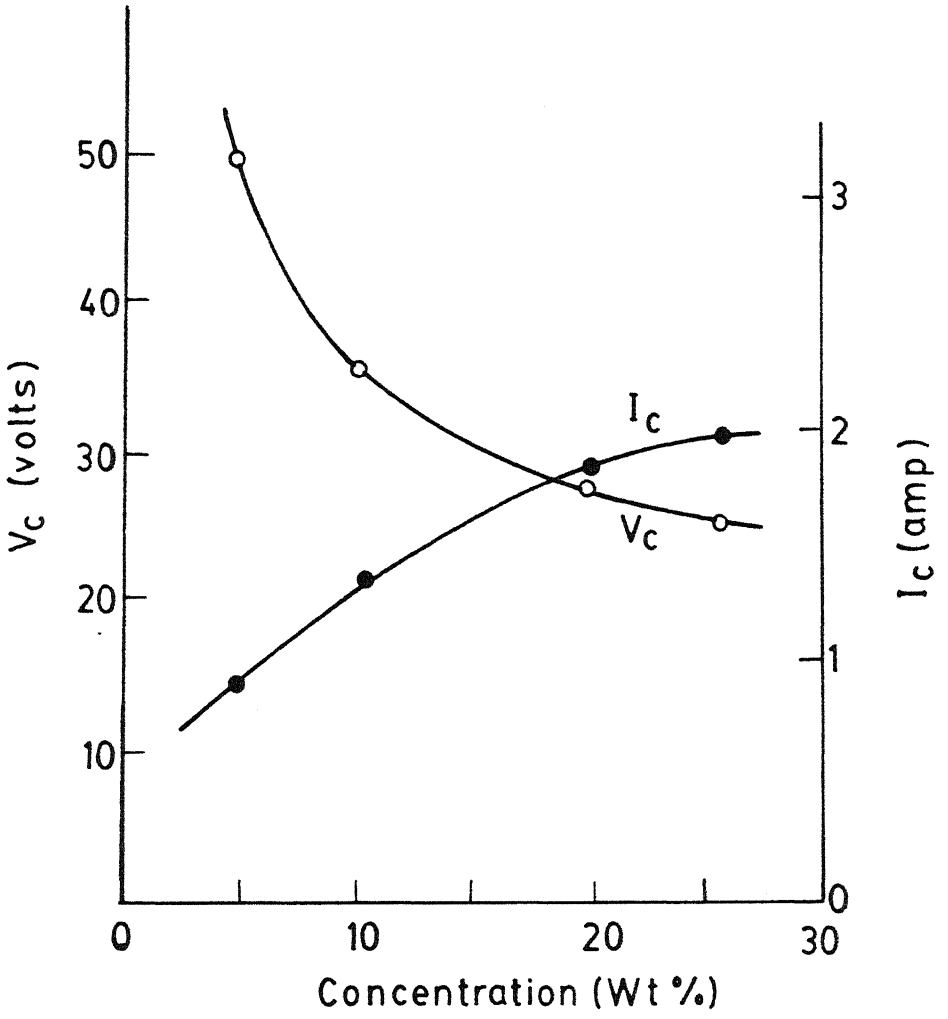

Tool dia = 0·11 cm ; Tool depth = 0·2 cm ;
Electrolyte = NaCl ; Smooth D.C.

Fig. 2·7 b Critical voltage and current at different concentration (NaCl)

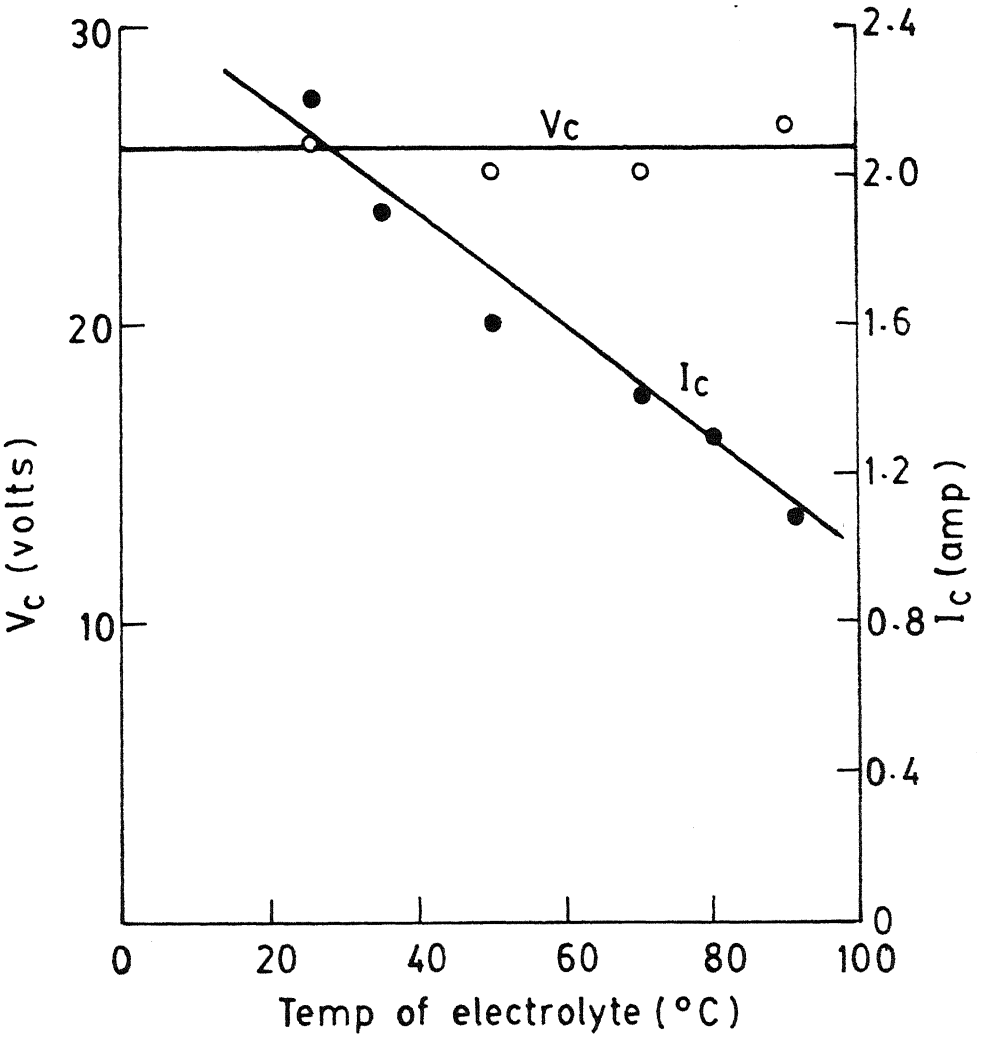

Electrolyte = 25 % NaCl ; Tool dia = 0·15 cm ;
Tool depth = 0·2 cm; 100 Hz full wave rectified D.C.

Fig. 2·8 Critical voltage and current at different electrolyte temperature

electrochemical reaction and the interface heating of the electrolyte are the reasons for the blanket formation. An arrangement was made to heat the electrode by electric heater externally maintaining the required depth of the electrode in the electrolyte. This resulted in nucleation of vapour bubbles on the electrode surface, though in much lesser number than that required for blanketing. It was expected that this effect might reduce the power requirement at the critical condition, which was found to be true. The schematic setup as well as the result obtained by this experiment are shown in Fig.2.9. The last two observations indicate the role of vapour generation at the interface for the initiation of the discharge.

(viii) Effect of the interelectrode gap and the size of the nonmachining (larger) electrode: The interelectrode distance was varied, keeping the applied voltage and the depth of the tool electrode in the electrolyte constant. There was no significant change in the current magnitude when the interelectrode distance is reduced from 5 cm. to 0.8 cm., indicating insignificant effect of the interelectrode distance. In the next step, the depth of the larger electrode in the electrolyte was increased from zero to 2 cm, at a distance of 5 cm. from the tool, again keeping the applied voltage constant. It was noticed that initially the current increased with the depth. But after reaching a depth of 0.03 cm the current did not increase any further. From the diameters of the electrodes used, it was found that when the area of contact between the larger electrode and electrolyte is more than four times of that between the tool and electrolyte, the size

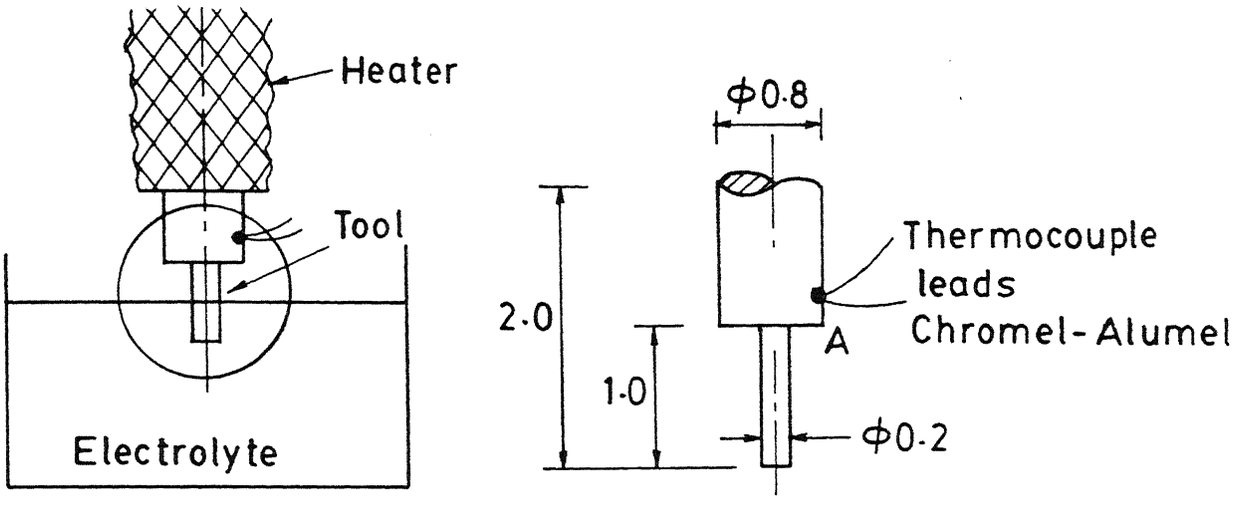

ELECTROLYTE	30% NaOH		25 % NaCl	
Temp. at pt. A (°C)	V_c	I_c	V_c	I_c
25	20	3·5	29	3·6
150	15	2·0	25	2·0

Fig. 2·9 Setup to find the effect of electrode temperature on V_c & I_c and obtained result

of the larger electrode does not effect the V-I characteristics. Figures 2.10a and 2.10b illustrate of these experiments.

2.3.2 The waveshapes of the applied voltage and the corresponding current

An oscilloscope was used to investigate the nature of the waveshapes of the current for the applied voltage with different characteristics, both just before and during discharge. Figure 2.11a shows these waveshapes for 100Hz full wave rectified D.C. It may be noticed that the current trace deviates from the sinewave form when the applied voltage approaches the critical value. The bubble density increases with applied voltage and increases the interface resistance. Therefore the current does not remain proportional to the voltage. The sharp drops in the current trace at the discharging condition are the result of switching. The use of a capacitor across the circuit acts as a filter, which converts the rectified D.C. to a smooth one. The waveforms of the applied voltage and the corresponding current with a filter capacitor of 1500μf are shown in Fig.2.11b. The small oscillation of the current at the predischarge stage results from the disturbance at the electrolyte surface due to bubble movement which affects the area of contact between the electrode and the electrolyte. The current trace in the discharging condition indicates the discharge is more frequent than the previous one which was shown in Fig.2.11a. Figure 2.11c shows the traces when an inductance of 100mH is added to the circuit. No filter capacitor was used in this case. The sharpness of the

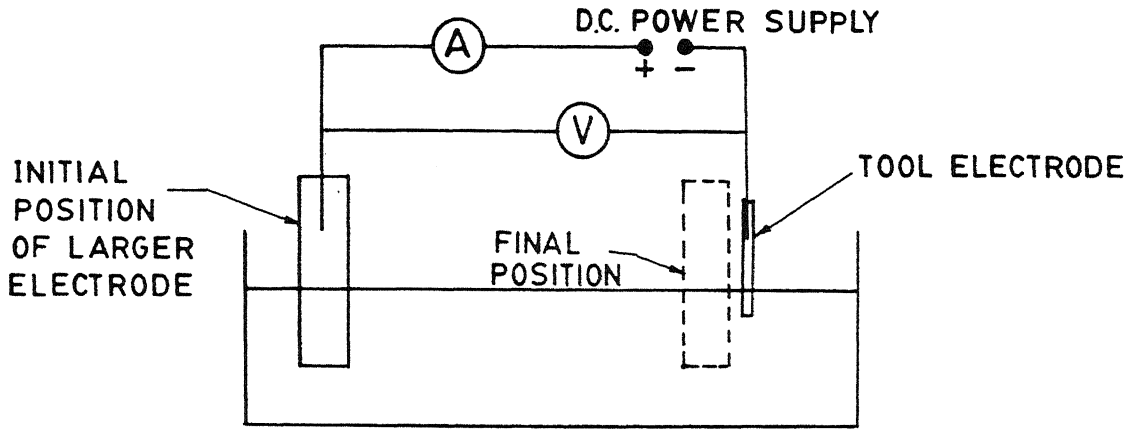

Depth of larger electrode in electrolyte = 1·0 cm
Depth of tool electrode in electrolyte = 0·2 cm

(a)

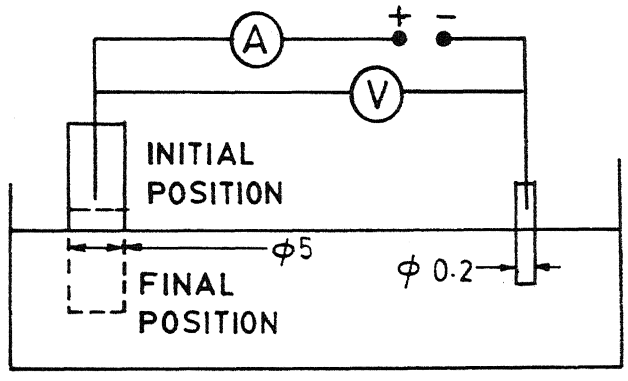

(b)

Fig. 2·10 Scheme to investigate the effects of
(a) Inter electrode gap
(b) Size of larger electrode

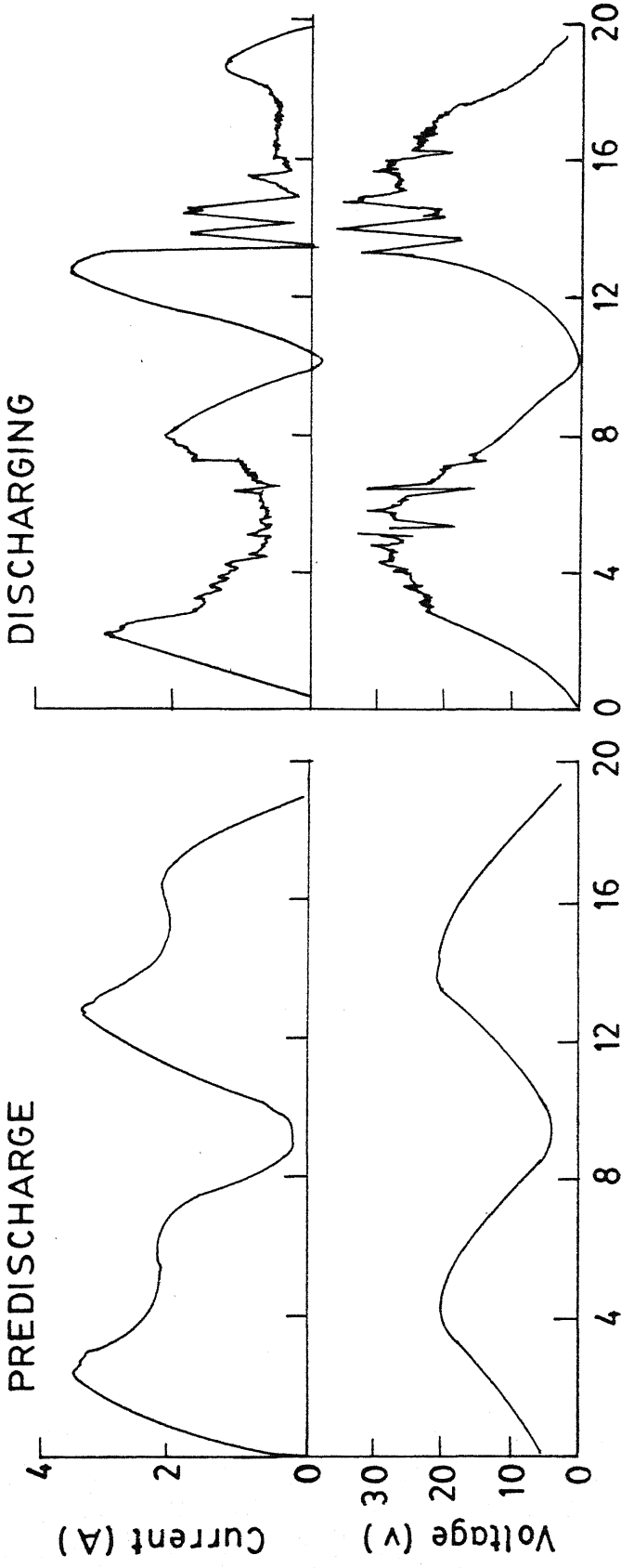

100 Hz, Full wave rectified DC

Fig. 2.11 (a) Waveshapes of voltage and current

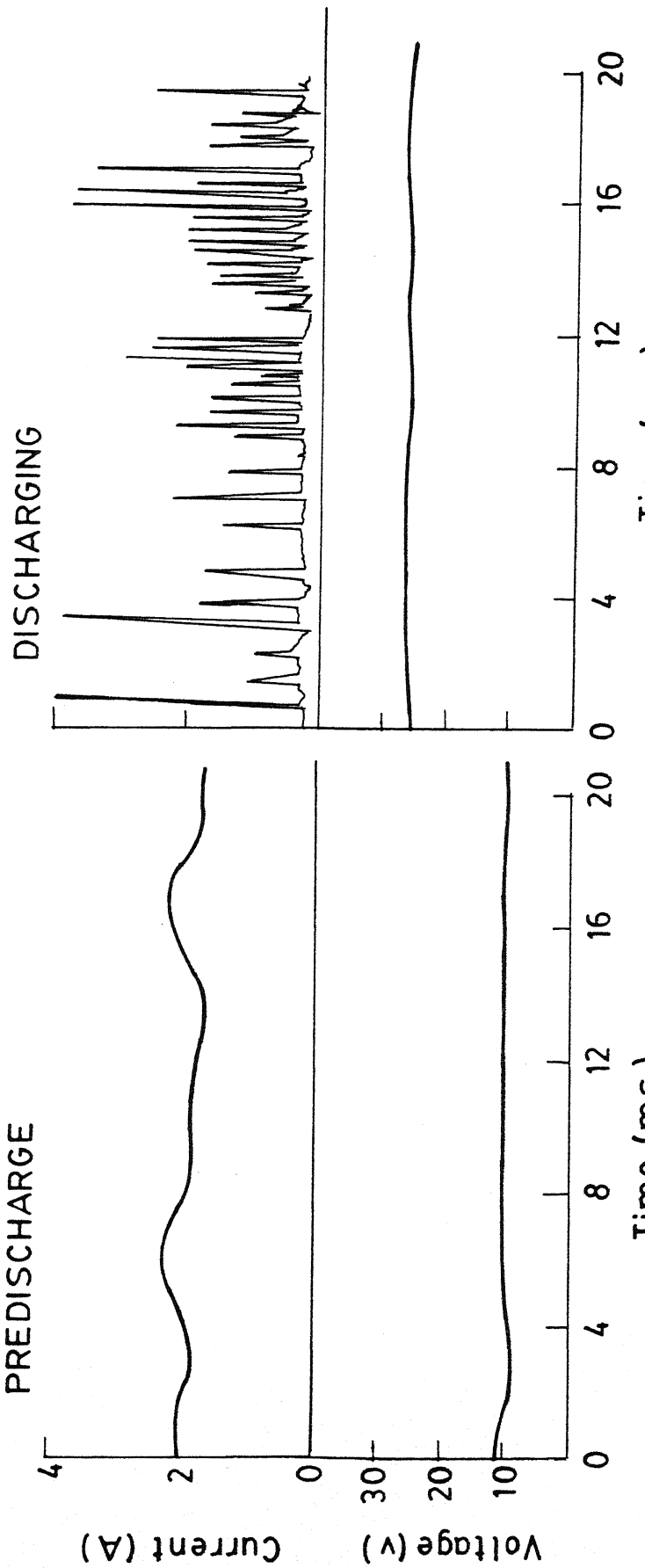

Smooth DC with C = 1500 μF

Fig. 2.11 (b) Waveshapes of voltage and current

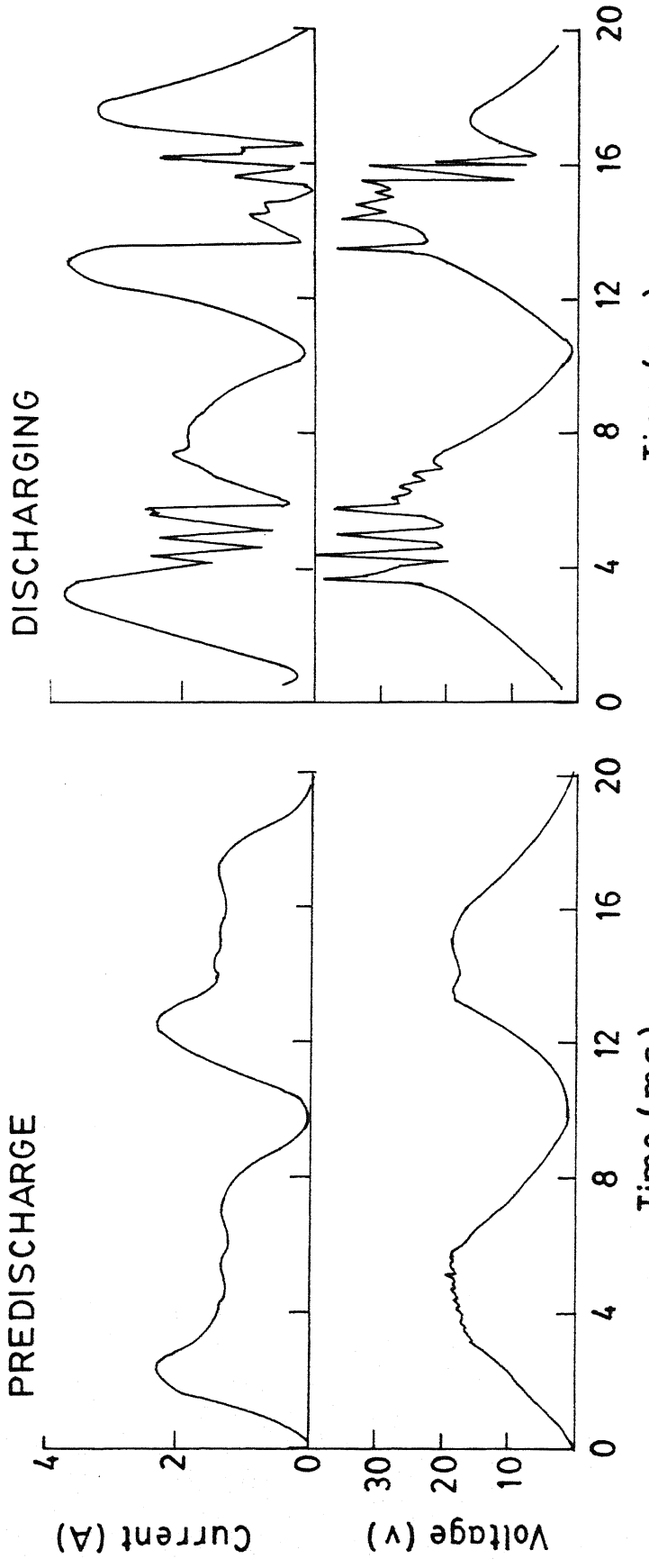

100 Hz Full wave rectified DC with L = 100 mH

Fig. 2.11 (c) Waveshapes of voltage and current

current spikes vanishes, but the applied voltage waveshape distorts due to the high switching e.m.f. in the discharging condition.

It was found difficult to evaluate the discharge frequency from the above traces and it was decided to analyse the spectrum of the discharge signal using a signal analyser.

2.3.3 Spectrum analysis of the discharge signal

The setup shown in Fig.2.1a was modified by replacing the oscilloscope by a signal analyser [Model:2100B, Iwatsu Electric Company, Japan] for spectrum analysis of the discharge signal. Different data lengths [1] ranging from 0.5K to 4K were selected for the analysis. However, the Forward Fourier Transformation [FFT] of the signal indicated no particular frequency. The FFT trace is shown in Figure.2.12. It indicates that a wide range of frequency, from very low to 50 KHz (the range of the frequency scale used), is present in the discharge signal.

2.3.4 The tool temperature

To investigate the tool temperature at different regions of the ECD process the following technique was adopted. The tool diameters were so small that it was difficult (practically impossible) to embed the thermocouple bead on its surface. The

---

[1] Data length of 1K means, signal has been sampled in 1000 points.

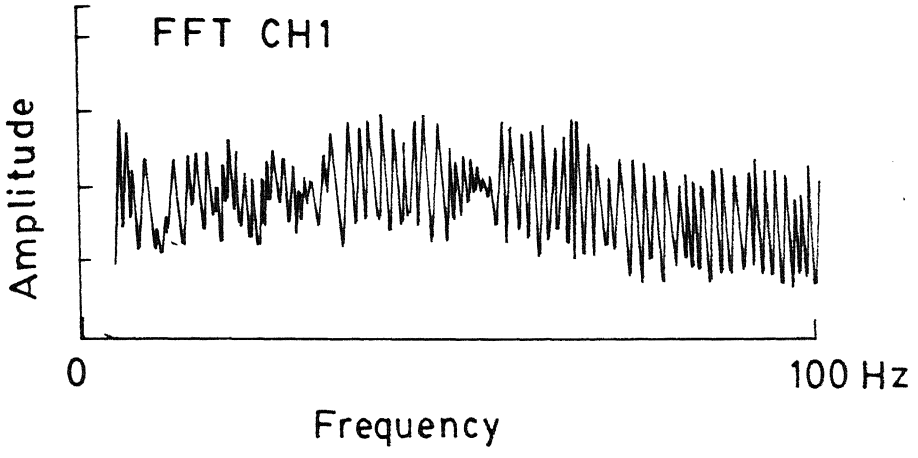

Range = 100 KHz
Cut off = 2 K
Linear scale

Fig. 2·12 FFT trace for discharge signal analysis.

attempt of using the thermocouple bead itself as a tool was proved to be successful (Fig.2.13a). It is to be noted that the thermocouple beads were prepared by the method developed by Allesu [1]. The induced e.m.f. in the thermocouple for different values of the applied voltage, ranging from zero upto the value where the bead failed due to intense arcing, was measured by a millivoltmeter. These millivolt readings were converted to the corresponding temperatures using the standard conversion table. Chromel-alumel thermocouples were used in this experiment. Figure 2.13b shows the variation of the temperature of the tool (thermocouple bead) with the applied voltage.

2.4 General Characteristics of Electrochemical Discharge Machining

As a general overview of ECDM is available from the published works, only a few characteristics were studied by the author mainly to maintain the consistency of the results.

2.4.1 Material removal rate (MRR) characteristics

A stable discharge establishes between the electrode and electrolyte at the tool edge when the applied voltage to the cell is above the critical value for that tool-electrolyte combination. Material can be machined if it is placed in the vicinity of the electrochemical discharge. Due to the gravity feed mechanism the discharging tool gradually penetrates into the workpiece showing the following characteristics.

(i) The MRR increases with the applied voltage, other input

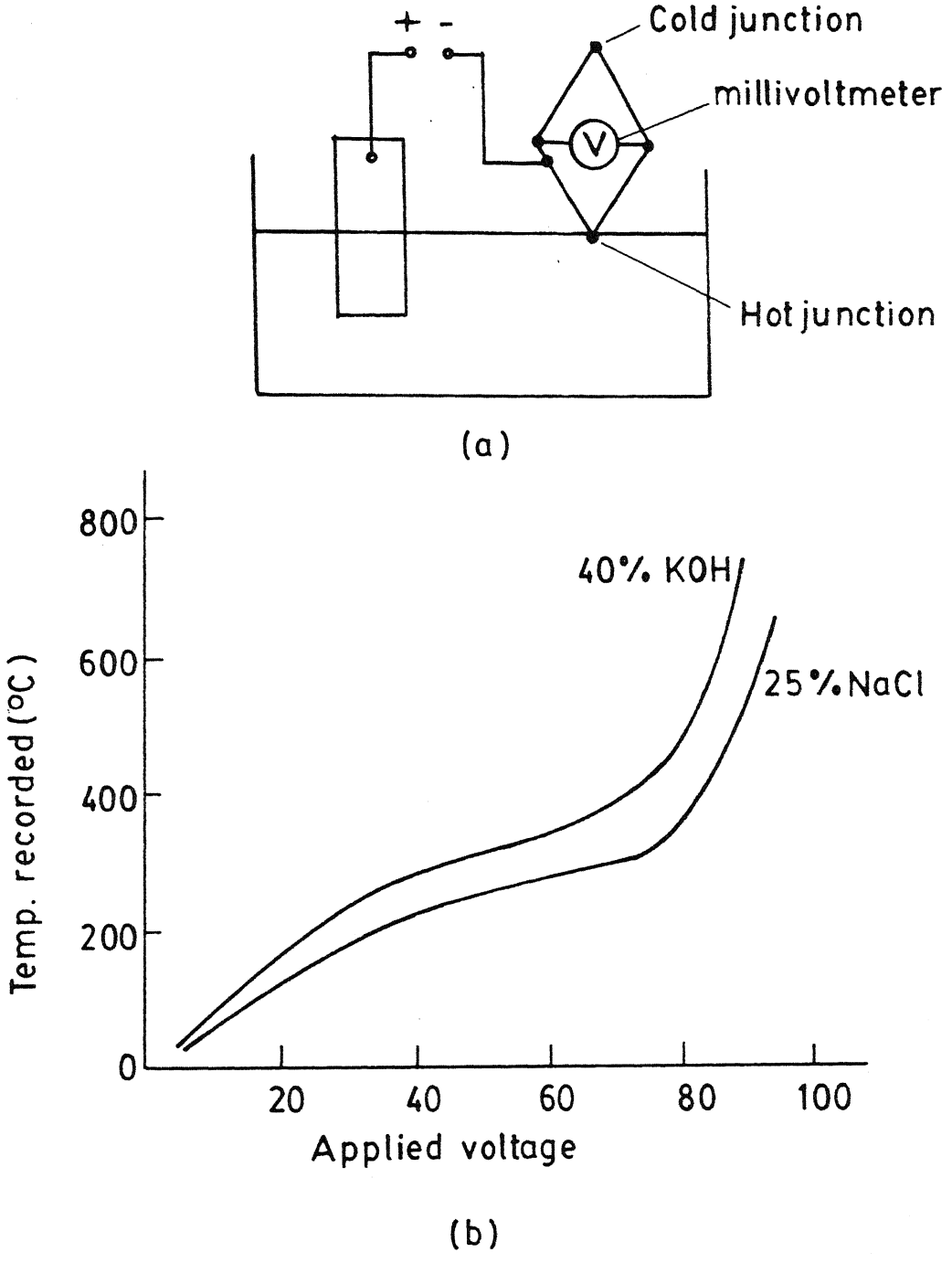

Fig. 2·13 (a) Setup to find electrode temperature
(b) Result obtained

parameter remaining same (Fig.2.14).

(ii)During vertical drilling of a blind hole MRR gradually decreases with time and after attaining a certain depth no more machining takes place (Fig.2.15).

This characteristic was also noticed and discussed by Allesu [1], who explained this as a result of loss of the potential at the electrode edge due to the accumulation of bubbles at the machining zone when scavenging was absent. Allesu also demonstrated it by a special set of experiments as discussed in Sec.1.2. For further proof of the explanation the author conducted an experiment with a different configuration. Machining of a glass wafer was done along its width by a tool whose diameter was larger than the wafer thickness (Fig.2.16a). This arrangement ensured no accumulation of vapour bubbles at the machining zone and continuous removal of the machined particles. A constant machining rate was obtained with this configuration (Fig.2.16b), in accordance with the explanation given by Allesu.

The effect of the electrolyte temperature on the MRR characteristic, was not investigated as it was decided beforehand not to include the electrolyte temperature as a process parameter.

2.4.2 Surface condition after ECDM

With the arrangement as shown in Fig.2.16a, machining of a glass wafer was done upto a depth of 0.25 cm. The machined wafer was cleaned and examined microscopically. An exaggerated view of the surface texture is represented in Fig.2.17. The machined surfaces was found parallel to each other indicating 'the

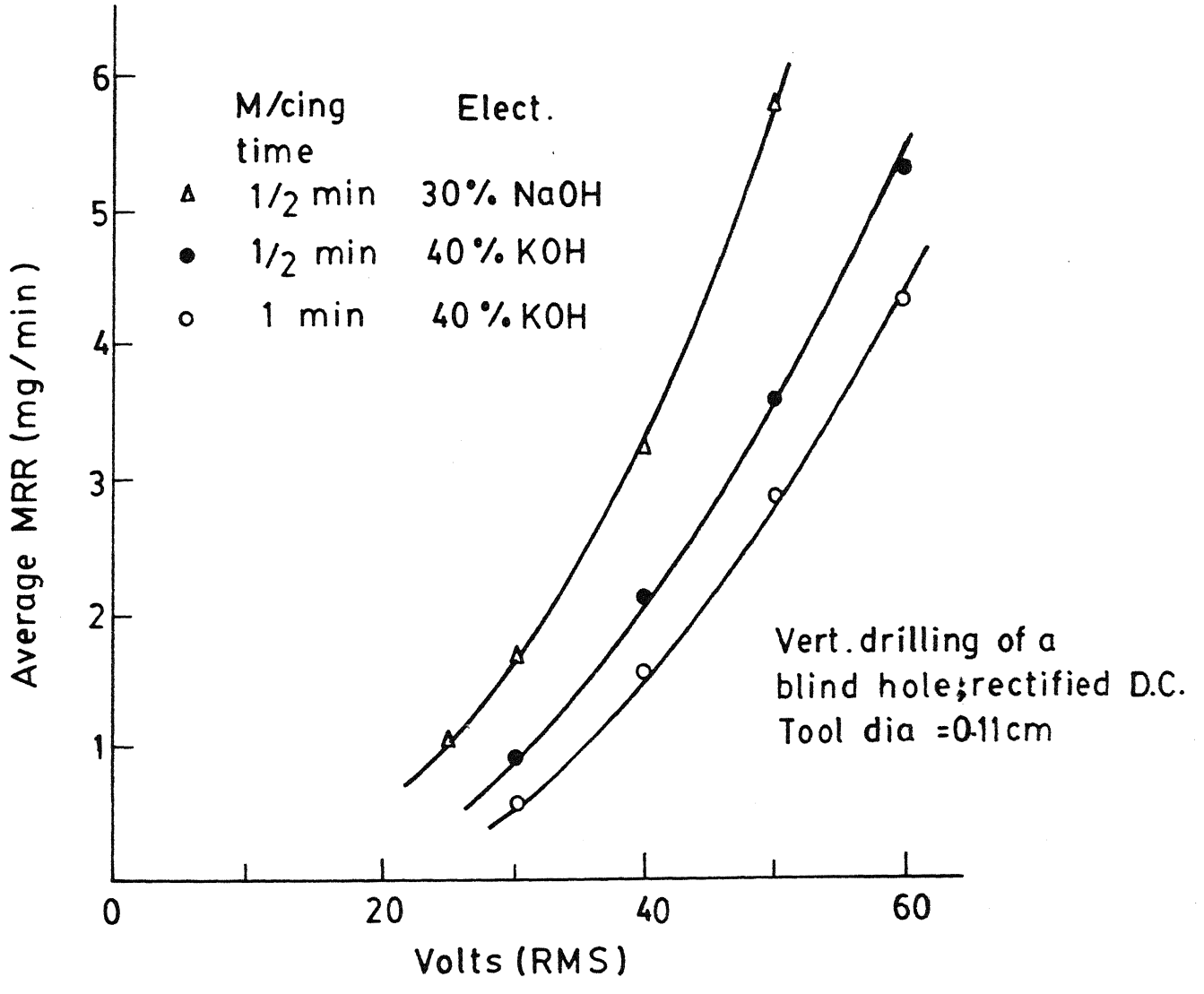

Fig. 2.14 MRR for different applied voltage workpiece : glass

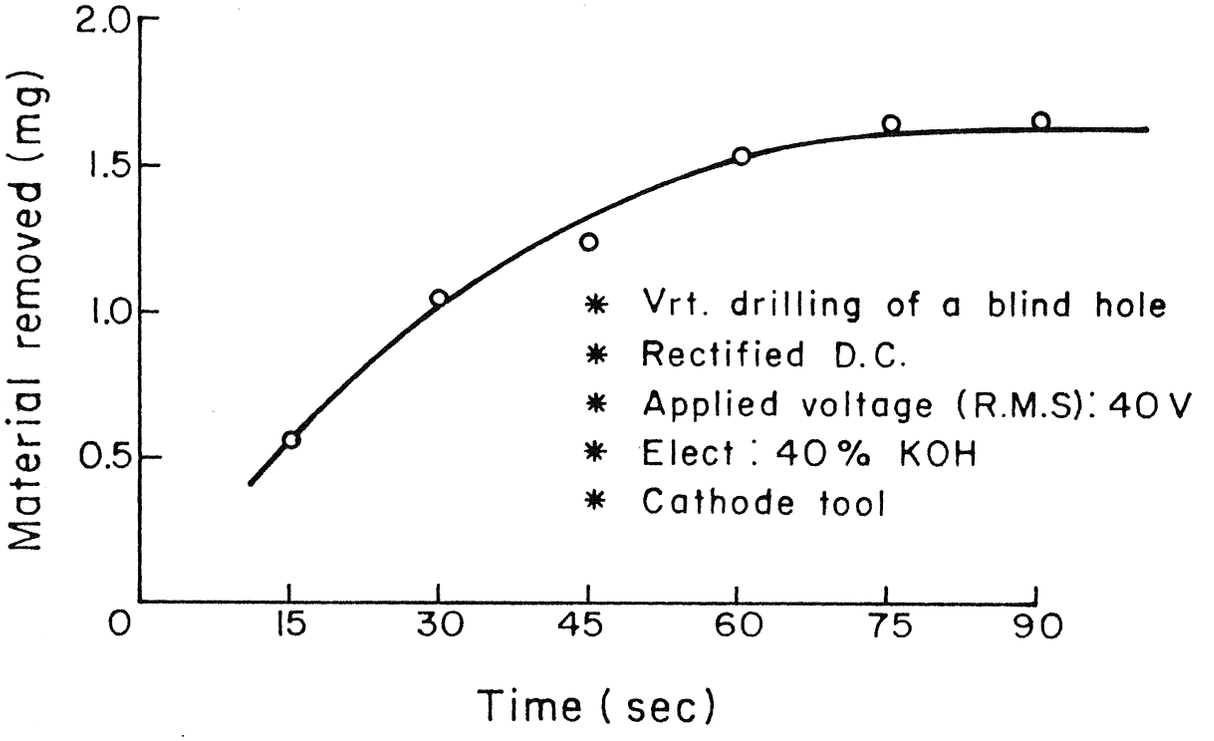

Fig 2.15 Variation of MRR with machining time approaching limiting depth. workpiece: glass.

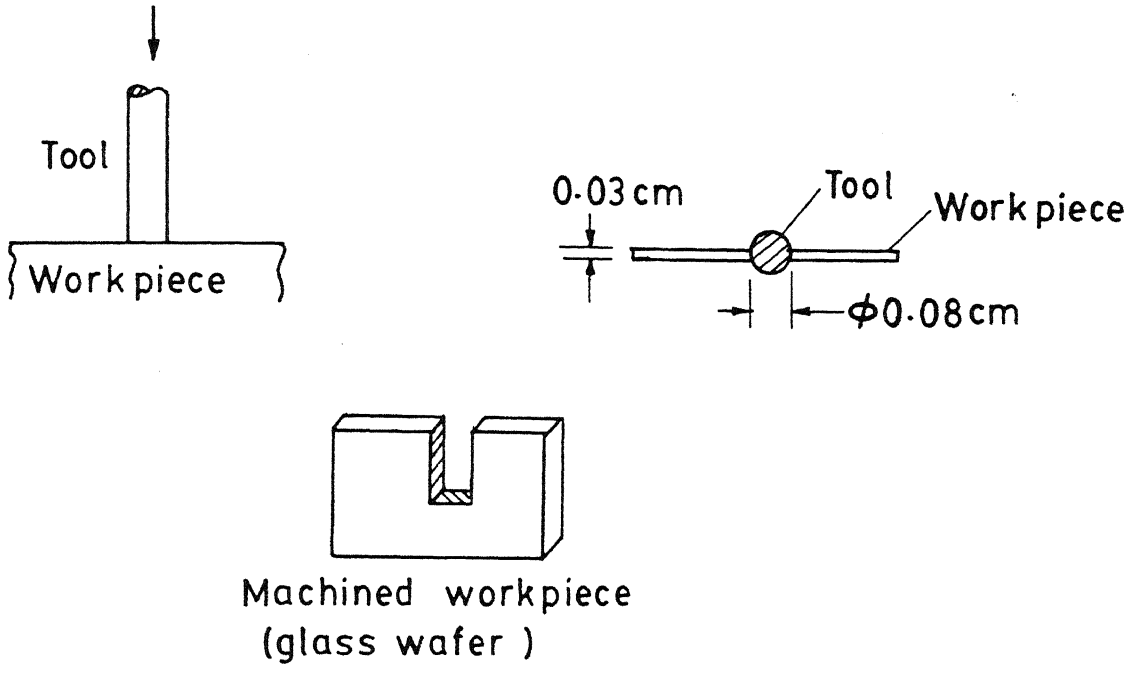

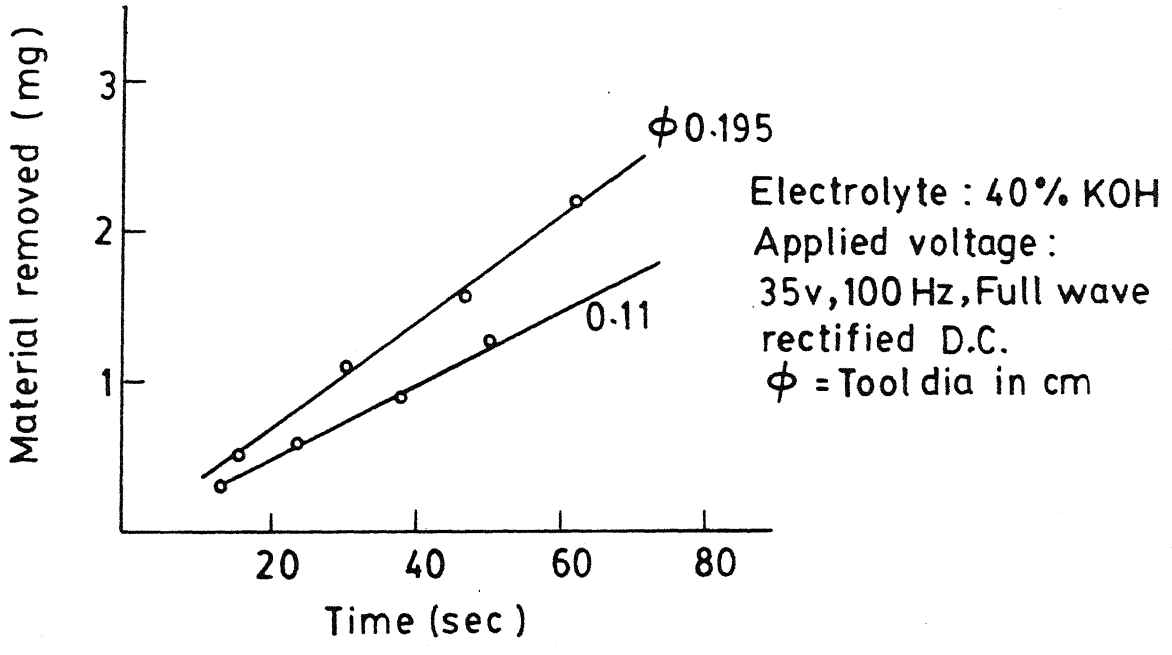

Fig. 2·16 (a) Configuration of transverse machining.
(b) Material removed vs. time obtained in above configuration.

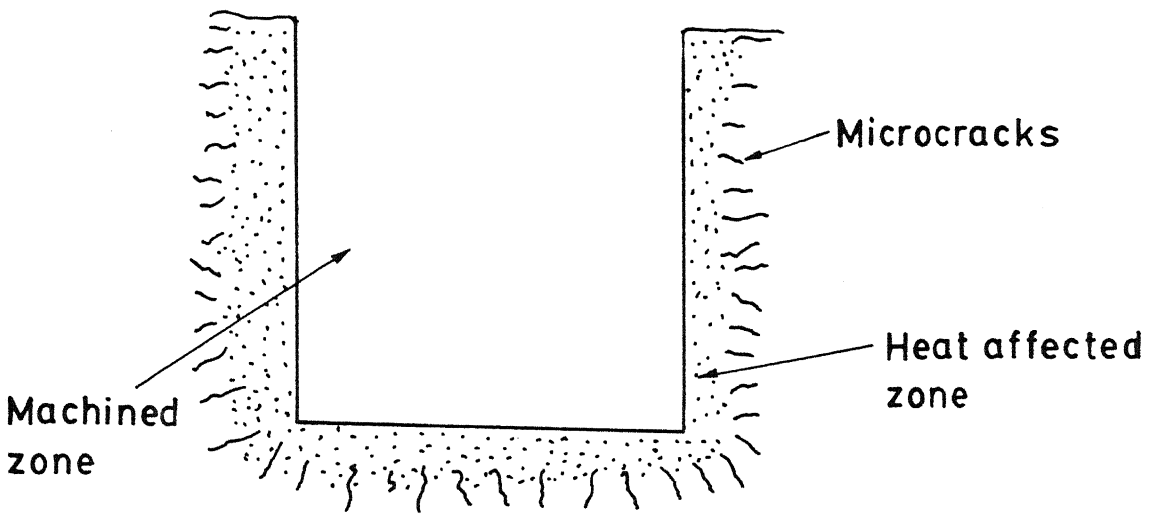

Fig. 2.17 Surface texture after ECDM

absence of any stray cut. The corner reproduction was good. The examination revealed that the subsurface contains a resolidfied surface and microcracks underneath the resolidified layer. These facts indicate that the machining process in ECDM is a primarily thermal one. The cracks were resulted from the sudden quenching of the workpiece by the surrounding electrolyte.

2.4.3 Range of ECDM

The range of ECDM is limited by the phenomenon of tool softening at a high applied voltage (90V) and by the tool size. Though with the application of higher potential the MRR increases, the temperature of the tool also rises simultaneously, as shown in Fig.2.13b. At a certain applied voltage, the stable discharge between the tool and the electrolyte converts to an arc and the tool temperature rises substantially. This causes tool softening as well as thermal cracking of the workpiece. Characteristically, the discharge is confined at the tool edge. For small diameter tool the effect of the discharge is such that the whole material under the tool melts and machining can be done. If the tool diameter is increased too much, material under the tool end can not melt fully by the discharge which takes place at the edge region only. As a result the indentation of the tool in the workpiece in such cases is not possible for the residual central portion of the workpiece. Practically, the ECDM can be performed for voltage ranging from a few volts above the critical voltage to 90V. The alkaline medium was found suitable for ECDM.

2.5 Identification of the system and its Basic Parameters

Development of a theoretical model needs the proper identification of the system and the selection of the basic parameters. The system of ECDM can be expressed in the form of a number of sequenced events. The application of an above-critical voltage to an electrochemical cell results enough bubble density on the tool electrode to blanket it which leads to discharge at the tool edge. A part of the energy released by the sparks is conducted to the workpiece (placed in the vicinity of the discharge) and melts it locally. The molten part is removed by shock and the material removal takes place.

It is clear from the V-I characteristics of the ECD phenomenon that the electrolyte and its concentration are the main parameters for the determination of the critical voltage. In addition to these, the contact area between the tool and the electrolyte is another factor to determine the critical current. The applied voltage, line inductance and the electrolyte temperature alongwith the electrolyte and its concentration determine MRR in ECDM. However, the electrolyte temperature is not included as an input parameter in the present model.

CHAPTER 3

ONSET OF ELECTROCHEMICAL DISCHARGE: A THEORETICAL MODEL AND EXPERIMENTAL VERIFICATION

3.1 Introduction

Electrical discharge in electrolyte was observed by many researchers in different circumstances. In all instances it was treated as a factor detrimental to the concerned processes. Thus, the primary motive behind all investigations concerning ECD had been to eliminate such discharge. As a result the mechanism of such discharge and the critical conditions leading to the onset of the phenomenon remain unexplored. The different characteristics of ECD were discussed in chapter 1. The characteristics provided the idea of the existence of a critical condition leading to the onset of electrochemical discharge. From the previous studies, the bubble nucleation on the tool electrode surface emerges as the main cause of discharge onset. The electrochemical reaction at the electrode and boiling of electrolyte at the interface region produce the bubbles. Therefore, some observations made by the researchers regarding the bubble formation and its dynamics in the concerned field of electrochemistry and boiling phenomenon were consulted and were found useful to develope the present model.

3.2 Basic Scheme of Discharge Onset

The schematic diagram of an ECD set up is shown in Fig.3.1a. Any electrical circuit inherently consists of elements such as resistance, capacitance and inductance. The contact area between the electrode and the electrolyte constricts due to the bubble nucleation on the electrode surface. This constriction produces the effect of an extra electrical resistance. The current path to the electrode with and without bubbles on it are shown in Fig.3.1b. The interionic repulsive force restricts the ion movement in the electrolyte and produces electrical resistances. The connecting leads, joints etc are also the source of electrical resistance. The electrodes attract the oppositely charged ions due to the electrostatic force. At any instance of the process, some unneuralised ion remain stagnant near the electrodes. These oppositely charged elements separated by a small distance at the electrode-electrolyte interface is equivalent to the situation in a charged capacitor (Fig.3.1c). The constriction of the current due to the bubble formation causes nonuniformity in the current path and results in an inductive effect [21] apart from the resistive one , as mentioned earlier. Even joining of two wires by twisting can introduce some inductive effect. Thus, the circuit of an ECD setup can be represented as

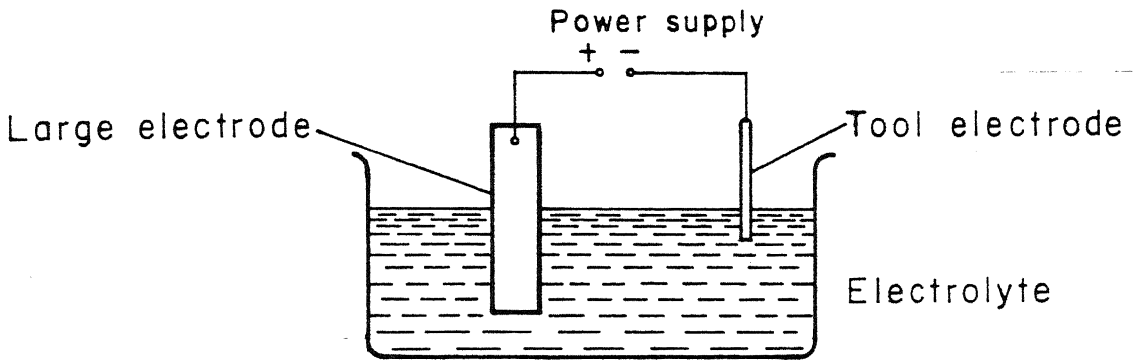

Fig.3.1(a) Schematic diagram of ECD set up

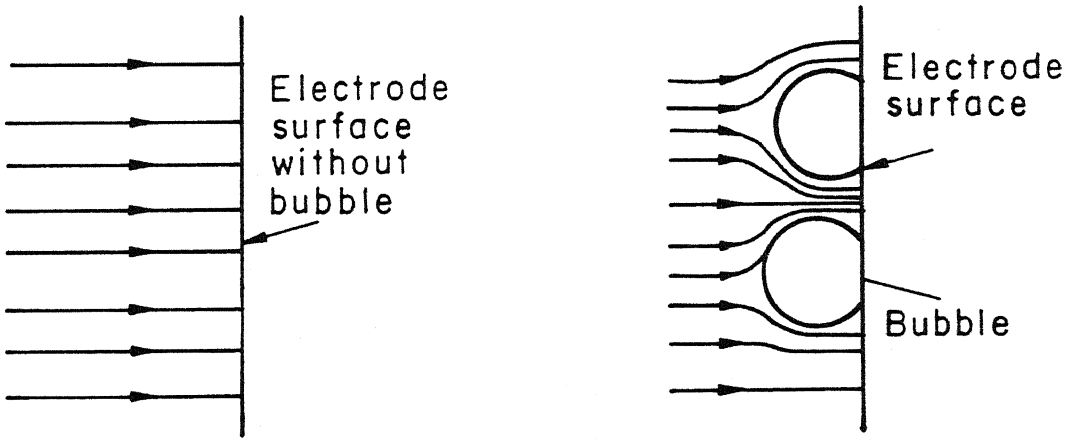

Fig.3.1(b) Current distribution on the electrode surface without and with bubbles

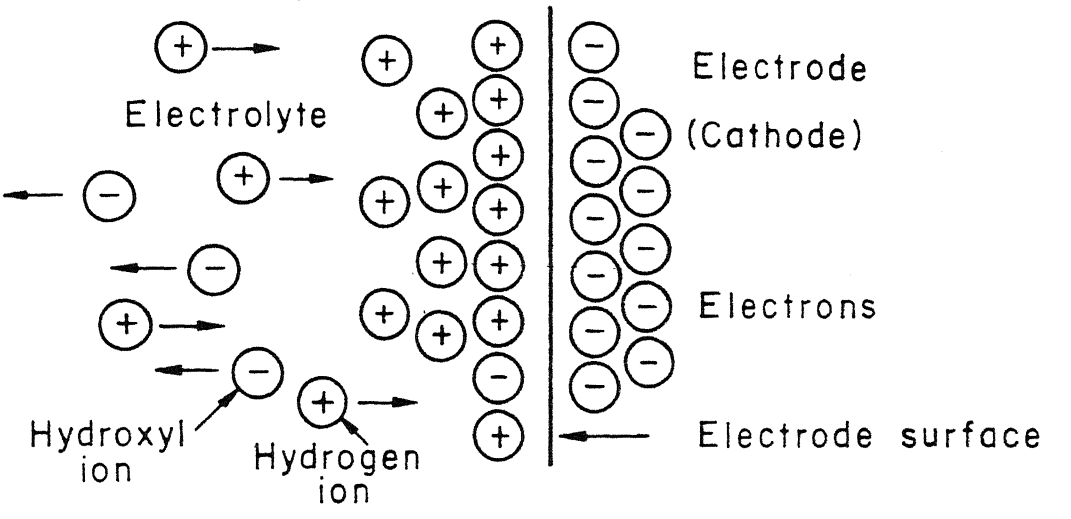

Fig.3.1(c) Accumulation of opposite charges at the interface.

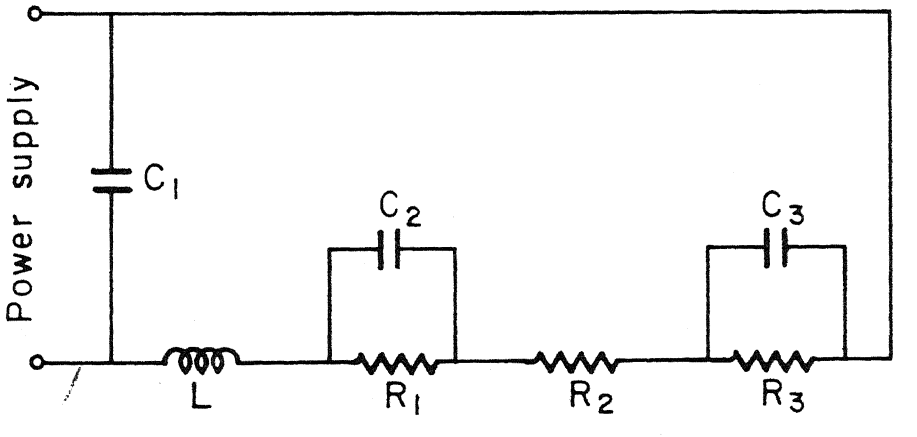

Fig.3.1(d) Equivalent electrical circuit of the E.C.D set up.

shown in Fig.3.1d. Referring to this figure C_1 and L are the capacitance and inductance which are inherent permanent features of the circuit. C_2 and C_3 are the capacitance values of the interfaces which arise due to the accumulation of the opposite charges at those regions. R_1 and R_3 are the resistances at the interfaces due to the constriction effect of the bubbles and R_2 is the resistance of the bulk electrolyte.

The effect of the current concentration takes place if there is any sharp edge present in the current path. This disturbs the current distribution of the systems, and a potential field is developed at the region. Due to this characteristic current concentration appears at the tool edge (Fig.3.2). As a result the discharge is mostly confined to this region. The bubbles move upward to the electrolyte surface due to the buoyant force exerted by the electrolyte. But, the bubbles at the bottom surface of the electrode cannot move such freely as its upward movement is restricted by the electrode surface itself (Fig.3.3). So, it can be assumed that the bottom faces of the electrodes are permanently insulated from the electrolyte by these stagnant bubbles.

3.2.1 Switching phenomenon

Electrical discharge can take place either due to the dielectric breakdown of the medium or due to switching action. When the applied potential between two electrodes separated by a

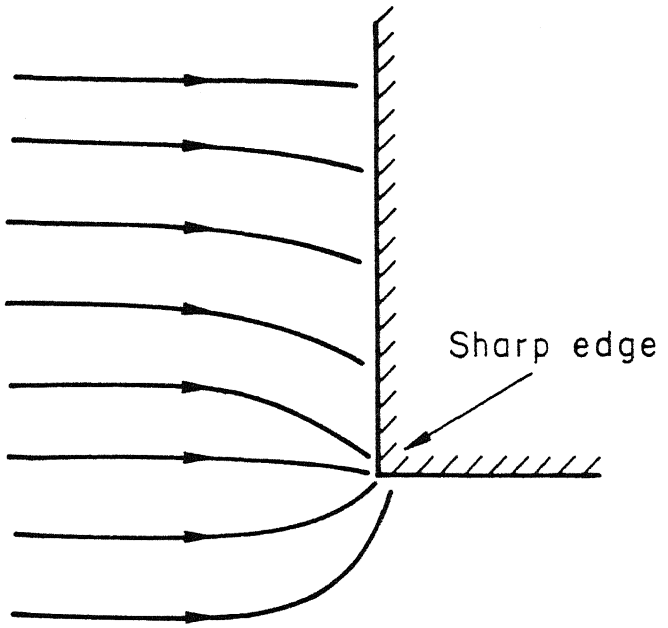

Fig.3.2 Distribution of current near a sharp edge.

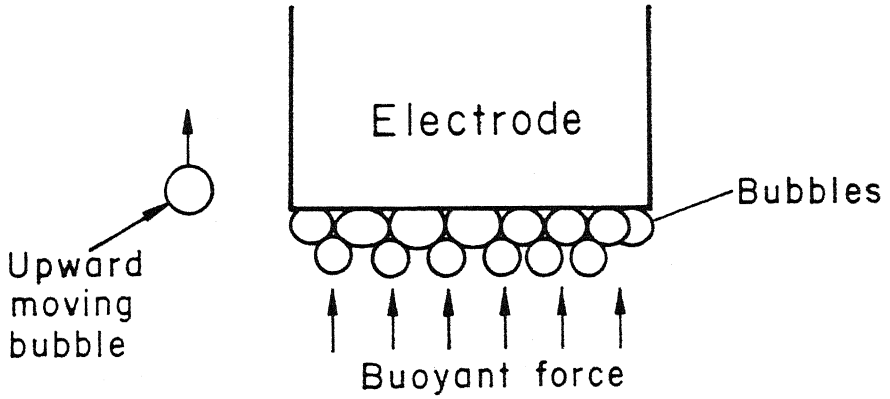

Fig.3.3 Bubble blockage at the bottom edge of the electrode.

dielectric medium is high enough, the breakdown of the medium takes place. Spark appears between the electrodes through the highly ionised channel developed due to dielectric breakdown. In a similar manner discharge between electrodes can also take place, when the medium is gaseous one. The required potential difference between the electrodes to cause such discharge through the air is given by the Paschen's curve [22] (Fig.3.4). The horizontal axis of the figure represents the product of the pressure of the gas and the distance between the electrodes. The value of the required potential difference is given by the vertical axis. For other gases the value of the potential required is in the same order.

The other type of discharge takes place at the interruptor switches of electrical circuit. If the inductance of the circuit is L, then at the instant of opening the circuit the induced e.m.f. V_s, is given by

$$V_s = - L \frac{dI}{dt}$$

where I is the current at the instant of circuit opening and t is the time to break the circuit. This e.m.f. is termed as back or switching e.m.f. The energy stored in the inductance is released through this spark. There are different explanations of this phenomenon. The discussion on those are out of the scope in the present context. However, it should be mentioned that this phenomenon occurs in the telecommunication switches where the operating voltage is less than 50V. This type of discharge can

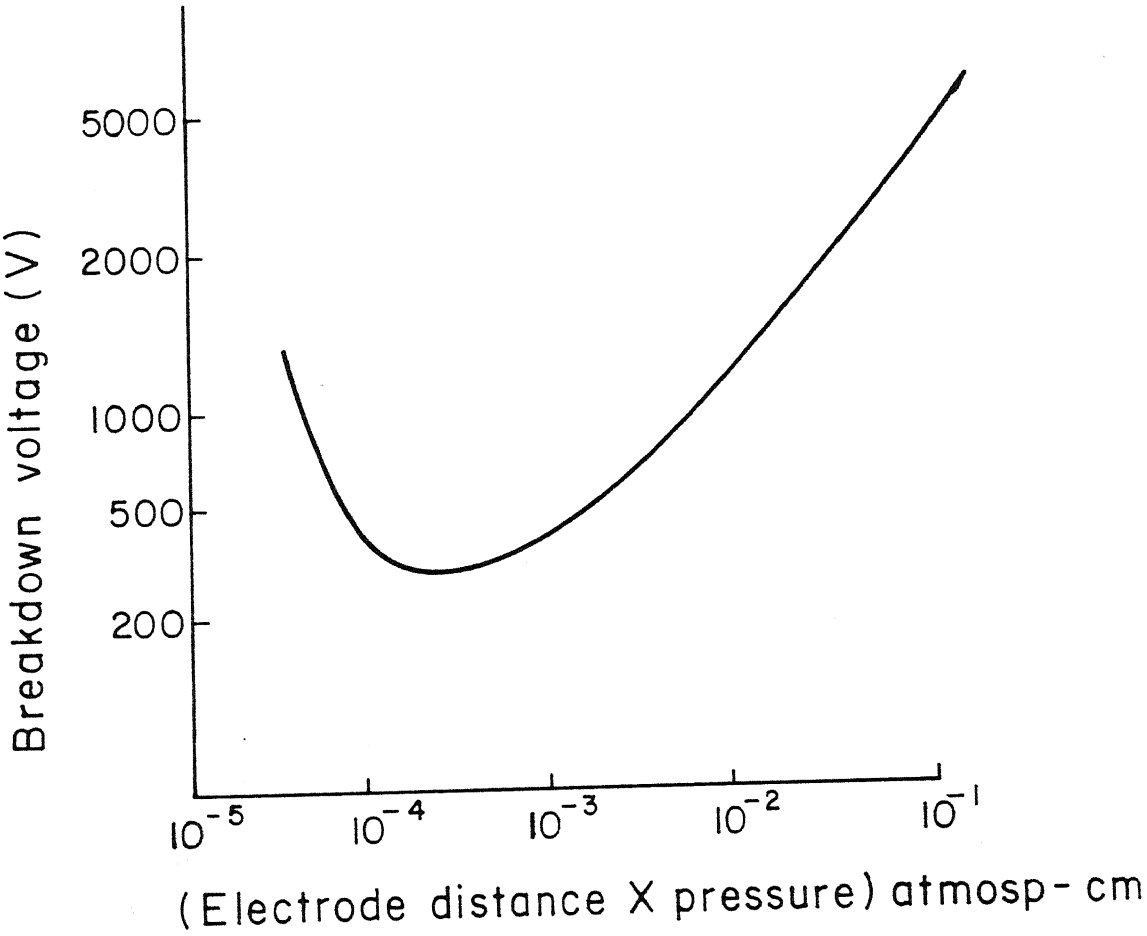

Fig 3.4 Paschen's curve for breakdown voltage,(for air filled gap at 20 °C for plane parallel electrode)

also be noticed in a circuit whose operating voltage is much less (<10V), but carries enough current. For example, short circuiting a car battery can produce a disturbing discharge. A discharging switch is shown schematically in Fig.3.5.

From Paschen's curve it can be seen that the minimum required potential difference to initiate a discharge through an air gap is in the order of 280V. Whereas in ECD cell the discharge occurs at an applied voltage in the range of 15V-50V. Hence, it is logical to conclude that the discharge in the electrochemical cell is due to the switching phenomenon and not the electrical breakdown of the gas bubbles.

3.2.2 Blanketing and the discharge

Hydrogen gas is liberated in the form of bubbles at the cathode, due to electrochemical reaction. The bubbles gradually grow in size and after attaining a critical size, they detach from the electrode surface. During the growth their shapes remain hemispherical for the reason described later. The base diameter of the bubbles prior to departure is D_d. Nucleation site density of H_2 bubble increases with the applied voltage (i.e. with the current density also) to the cell. When the nucleation site density of H_2 becomes sufficiently high, substantial constriction of the current path takes place at the interface. Figure 3.6 shows the nucleation site density on the electrode surface at

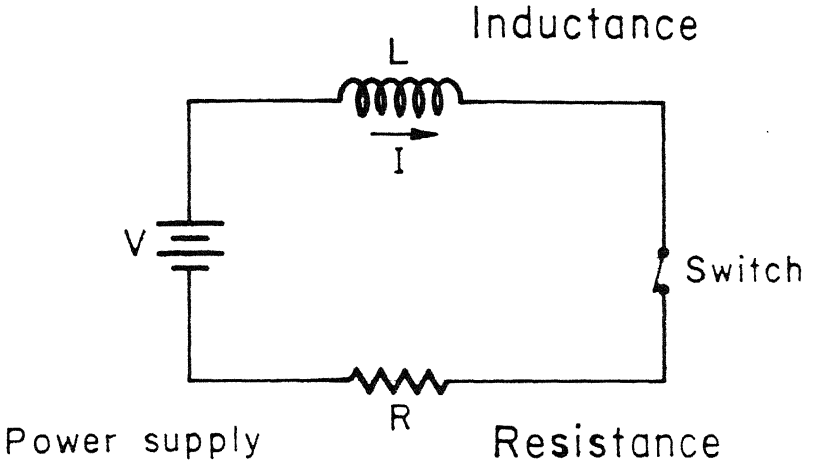

$$\text{Current, } I = \frac{V}{R}$$

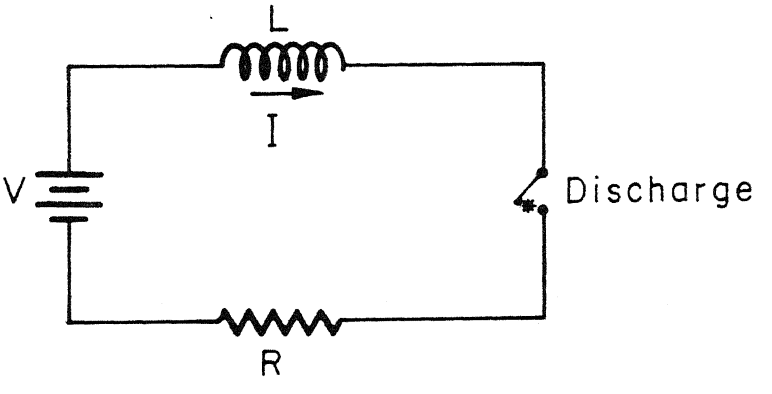

$$\text{Energy released in the discharge} = \frac{1}{2} LI^2$$

Fig. 3.5 Discharging (arcing) switch

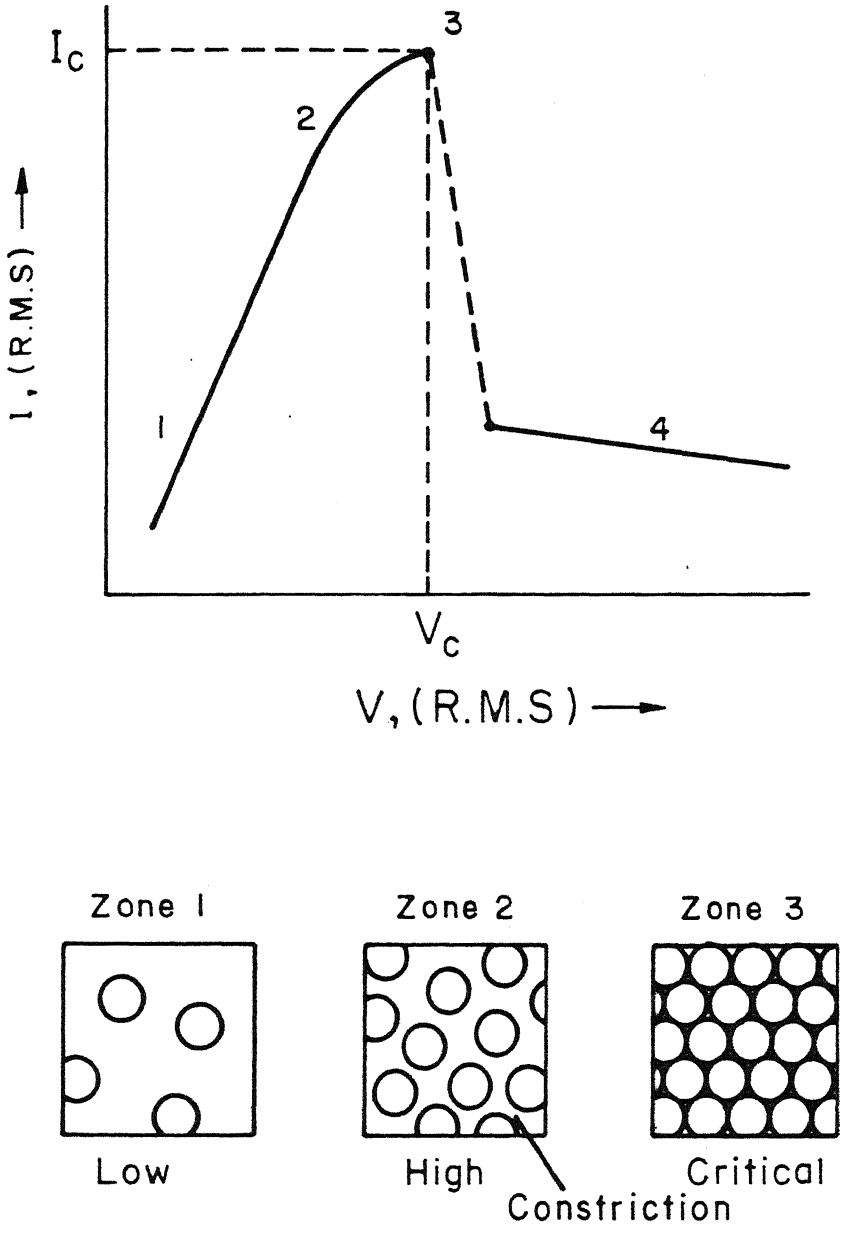

Fig. 3.6 Bubble density on tool electrode at different applied voltage.

different value of the applied voltage and the location of the constrictions. This causes an increased resistance at that region and the ohmic heating of the electrolyte becomes significant. This causes the onset of vapour bubble nucleation on the electrode surface in addition to the H_2 bubbles. Beyond this stage the number of the combined nucleation sites increases very rapidly with the applied voltage. It was observed by Janssen and Hoogland [23] that with the increase of current density through an electrochemical cell, more and more nucleation sites for H_2 generation become active. While investigating the boiling phenomenon, Staniszewski [24] noticed that the number of nucleation sites of the vapour bubbles is proportional to the heat flux at low heat flux condition, but it becomes proportional to the square of the heat flux when the heat flux is high. As the nucleation site density reaches a critical value, vapour blanketing of the electrode occurs. This was also noticed by Griffith et. al. [25] and Zuber [26]. The author suggests that at the critical value of the nucleation site density, maximum possible coverage of the electrode surface takes place with the full grown hemispherical bubbles of base diameter, D_d. At this stage the points of contact between the electrolyte and the tool electrode, known as bubble bridge, blows off instantly due to intense heating (Fig.3.7a). Consequently the current through the circuit drops to zero within a very short time span, which is analogous to the switching off in an electrical circuit

(Fig.3.7b). Discharge takes place along the locations of the bubble bridge, reducing the circuit to that shown in Fig.3.7c. The bubbles dislodge from the electrode surface due to bridge blowing and the contact between the electrode and the electrolyte is reestablished. This cycle repeats continuously.

3.2.3 Simplifying assumptions and idealisation

The phenomenon of ECD is a very complex one. To make the problem tractable some idealization of the real system and simplifying assumptions are unavoidable. In the idealised circuit, shown in Fig.3.1d, C_2 and C_3 can be neglected as there values are very small. As discussed earlier, current concentration at the tool end takes place, because of the sharp edge. To tackle the situation, the current at the edge is assumed to be distributed uniformly, as in the other part of the electrode, on an imaginary extended length (l_i) of the tool (Fig.3.8). Thus, the total equivalent length of the electrode dipped in the electrolyte is the sum of the actual physical length and the imaginary length (l_i). This assumption does not affect the V-I characteristics in any major way. Only the scale of the depth axis of the V-I characteristic for tool depth changes. This is likely to affect only the constants of proportionalities of the model, which are in any way to be determined by the pilot experiments. The nature of interdependence of various process

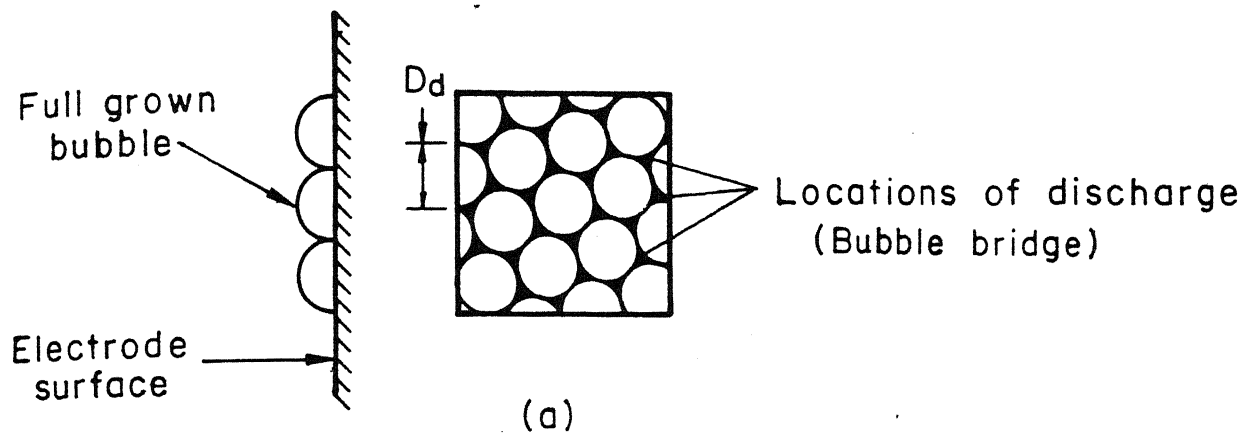

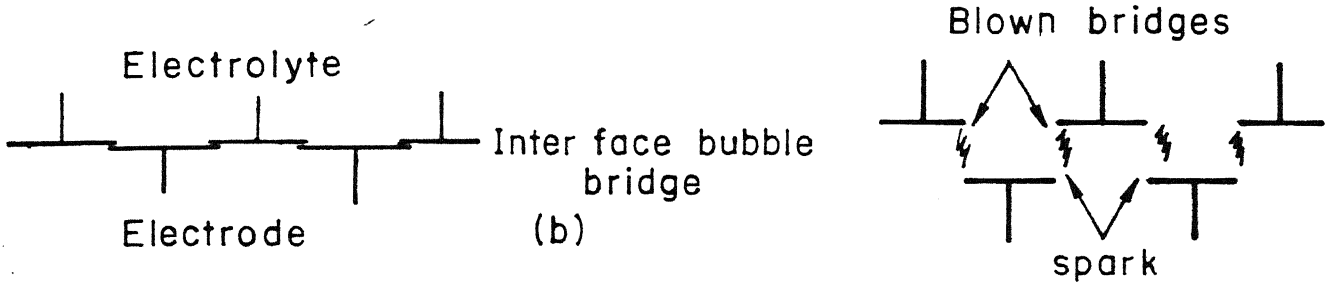

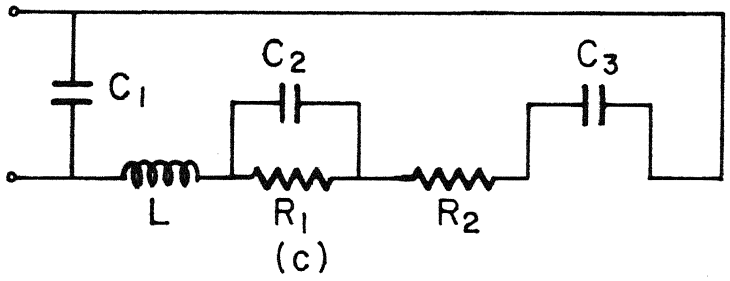

Fig 3.7 (a) Discharge locations with bubble distribution at critical condition
(b) Idealised switching off situation, and
(c) Idealised equivalent circuit at discharge

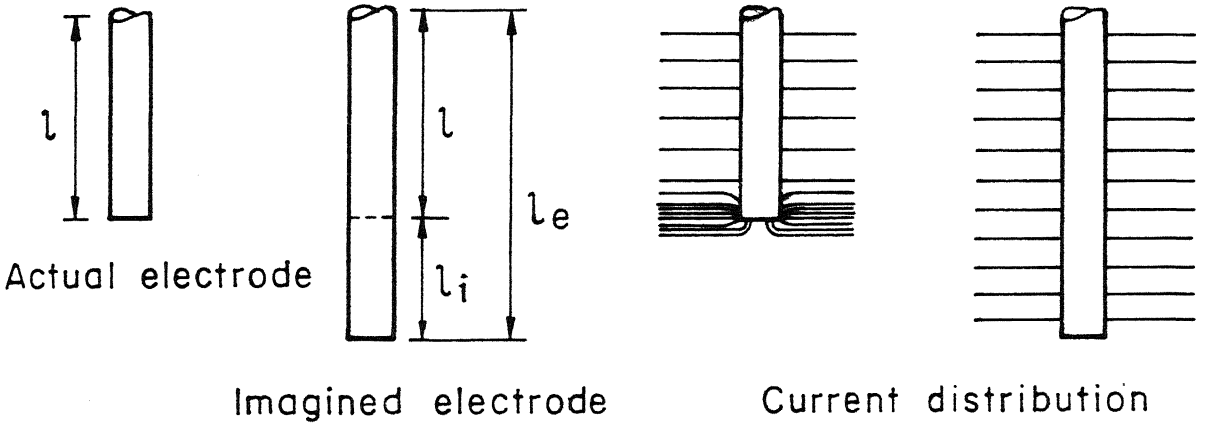

Fig 3.8 Actual and idealised electrode with corresponding current distribution.

parameters also are not expected to be affected by this simplification. To simplify the analysis without sacrificing any basic characteristic feature of the process, the following assumptions are made:

(i) A set of identical bubbles nucleate, grow to the critical size (with base diameter D_d) and then detach simultaneously over the whole equivalent surface of the tool.

(ii) The nucleation sites of both the H_2 and vapour bubbles are uniformly distributed over the whole equivalent surface of the electrode.

(iii) H_2 bubbles and vapour bubbles behave in identical fashion.

(iv) Current distribution is uniform over the whole equivalent surface of the tool, as discussed earlier.

(v) Characteristic of the electrolytes do not change with time.

(vi) The growth of all bubbles are rapid.

3.2.4 Some relevent observations in the field of the electrochemistry and boiling phenomenon

Apart from the simplifications made in the previous section, a few observations by the researchers in the field of electrochemistry and boiling phenomenon are also utilised for understanding the mechanism and developing the theoretical model.

These are as follows:

(i) The fast growing bubbles are hemispherical in shape and the diameter prior to detachment from the surface is independent of current density and is governed mainly by the buoyant force and the viscous properties of the electrolyte, as noticed by Venczel [27].

(ii) Ivey [28] showed that the relationship between the diameter prior to departure of the vapour bubble and the frequency of bubble generation at a particular site depends on the regime of the bubble growth. For very small bubbles, whose growth is dynamically controlled, $D_d.f^2$ = constant, where D_d is the departure diameter and f is the frequency of bubble generation at a particular site. On the otherhand for thermally controlled large bubbles, $D_d.f^{1/2}$= constant. In the intermediate regime the exponent on f is between 2 and 1/2.

(iii) It has been observed that the vapour bubble growth rate at the initial stage is in the form of $D(t) \propto t^{3/2}$, which changes to asymptotic growth, given by $D(t) \propto t^{1/2}$, at the later stage [29]. Electrolytic gas evolution at atmospheric pressure is completely controlled by mass diffusion and is of the form $D(t) \propto t^{1/2}$ [30].

3.3 Model of Blanketing and Onset of ECD

The following model is being developed according to the scheme discussed in section 3.2. As a general representation the values of the parameters at the critical condition (Sec.2.3.1) are denoted by the subscript c.

The bubbles on the electrode surface is hemispherical in shape due to their fast growing nature. Let, $\bar{N}$ be the nucleation site density and D_d be the base diameter of the bubbles at departure. $\bar{N}$ increases with the applied voltage and reaches a value $\bar{N}_c$ at the critical condition. The maximum possible coverage of the electrode surface takes place with the nucleation site density $\bar{N}_c$ and the bubble base diameter D_d, leading to the vapour blanketing and discharge. Under these conditions the combined H_2 gas and the water vapour (henceforth termed as the combined gas) bubble generation rate is

$$\left(\frac{d\bar{v}}{dt} \right)_c = \dot{\bar{v}}_c = k_1 D_d^3 f \bar{N}_c \qquad (3.1)$$

where $\bar{v}$ is the volume of the combined gas generated per unit area, $\dot{\bar{v}}_c$ is the combined gas generation rate per unit area, f is the frequency of the bubble generation, independent of voltage, from a particular nucleation site and k_1 is a constant of proportionality. A two-dimensional close-packed formation of the bubbles is required to provide the maximum coverage of the

electrode surface (Fig.3.7a). For this configuration

$$\frac{\pi}{4} k_2' D_d^2 \bar{N}_c = 1$$

$$\text{or,} \quad \bar{N}_c = \frac{k_2}{D_d^2} \qquad (3.2)$$

where $1/k_2'$ is the critical packing density and constant and

$k_2 = 4/\pi k_2'$.

From the observation (iii) (Sec.3.2.4), we can assume that

$$D(t) \propto t^{1/2}$$

$$\text{or} \quad t_d = k_3' D_d^2 \qquad (3.3)$$

where, t_d is the time taken by the bubble to attain the departure diameter, D_d, and k_3' is the constant of proportionality.

Neglecting the delay time (the time required to nucleate the next bubble after the departure of the previous one), the bubble frequency, f, is given by

$$f = \frac{1}{t_d} = \frac{k_3}{D_d^2} \qquad (3.4)$$

where, $k_3 = \frac{1}{k_3'}$ = constant.

From the observstion of Ivey [Obvs.(ii), Sec 3.2.4] we can assume an overall regime of bubble growth, where both the

thermally and dynamically controlled bubble growth are taking place. Under this condition

$$D_d . f^n = k_4 \qquad (3.5)$$

where, k_4 is constant and $\frac{1}{2} < n < 2$. From (3.4) and (3.5)

$$D_d \left(\frac{k_3}{D_d^2} \right)^n = k_4$$

or, $$D_d = \left(\frac{k_4}{k_3^n} \right)^{\frac{1}{1-2n}} \qquad (3.6)$$

In (3.6) the right hand side is a constant, provided n is a constant. The value of n depends on the regime of the bubble growth. If that regime is same for all electrolytes, the departure diameter comes out to be almost constant. Equation 3.6 also indicates another significant result that the departure diameter of the bubble is same under all conditions. This result is in agreement with the observation made by Venczel, at high current density [Obv. (i), Sec 3.2.4].

Substitution of the values of $\bar{N}_c$ from (3.2) and f from (3.4) in (3.1) yields

$$\bar{v}_c = k_1 D_d^3 \left(\frac{k_3}{D_d^2} \right) \left(\frac{k_2}{D_d^2} \right)$$

$$\text{or, } \bar{v}_c = \frac{k_5}{D_d} \qquad (3.7)$$

where $k_5 = k_1 k_2 k_3$ =.costant.

Equation 3.7 indicates that the combined gas generation rate per unit area, at the critical condition is constant as both k_5 and D_d are constants.

For any given tool size the critical combined gas generation rate, $\dot{v}_c$, can be obtained by multiplying $\bar{\dot{v}}_c$ with the equivalent surface area of the electrode, A_e. Thus,

$$\dot{v}_c = \bar{\dot{v}}_c . A_e \qquad (3.8)$$

$$\text{with } A_e = \pi d l_e = \pi d (l + l_i) \qquad (3.9)$$

where d is the diameter of the tool, l is the actual length of the electrode dipped in the electrolyte and l_i is the imaginary extension of the electrolyte length to account for the current concentration at the edge, as discussed earlier. The face area is neglected in the calculation of the surface area, due to the reason which is also stated earlier.

It is already mentioned that the combined generation rate is the sum of the H_2 gas generation rate and water vapour generation rate. Let those be denoted by $\dot{v}_1$ and $\dot{v}_2$, respectively, so that,

$$\dot{v} = \dot{v}_1 + \dot{v}_2$$

At the critical condition

$$\dot{v}_c = \dot{v}_{1c} + \dot{v}_{2c} \qquad (3.10)$$

3.3.1 Mechanism of hydrogen gas generation

When electric current passes through an electrochemical cell electrolysis of the aqueous electrolytes takes place. As a result the following reactions take place to liberate hydrogen gas at the cathode. (The anode reactions are not shown here).

$$H_2O = OH^- + H^+$$

$$H^+ + e = H$$

$$2H = H_2 \quad \text{(at cathode)}$$

When the liberated hydrogen gas saturates the neighboring electrolyte, it comes out in the form of bubbles. The quantity of H_2 liberated by the electrochemical reaction is given by the Faraday's law of electrolysis. The law states that the quantity of element deposited or dissolved at the electrode is proportional to the charge passed through the cell and the constant of proportionality is termed as the electrochemical equivalent. If w be the deposited or liberated quantity of element, then

$$w = \varepsilon It$$

where ε is the electrochemical equivalent, I is the current and t is time. When I is in amp and t is in second, then the product 'It' is termed as coulomb and the electrochemical equivalent of H_2 is 1.045×10^{-5} mg/coloumb.

In our present configuration of the bubble generation, both the H_2 gas and water vapour generate simultaneously. It will be logical to assume that the bubble are at a temperature of 100°C. By Avogadro's law the density of a gas at 0°C and 1

atmospheric pressure is

$$\rho = \frac{1}{22400} \text{ gm-mole/c.c}$$

For H_2 , $\rho_H = \frac{2}{22400}$ gm./c.c = 8.9×10^{-5} gm/c.c

The density of H_2 at 100°C or 373°K is

$$\rho_H \text{ (at } 100^\circ C) = \frac{273}{373} \times \frac{2}{22400} = 6.535 \times 10^{-5} \text{ gm/c.c}$$

when the electrochemical equivalent of H_2 at 100°C is expressed in volume

$$\gamma = \varepsilon / \text{ (density of } H_2 \text{ at } 100^\circ C)$$

$$= \frac{1.045 \times 10^{-5}}{6.535 \times 10^{-5}} \text{ cm}^3/\text{Col.}$$

$$= 0.16 \text{ cm}^3/\text{A-Sec.} \quad (\text{As 1 A-sec = 1 Col})$$

Hence, $\dot{v}_1 = \gamma I$, where $\gamma = 0.16$ cm^3/A-sec and at critical condition

$$\dot{v}_{1c} = \gamma I_c = \gamma J_c A_e \qquad (3.11)$$

3.3.2 Mechanism of water vapour generation

The water vapour forms on the electrode surface due to ohmic heating . If I be the current and R_3 be the interface

resistance, then the rate at which heat liberates is I^2R_3. A major part of this heat generated is lost due to conduction in the tool and convection in the electrolyte. Only a small part is utilised in vapour formation. Let, β be the fraction of heat utilised in the vapour formation, T_a be the ambient temperature and T_b, L and s be the boiling point, latent heat of vaporisation and the specific heat of the electrolyte, respectively. Then the rate of vapour formation is given by

$$\dot{v}_2 = \frac{\beta I^2 R_3}{\rho[s\ (T_b - T_a) + L]} = \delta I^2 R_3$$

where, ρ is the density of water vapour. It is difficult to calculate β theoretically. Therefore it was decided to evaluate the factor δ by an indirect method which will be discussed afterward. It was termed as the coefficient of vapour formation and expressed in cm^3/watt-sec. At critical condition,

$$\dot{v}_{2c} = \delta I_c^2 R_{3c} \qquad (3.12)$$

3.3.3 Determination of the critical current (I_c) and the critical voltage (V_c):

Substituting the values of $\dot{v}_{1c}$ and $\dot{v}_{2c}$ from (3.11) and (3.12) in (3.10)

$$\dot{v}_c = \gamma I_c + \delta I_c R_{3c} \qquad (3.13)$$

when expressed in terms of unit area,

$$\bar{v}_c = \gamma J_c + \delta I_c^2 R_{3c} \left(\frac{1}{A_e}\right)$$

$$= \gamma J_c + \delta J_c^2 R_{3c} A_e$$

$$\text{or,} \quad \delta R_{3c} A_e J_c^2 + \gamma J_c - \bar{v}_c = 0 \qquad (3.14)$$

The positive root of J_c in (3.14) is the critical current density. So that,

$$J_c = \frac{-\gamma + (\gamma^2 + 4\delta R_{3c} A_e \bar{v}_c)^{1/2}}{2 \delta R_{3c} A_e} \qquad (3.15)$$

The critical voltage, V_c, can be determined from (3.15) and the idealised ECD circuit as shown in Fig.3.1d. This yields

$$V_c = J_c A_e [R_{1c} + R_{2c} + R_{3c}] \qquad (3.16)$$

where, R_{1c}, R_{2c} and R_{3c} are the critical values of the resistances R_1, R_2 and R_3.

3.4 Determination of the Invariant Quantities and Evaluation of Various Constants.

It is extremely difficult to estimate all the constants in (3.7) and (3.12), without taking help of any experimentation. Furthermore, it is also very difficult to estimate the values of R_{1c}, R_{2c} and R_{3c} theoretically, due to their transient nature involving complex bubble dynamics. The experimental setup shown in Fig.2.1a was used for conducting the pilot experiments to

evaluate these constants, critical resistances and the invariant parameter, l_i.

3.4.1 Determination of l_i

The depth of a tool in the electrolyte was varied in the range 0.05cm to 0.25cm keeping its diameter constant. KOH of 40% concentration was used as the electrolyte. Smooth D.C. supply of 15V was applied to the cell, so that the V-I characteristic remains within the predischarge region. The currents through the cell ware plotted corresponding to different tool depths in the electrolyte. The same procedure was followed with the tools of other diameters. The plots were extended to intercept the horizontal axis (the tool depth axis). It was observed that all the plotted curves were straight lines and intercepted the depth axis at - 0.12 cm (Fig.3.9a). To check whether this intercept changes with applied voltage or not, the same procedure was repeated with the voltage magnitude at the critical condition. Interestingly, the same location of intercept was obtained as in the previous sets of experiments. (Fig.3.9b). As the current depends on the area of contact between the tool and the electrolyte, it is expected that the current will be zero when the area of contact between tool and electrolyte is zero. The zero current corresponds to the point where the plotted straight lines intersect the tool depth axis. This signifies that the

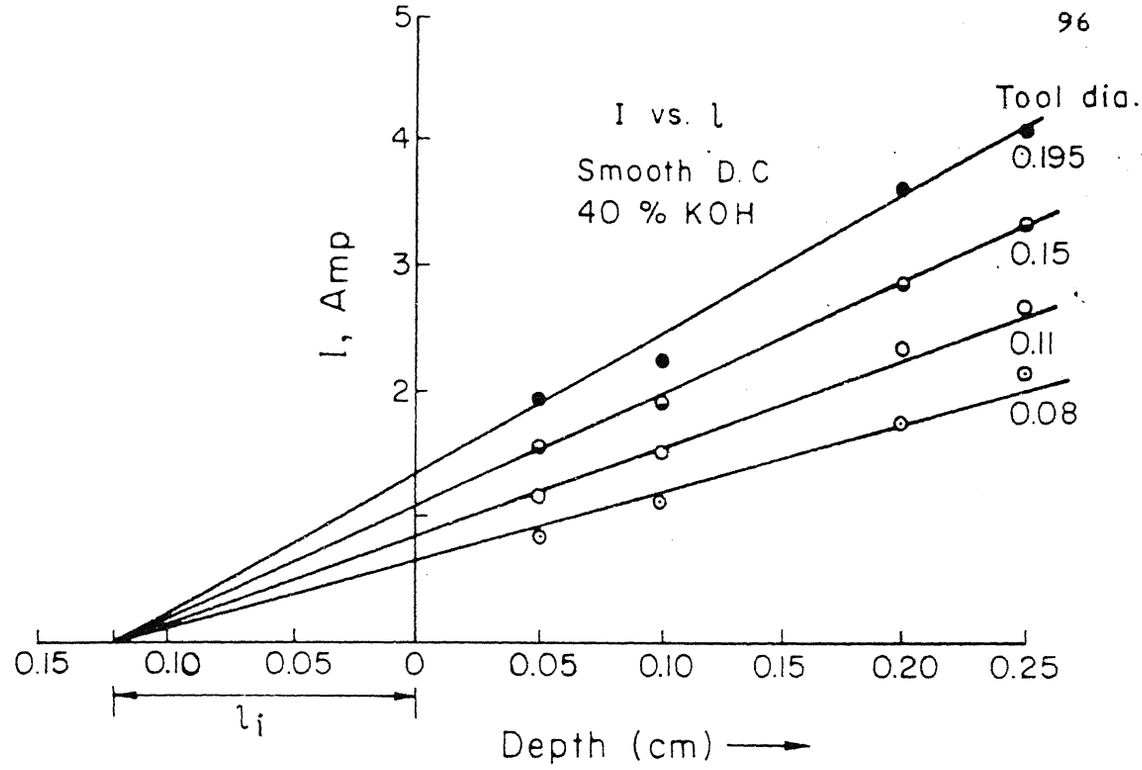

(a)

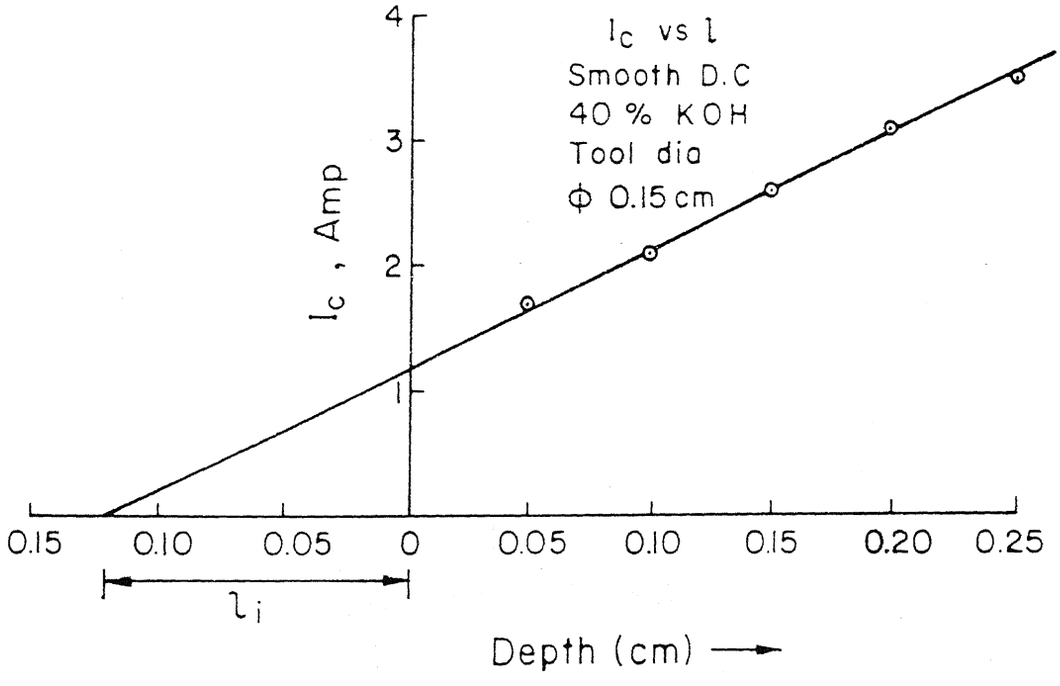

(b)

Fig 3.9 Evaluation of l_i

effective length of the electrode in contact of the electrolyte is the sum of the actual length and that intercept. Hence the imaginary extension of the electrode length is that intercept, which gives

$$l_i = 0.12 \text{ cm}$$

3.4.2 Determination of the critical resistances

The total resistance of the electrochemical circuit is the sum of the three components R_1, R_2 and R_3 [Fig.3.1d]. Out of these R_1 and R_3 result from the constriction effect at the electrode surface due to the bubbles. The nucleation site density of the bubbles on the nonmachining electrode is much less compare to that on the tool electrode, owing to its much larger area of contact with the electrolyte. The nucleation sites on the larger electrode is distributed enough sparely to have no constriction effect [31] and hence, R_1 can be neglected. It was decided to conduct a special set of experiments to investigate the behavior of R_2. The experiments were planned to conduct at a very low value of applied voltage, so that the bubble density on the tool electrode remained low. In this situation R_3 can also be neglected, so that the only R_2 component will be effective.

A full wave rectified D.C. (much lower than the critical value) was applied to the cell and the waveshapes of the applied voltage and the corresponding current were monitored by the oscilloscope. The applied voltage was gradually increased and it

was observed that the current waveshape distorted beyond a certain limit of the applied voltage (Fig.3.10). this indicated that R_3 was no more negligible beyond that value of the applied voltage. Within the limit found above, the ratio of the instantaneous voltage and the instantaneous current was constant throughout. This revealed the fact that R_2 is not a function of the applied voltage and remain constant throughout the region of the applied voltage upto the critical point. To investigate the variation of R_2 with the concentration of electrolyte, the above technique was repeated for different concentration of the same electrolyte. It was found from the variation that R_2 can be expressed in terms of the mole fraction of the electrolyte and the equivalent area of the electrode A_e as. [Appendix A]

$$R_2 = \frac{K_2 M^{\lambda_2}}{A_e}$$

where K_2 and λ_2 are constants and depend on electrolyte. The mole fraction M is expressed as

$$M = \frac{m_2}{m_1 + m_2}$$

where, m_2 moles of the electrolyte are present in m_1 moles of water. The values of K_2 and λ_2 for four commonly used electrolytes, as obtained, are given in Table 3.1.

The interface resistance R_3 depends on the bubble density on the electrode surface. The bubble density increases with the applied voltage, i.e., current. So, R_3 is also expected

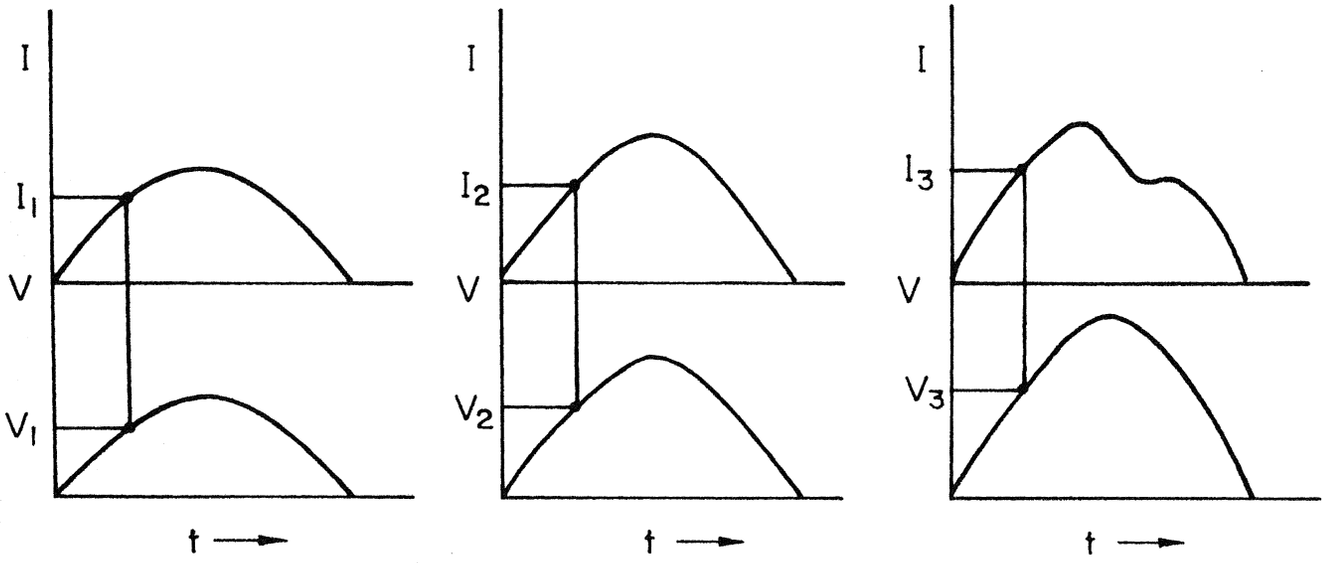

Power supply: Full wave rectified D. C.

$$R_2 = \frac{1}{p}\left[\frac{V_1}{I_1} + \frac{V_2}{I_2} + \frac{V_3}{I_3} + \cdots\cdots + \frac{V_p}{I_p}\right]$$

Fig 3.10 Oscilloscope traces for evaluation of $R_2(=R_{2C})$

to increase with the applied voltage. Therefore, the concerned investigating experiments were conducted in the critical condition. The total resistance at the critical condition can be calculated from the values of the current and the voltage at the critical point of the V-I characteristic curve. Let at the critical condition, V_c and I_c be the values of the voltage and the current respectively. This gives the critical resistance

$$R_c = \frac{V_c}{I_c}$$

which is the sum of R_{2c} and R_{3c}. R_{3c} is the critical values of the interface resistance and $R_{2c} = R_2$, as R_2 remains constant throughout predischarge the region, as found earlier. Thus R_{3c} for any combination of the tool and the electrolyte can be given by

$$R_{3c} = R_c - R_{2c}$$

The values R_{3c} for different concentration of a single electrolyte were obtained and found to follow the same pattern as that of R_2 ($=R_{2c}$) [Appendix A] and can be expressed as

$$R_{3c} = \frac{K_3 M^{\lambda 3}}{A_e}$$

The values of K_3 and λ_3 for the same four electrolyte are given in Table 3.1. It is interesting to note that λ_2 and λ_3 values are independent of the electrolyte.

Table 3.1

Electrolyte	K_2 ($\Omega cm^2\ mole^{-0.5}$)	K_3 ($\Omega cm^2\ mole^{-1.0}$)	λ_2	λ_3
NaOH	0.15	0.03	-0.5	-1.0
KOH	0.15	0.055		
NaCl	0.22	0.055		
KCl	0.22	0.03		

3.4.3 Evaluation of $\bar{v}_c$ and δ :

The only two invariants left to be evaluated were $\bar{v}_c$ and δ. The hydrogen and the water vapour are generated simultaneously at the electrode surface. It is difficult to measure the volume rate of generation of those elements as all the bubble released from the electrode surface do not come out from the electrolyte. The condition of the electrolyte boiling at the interface in an ECD setup is referred as subcooled boiling. In subcooled boiling the bulk of the fluid do not attain the boiling temperature. Most

of the vapour bubbles, detached from the electrode surface collapse, releasing the latent heat of evaporation to the relatively cold bulk electrolyte. Similarly, some part of the hydrogen gas diffuses into the electrolyte. Therefore, an indirect method was adopted to evaluate both the $\bar{v}_c$ and δ simultaneously. A few sets of pilot experiments were conducted with different configurations of the tool and the electrolyte. The corresponding values of R_{3c} and I_c and constant value of γ were substituted in (3.14) [Appendix B]. The resultant quadratic equations were solved and the values of $\bar{v}_c$ and δ were found to be as follows:

$\bar{v}_c$ = 6.28 cm/sec

and δ = 0.018 cm^3/watt sec.

3.4.4 Summerization of the result

The final forms of the expressions predicating the critical current and critical voltage can be arranged as follows

$$I_c = J_c A_e = A_e \left[\frac{-\gamma + (\gamma^2 + 4\delta K_3 M^{\lambda_a} \bar{v}_c)^{1/2}}{2\delta K_3 M^{\lambda_a}} \right] \qquad (3.17)$$

$$V_c = \frac{I_c}{A_e} \left[K_2 M^{\lambda_2} + K_3 M^{\lambda_a} \right]$$

$$= J_c \left[K_2 M^{\lambda_2} + K_3 M^{\lambda_a} \right] \qquad (3.18)$$

where γ = 0.16 cm^3/A-sec

δ = 0.018 cm^3/watt-sec

$\bar{v}_c$ = 6.28 cm/sec

λ_2 = - 0.5; λ_3 = -1.0 and

K_2 and K_3 are the coefficients given in Table 3.1

3.5 Verification of the Model:

The model developed in Sec.3.3 and the formulations in Sec.3.4 on the basis of that model were verified to establish the accuracy. Verification was done by comparing the results obtained from the verifying experiments with those predicted by the model. Figure 3.11 shows the comparison between the critical currents for four different electrolytes at two different tool depth of 0.1 cm and 0.2 cm, obtained experimentally and calculated on the basis of the model. The comparison for the critical voltages are shown in Fig.3.12. The critical voltages being independent of the tool depth, the plots for 0.1cm and 0.2 cm coincide. Figure 3.13 compares the calculated and the observed critical voltages and critical currents for different tool diameters, other parameter being the same.

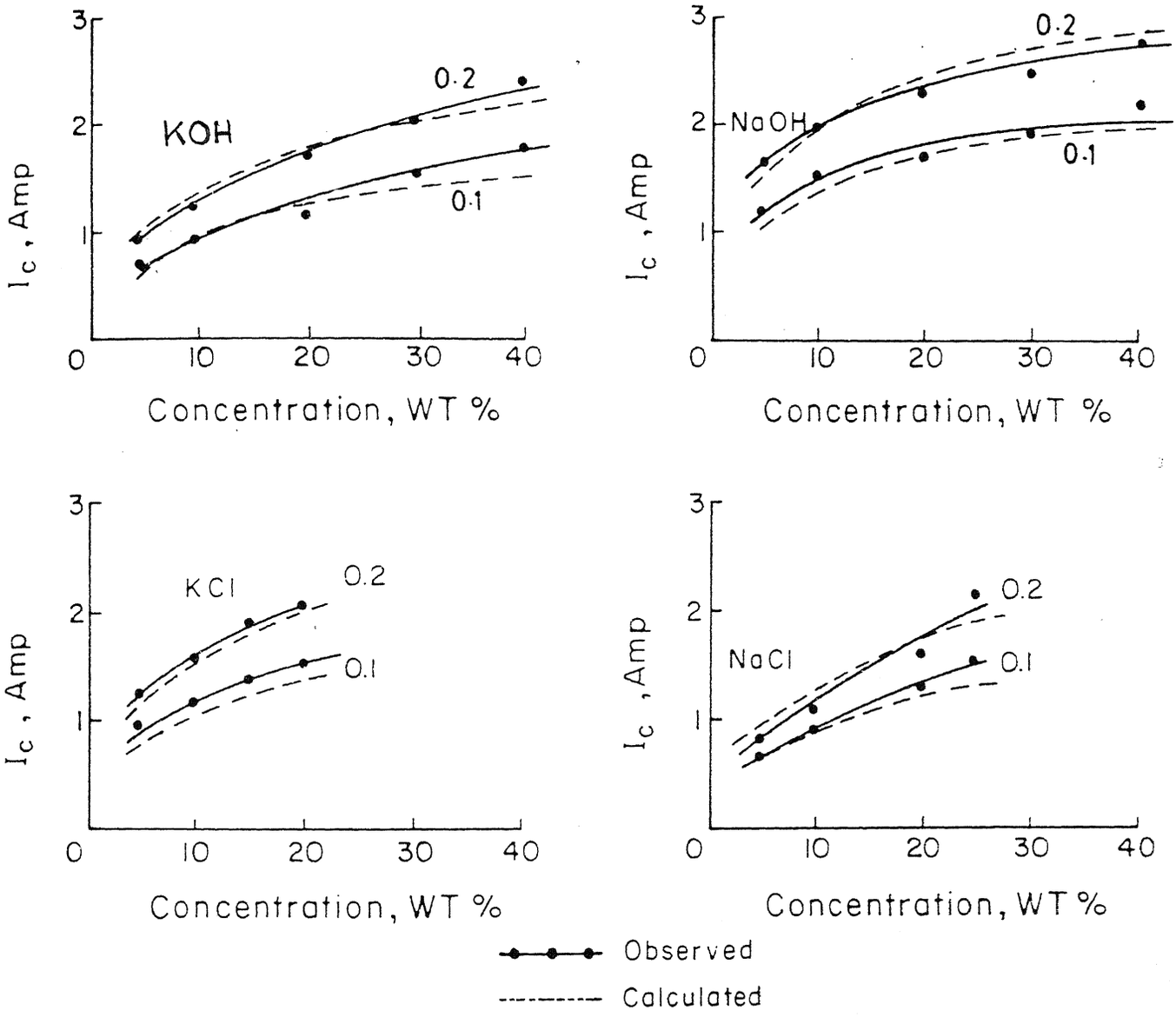

Fig 3.11 Comparison of calculated and observed I_c for tool diam. 0.11 cm and depth 0.1 cm & 0.2 cm., power supply: Smooth D.C.

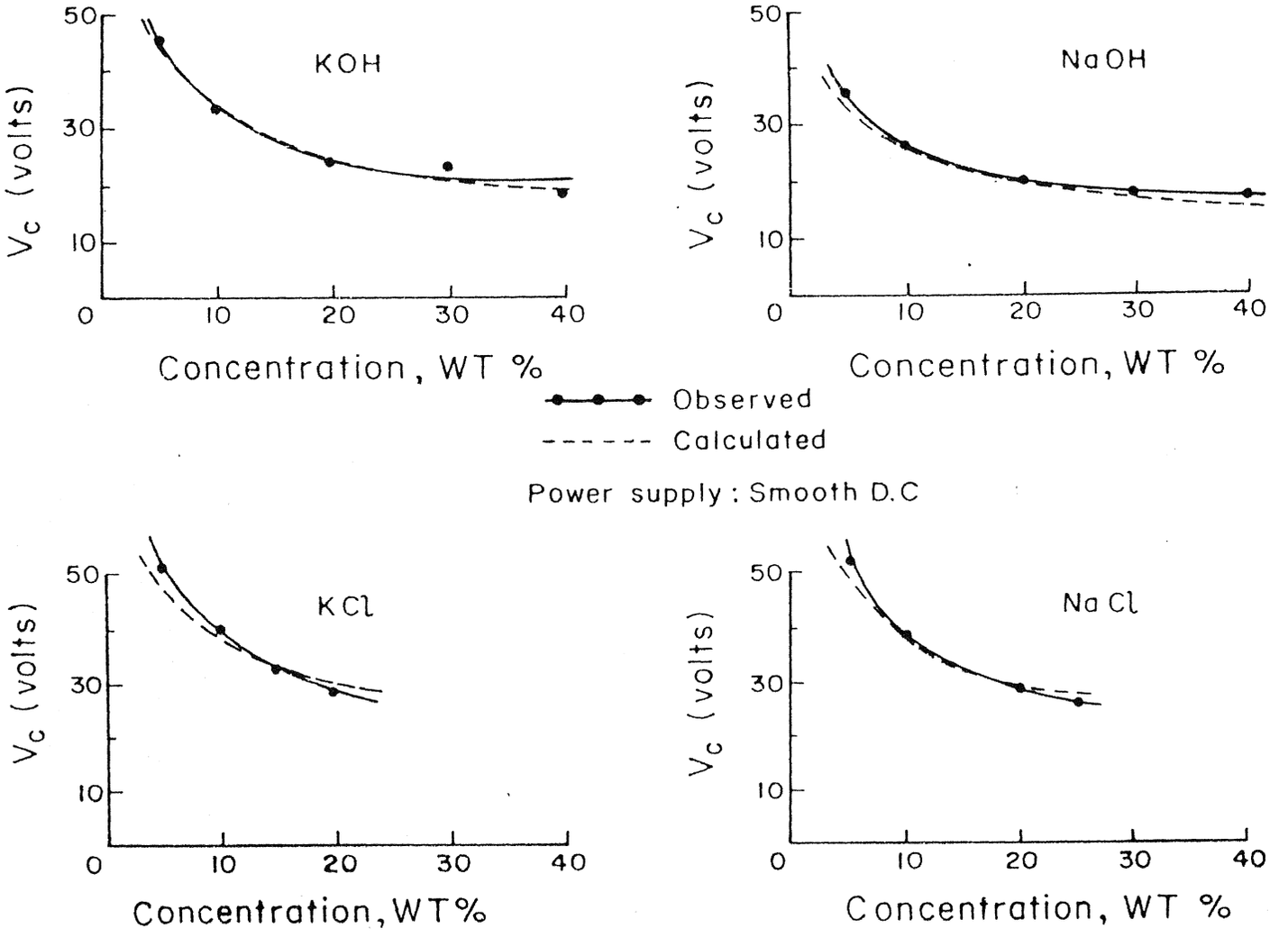

Fig 3.12 Comparison of calculated and observed V_c for tool diam. 0.11 cm and depth 0.1 cm. & 0.2 cm.

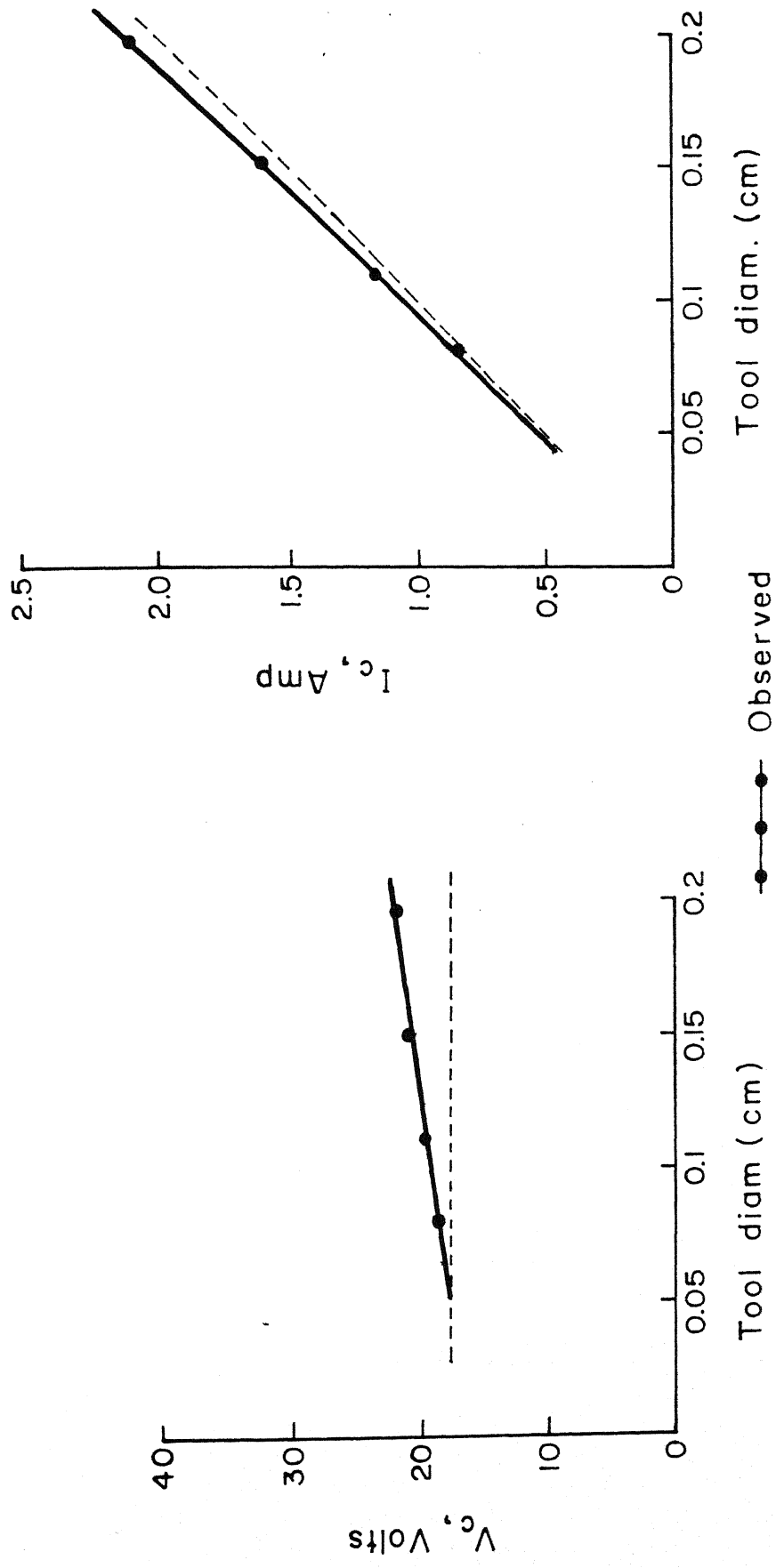

Fig 3.13 Comparison of observed and calculated V_c & I_c for different tool diameter (power supply : Smooth D.C)

3.6 ECD Phenomenon Above the Critical Condition

In the present chapter emphasis has given to model the critical condition, where ECD phenomenon initiates. If the applied voltage to the cell is slightly more than the critical value a stable discharge at the tool edge takes place. It is already pointed out that the intensity of the discharge increases with the applied voltage. This is due to the fact that larger amount of energy are released with the increase of the applied voltage. The stabilisation of the discharge occurs due to the switching action at a quick succession. The spark point moves rapidly throughout the edge region forming a luminous ring of discharge. Though the RMS current value is low at this stage, the instantaneous peak value increases with the applied voltage.[1] Electrochemical discharge machining can be done with the help of this stabilized discharge.

---

[1] This can be noticed from the Fig.2.2 and 2.11b. The region 4 of fig.2.2 shows a low RMS value of circuit current but the corresponding current wave shape in fig.2.11b shows the peaks at high values indicating high instantaneous current.

CHAPTER 4

THEORETICAL MODEL OF ECDM AND ENHANCEMENT OF THE PROCESS CAPABILITY

4.1 Introduction

The basic mechanism of electrochemical discharge machining (ECDM) is the localised melting of the workpiece by the energy released from a series of electrochemical discharge (ECD). The basic parameters controlling the material removal rate (MRR) are identified from the investigating experiments as the input voltage, the electrolyte and its concentration and the temperature of the electrolyte. ECD being a type of switching phenomenon the effect of the circuit inductance as a parameter is also investigated. In addition to these tool polarity as well as the type of power supply also influence the MRR. However, in the present work the temperature and the tool polarity are not included in the model. The temperature is taken as constant at room temperature and the cathode tool is used. The verification of the model is done with 100 Hz full wave rectified D.C.

4.2 Basic Scheme of ECDM

The process of material removal in ECDM is a thermal one. A part of the energy released by the discharge is conducted to the workpiece and raises the temperature of the workpiece to a high value. this temperature rise is confined to a localised region. If the maximum temperature attained is more than the melting temperature of the workpiece some part of the workpiece melts. the molten portion is removed by the shock due to the discharge and it ultimately results in a small crater. The mechanism of material removal in ECDM is comparable with that of electric discharge machining (EDM). In EDM the applied potential between the electrodes (tool and workpiece) causes breakdown of the dielectric medium. This results in electron emission from the tool through the gas bubbles, formed due to the dielectric breakdown. The resulting discharge strikes the workpiece and melts it locally. This type of discharge takes place from the end surface of the tool and between the points where the distance between the tool and workpiece is minimum. ECDM differs from EDM in the way that, the discharge in ECDM takes place between the tool and the electrolyte due to the switching action and only at the tool edge. However in both the cases the electrical discharge causes machining. A comparison between the initiation of

discharge and material removal in EDM and ECDM is shown exaggeratedly in Figs.4.1a and 4.1b for a single discharge. Though it was assumed that the sparking takes place at the edge, practically the sparking zone is a small area at the vicinity of the edge (Fig.4.2a). It was observed that with the increase of the applied voltage the region of sparking enlarges and the vacant area at the centre shrinks. Simultaneously the sparking zone also spread along the side of the tool. The region of sparking shown in the figure is qualitatively only and analytical treatment is kept outside the scope of the present work. The molten part of the workpiece surface due to the annular area in which the sources (developed by the discharge) are distributed is indicated in Fig.4.2b and 4.2c. In Fig.4.2b the distribution of the melting temperature of workpiece material is such that at the central region no melting takes place. This unmelted region restrict the penetration of the tool in the workpiece and machining becomes impossible. The thickness of the annular area of discharge expands towards the central region with increased current, i.e., with increased applied voltage. Also, the energy density of the sparking zone increases with applied voltage. When the molten area overlap at the central region (Fig.4.2c), the tool can move downward in the workpiece and drill continues. It can be seen that at a low machining voltage (though higher than the critical voltage) even a small diameter tool cannot machine material due to the reason shown in Fig.4.2b. With large diameter tool ECDM is

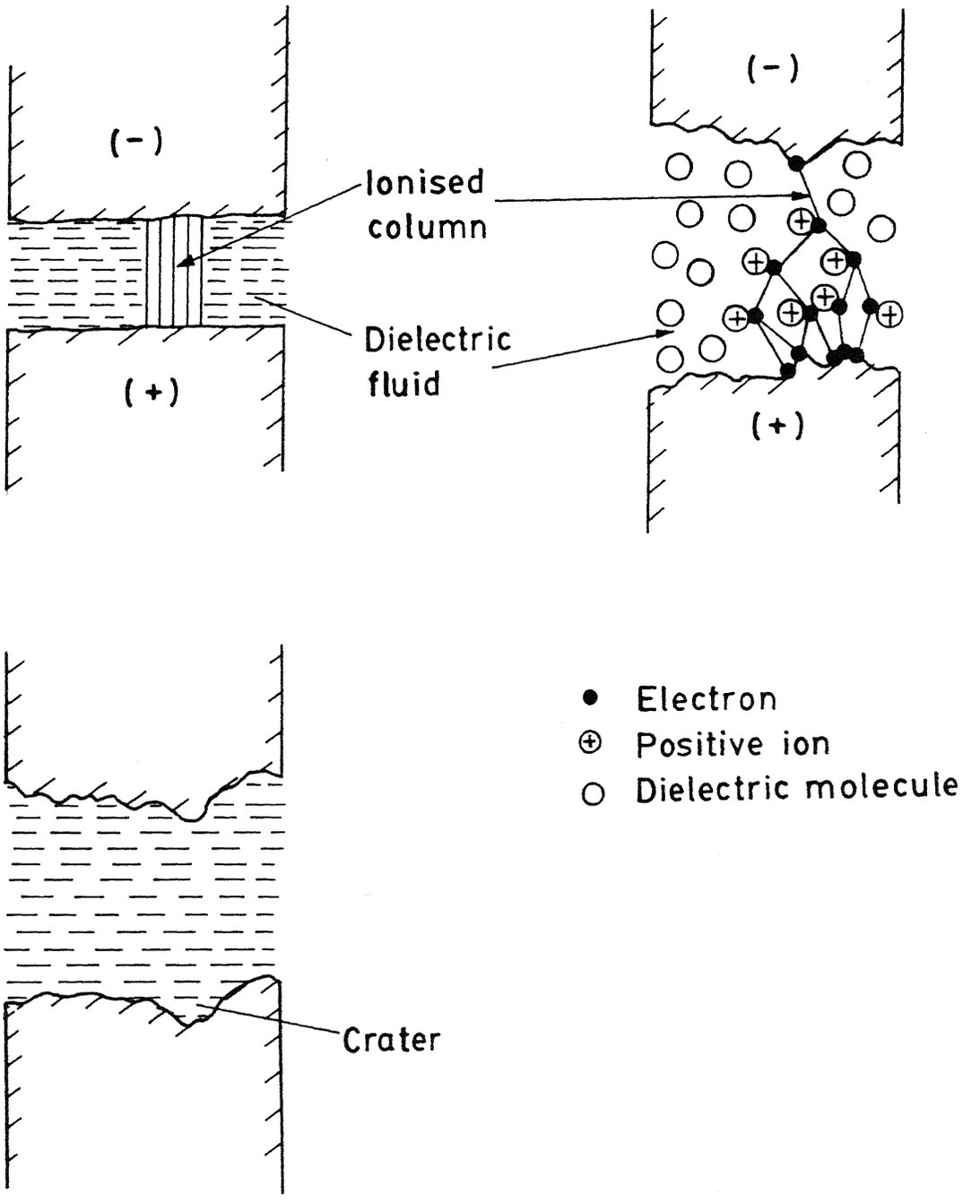

Fig. 4.1a Mechanism of discharge and material removal in EDM

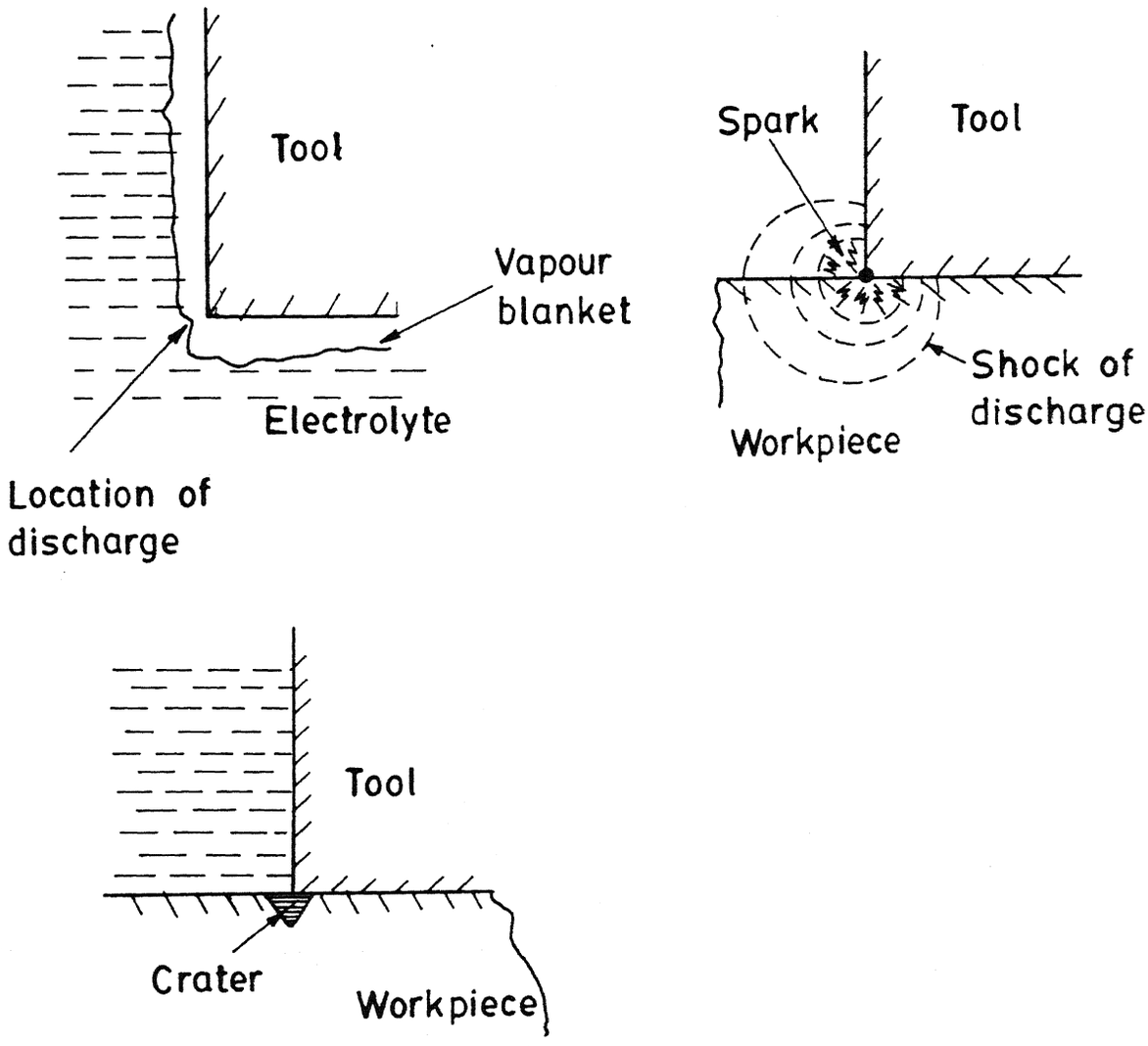

Fig. 4.1b Mechanism of discharge and material removal in ECDM

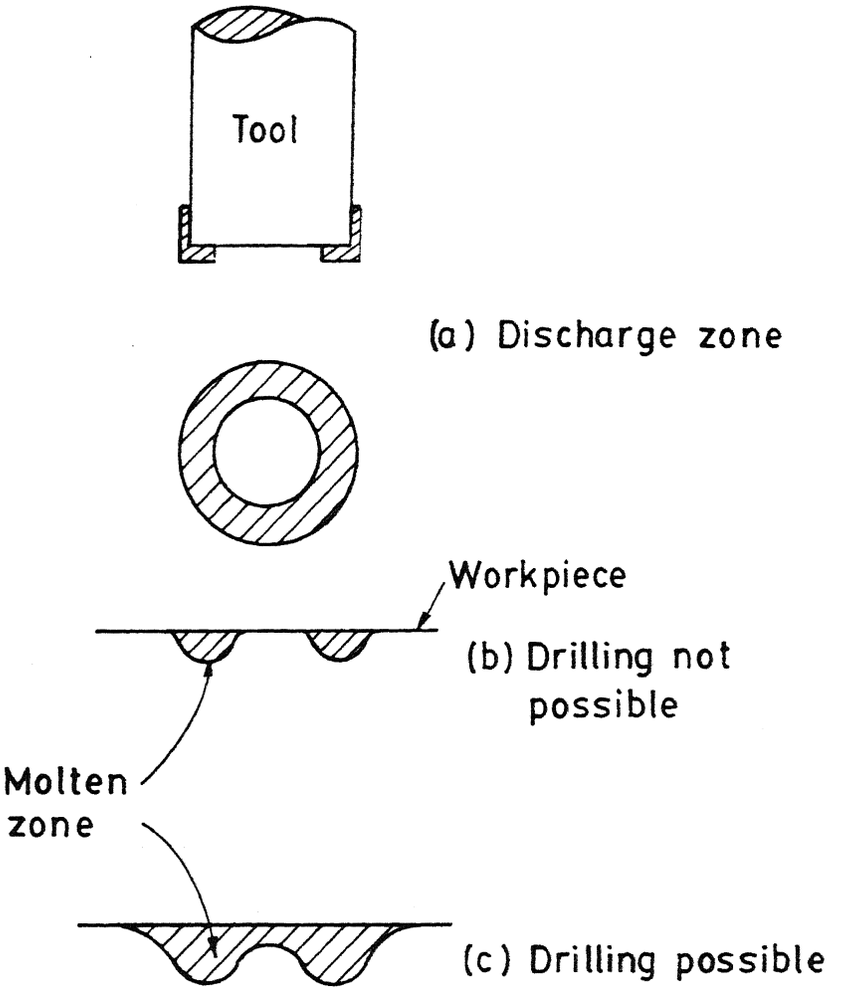

Fig. 4.2 Drilling by ECDM

not possible as the molten area never overlap.However, trepanning can be done with hollow tools with relatively larger diameters which is explained by Fig.4.3. It will be logical to formulate the problem in the manner which has been done generally in case of the EDM.

4.2.1 Assumptions

The following assumptions and idealisations are proposed to simplify the model of material removal in ECDM.

(i) The workpiece is homogeneous semiinfinite body.

(ii) The thermophysical properties of the workpiece material are identical for the solid and the liquid phase.

(iii) During the discharge the current through the other part of the electrode surface, except near the edges, is negligible.

(iv) All spark are identical and homogeneously distributed near the bottom edge of the tool.

(v) The energy density of the spark column is constant and the spark channel is cylindrical in shape.

(vi) The duration of the discharge is same for all the sparks.

(vii) The molten part of the workpiece material is continuously removed from the machining zone.

(viii) The machining rate is constant.

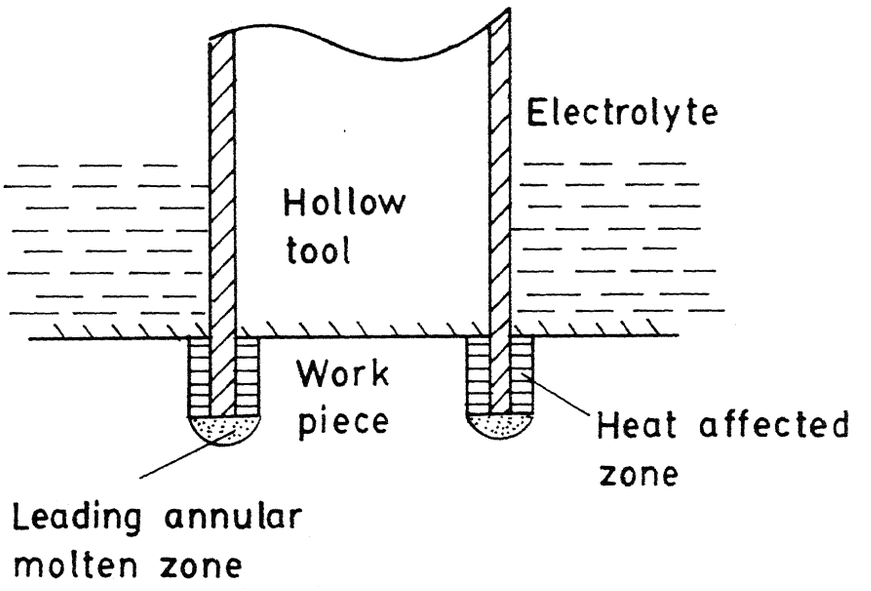

Fig. 4.3 Trepanning with hollow tool

4.2.2 Problem formulation and the solution procedure

The mechanism of the material removal is formulated as a heat conduction problem. A cylindrical source of heat acts on the workpiece surface for a certain duration and heat is conducted into it. Then the source disappears and the conducted heat melts some portion of the workpiece. The treatment is similar to that done by Yoshitsuge et.at [32] and Konig et. al, [33] in the field of EDM. The coordinate system used is shown in Fig.4.4 with respect to the spark column. The temperature at any point of the workpiece due to the action of the heat source is given by the Fourier's equation of heat conduction [34].

$$\frac{\partial T}{\partial t} = \alpha \nabla^2 T \qquad (4.1)$$

In cylindrical coordinate system, as shown in Fig.4.4, $T = T(r,\theta,z,t)$, t being the time, α is the thermal diffusivity of the workpiece material and ∇^2 is the Laplace operator given by

$$\nabla^2 = \frac{\partial^2}{\partial r^2} + \frac{1}{r}\frac{\partial}{\partial r} + \frac{1}{r^2}\frac{\partial^2}{\partial \theta^2} + \frac{\partial^2}{\partial z^2}$$

in cylindrical coordinate system. From the physical configuration of the present problem, it is quite clear that the temperature distribution will be symmetric about the z-axis and T is independent of θ. Denoting the spark channel diameter as 2a, the respective initial and boundary conditions are as follows :

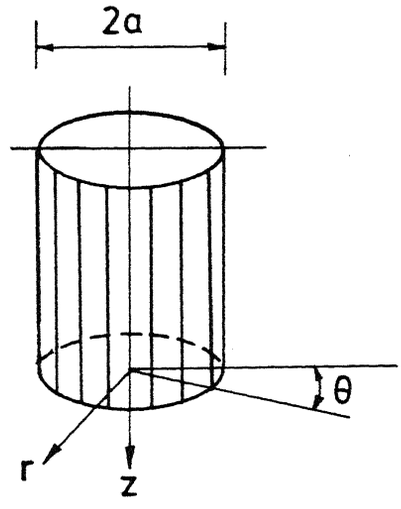

Fig. 4.4 Spark channel shape and coordinate system

$$T(r,z,t) = 0 \text{ for } t \leq 0$$

$$\left.\frac{\partial T}{\partial z}\right|_{z=0} = 0 \qquad \text{for } t > 0,\ r > a$$

$$-k \left.\frac{\partial T}{\partial z}\right|_{z=0} = \frac{\lambda Q}{\pi a^2 t_d} \qquad \text{for } t > 0,\ 0 < r \leq a$$

where, k = thermal conductivity of the workpiece material, Q = total heat released by each spark, t_d = duration of discharge and λ = fraction of released heat conducted into the work piece.

It is obvious that the maximum temperature attained will be along the z-axis due to the axial symmetry. It can also be assumed without introducing much error that the peak temperature is reached at the end of the discharge, i.e., at $t = t_d$. The solution of interest is the temperature at $T(0,z,t_d)$, which is given by,

$$T(0,z,t_d) = \frac{\lambda Q}{2\pi k a t_d} \int_0^\infty J_0(\xi a) J_1(\xi a) \left[e^{-\xi z} \operatorname{erfc}\left\{ \frac{z}{2\sqrt{\alpha t_d}} - \xi\sqrt{\alpha t_d} \right\} \right] \frac{d\xi}{\xi}$$

where, ξ is a dummy variable and $J_o(\xi a)$ and $J_1(\xi a)$ are the Bessel's functions of zero and first order, respectively. If z_m

be the depth upto which the temperature reaches the melting point, T_m, along the z-axis, then

$$T_m = \frac{2\lambda Q \sqrt{\alpha t_d}}{\pi k a^2 t_d} \left[\text{ierfc} \frac{z_m}{2\sqrt{\alpha t_d}} - \text{ierfc} \frac{\sqrt{z_m^2 + a^2}}{2\sqrt{\alpha t_d}} \right] \qquad (4.2)$$

where, $$\text{ierfc}(\eta) = \frac{1}{\sqrt{\pi}} e^{-\eta^2} - \eta \, \text{erfc}\, \eta$$

$$\text{erfc}(\eta) = 1 - \text{erf}(\eta)$$

and $$\text{erf}(\eta) = \frac{2}{\sqrt{\pi}} \int_0^{\eta} e^{-x^2} . dx$$

Some part of the heat released by the spark will be absorbed by the workpiece as latent heat during melting and a major part will be lost to the electrolyte. The part of the released heat conducted in the workpiece is λ. For simplicity of the analysis the intensity of the heat flux of the spark column, i.e., $Q/\pi a^2$ is taken as uniform.

4.2.3 Numerical evaluation of the solution

Equation 4.2 indicates that the depth upto which the melting temperature of the workpiece material is reached is a function of the spark channel diameter as well as the thermophysical properties of the workpiece material and the duration of discharge. To establish the relation between the energy released by the spark and the depth of the melting

temperature, it is essential to identify the values of T_m, k, λ, α, t_d and $Q/\pi a^2$ appearing in (4.2). The values of the thermal conductivity k and the thermal diffusivity α are 0.12 watt/cm°C and 0.07 cm^2/sec, respectively for sodalime glass. The melting temperature, T_m for sodalime glass is about 1400°C [35,36]. The magnitudes of λ and $Q/\pi a^2$ are assumed from the discharge characteristics of EDM and that of t_d from the switching phenomenon.

During the operation of the metallic contacts, small discharge occurs between the contacts. This results in some material transfer from one contact to the other (Fig.4.5) leaving some marks of discharge on the bodies as shown. Examining such a crater produced after a single discharge in Pd contacts, Riddlestone [37] computed that $2a \simeq 10^{-6} I_b$, where 2a is the spot diameter in meter and I_b is the current in ampere at the instant when the circuit opens. In an inductive circuit with constant inductance the energy released by the spark caused by circuit opening

$$E \propto I_b^2 \qquad (4.3)$$

From the abovementioned observation of Riddlestone,

$$2a \propto I_b$$

which implies that the area of the spot

$$A \propto I_b^2 \qquad (4.4)$$

where, $A = \pi a^2$. Thus, from (4.3) & (4.4)

$$A \propto E$$

$$\text{or, } \frac{E}{A} = \text{constant}$$

Therefore, the assumption of the constant energy density of the spark channel is justified.

When an electrical contact switch opens a current carrying circuit a minute portions of the contact vaporise and forms a bridge, quite analogous to the electrolyte bridge in ECD (Fig 4.6). The metal vapour bridge formation and material transfer depend upon the time taken to open the contact. Regular discharge requires a voltage of the order of 10V and the duration of discharge depends on the energy delivered by the inductance of the circuit. The discharge duration satisfies the relation

$$t_d \cong \frac{1}{10} L I_b$$

where L is the circuit inductance in Henry [38]. However, the discharge duration is influenced by the speed with which the contact breaks. It was observed that if the discharge duration is more than 10^{-5} sec, enough energy is released in the discharge to cause metal transfer between the electrodes, particularly in the telecommunication switches [39]. From the above observation the magnitude of discharge duration in ECD phenomenon is taken to be of the order of 10^{-4} sec.In ECD the discharge extinguishes only by blowing of the electrolyte bridge. Therefore, the excepted duration of discharge in ECD is longer than that in metal contact opening.

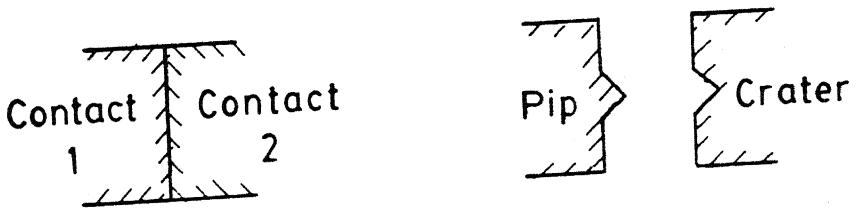

Fig. 4.5 Material transfer at contact opening (Exaggerated view)

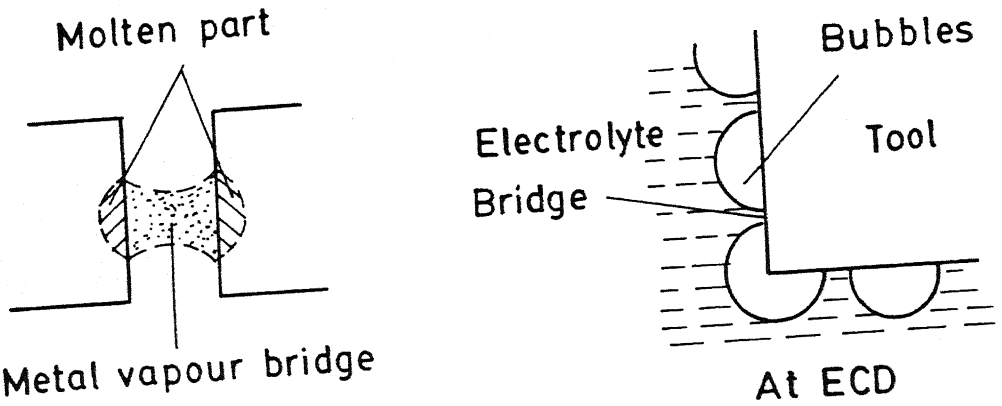

Fig. 4.6 Bridge formation before discharge

Appropriate data for the energy density in the discharge channel are not available in the literature on switching phenomenon. Therefore, relevant data available from the analysis of spark discharge during EDM were used. In EDM the energy per spark ranges from 0.1 J to 0.5J with spark channel diameters in the range of 0.005 cm to 0.01 cm. It indicates that the energy density in EDM spark channel ranges from 1000 J/cm^2 to 5000 J/cm^2. The energy density of the EDM spark channel can be controlled by the operative voltage and the worktool gap. Whereas in ECD with usual setup, the discharge initiates due to the vapour blanketing of the tool electrode and the energy density is not easy to control. Therefore, an intermediate value of the energy density of the spark channel in EDM was taken and the energy density of electrochemical discharge channel becomes of the order of 2000 J/cm^2.

The spark channel in EDM developes between the tool and the workpiece, whereas in ECD discharge takes place between the tool and the electrolyte and the workpiece is placed in the vicinity of the discharge. This configuration is likely to have lesser conduction of heat into the workpiece than that with the usual configuration for EDM. In EDM, under normal condition, 40%-80% of the heat released is utilised to melt the workpiece. Therefore, in ECDM it is assumed to be about 20% of the heat released by the spark. Thus, the magnitudes of $Q/\pi a^2$ and λ become 2000 J/cm^2 and 0.2, respectively. With these values (4.2) becomes

$$0.0079 = \text{ierfc } 189\ z_m - \text{ierfc } 189\ \sqrt{z_m^2 + a^2} \qquad (4.5)$$

and the energy released per spark can be expressed as $2000\pi a^2$ J, where a is in cm.

The volume of material removed per spark can be assumed to be conical in shape with base diameter as 2a and the height as z_m. Material removal per spark for different spark energy can be estimated using (4.5) and the characteristics is shown in Fig.4.7. The relationship between these two quantities can be approximately expressed (as derived from the plot) as

$$u = 0.52 \times 10^{-5}\ Q^{1.5} \qquad (4.6)$$

Where u is the volume of material removed per spark from the glass workpiece in cm^3 and Q is the heat released per spark in Joules. The amount of heat released per spark can be expressed as,

$$Q_s = \frac{1}{2} L I_o^2$$

where L is the inductance of the circuit in Henry and I_o is the instantaneous current at the beginning of discharge. However, when the current is equal to I_c, the condition is just adequate to initiate discharge, but hardly any material removal takes place. Hence, the actual amount of energy available for material removal can be taken as

$$Q = \frac{1}{2} L(I_o - I_c)^2 \qquad (4.7)$$

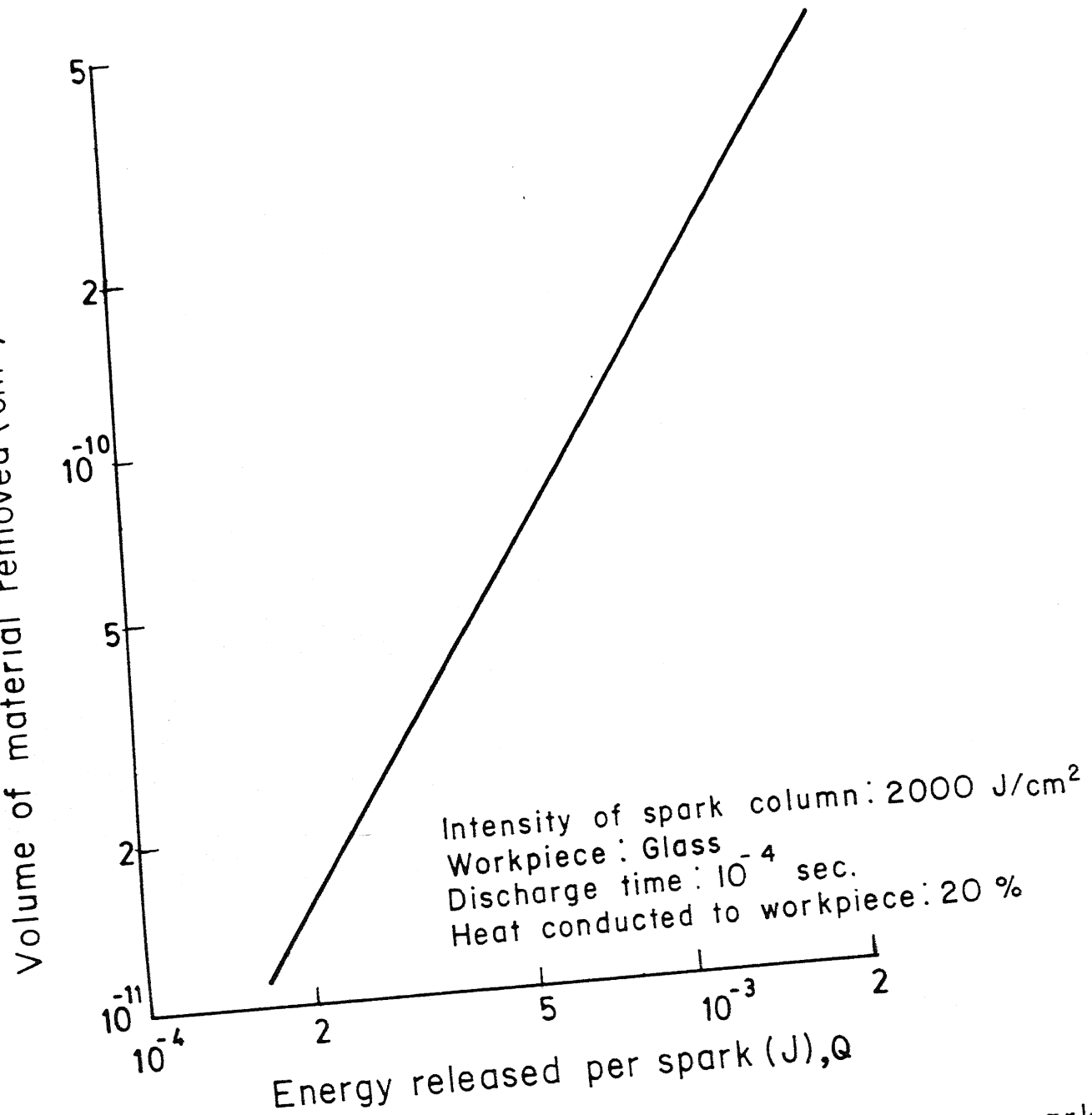

Fig 4.7 Energy per spark vs. material removed per spark (Derived from heat conduction equation).

However, it should be noted that both the energy delivered by the power source and the energy consumed by the circuit resistance during discharge are neglected for simplicity.

4.2.4 Determination of the sparking frequency in ECDM

It is necessary to determine the sparking (discharge) frequency to evaluate the MRR. It was found from the spectrum analysis of the discharge that no predominant frequency of the discharge during ECDM exists [Fig.2.12]. Therefore it was necessary to idealised the situation to calculate a representative theoretical frequency of discharge.

The discharge frequency is the reciprocal of the cycle time (=sum of the rise and fall time of the current). The cycle time can be calculated based on the simplified circuit shown in Fig.3.1d, assuming that the capacitances to be negligible. This reduces the ECD circuit to a R-L circuit. The current gradually increases from zero due to the presence of the inductance as shown in Fig.4.8a. The current at any time t is given by,

$$I(t) = \frac{V_o}{R}\left[1 - \exp\{-(R/L)\,t\}\right] \qquad (4.8)$$

where V_o is the applied voltage and R is the resistance.Theoretically it takes infinite time to reach the maximum current, I_m where

$$I_m = \frac{V_o}{R} \qquad (4.9)$$

In an ECD setup, when the circuit current is zero, no bubble nucleates on the electrode. Therefore, at the beginning of the cycle, when t = 0 only R_2 exists and the interface resistance R_3 is zero. With the passage of time circuit current rises and also nucleation of bubbles on the electrode surface begins. The interface resistance gradually increases from zero, and reaches its maximum value R_{3c} in course of time (Fig.4.8b). This shows that the maximum possible current in an ECD set up is,

$$I_o = \frac{V_o}{R_2 + R_3} \qquad (4.10)$$

where, V_o is the applied voltage. It is also observed from the current trace during discharge that the peak value of current increases with the applied voltage. To idealise the cycle the average resistance of the circuit is taken as $(R_2+0.5R_3)$. Actually, the circuit resistance increases from R_2 to $(R_2 + R_3)$ in the course of the cycle. Considering the average resistance $(R_2 + 0.5R_3)$, the current time characteristics can be approximated from (4.8) as follows

$$I(t) \simeq \frac{V_o}{R_2 + 0.5R_3}\left[1 - \exp\{-(R_2 + 0.5R_3)t/L\}\right] \qquad (4.11)$$

Figure 4.8c shows the idealised condition to determine the sparking frequency. The rising time of the current, t_1, is the time required to reach I_o. It is assumed that the blanketing takes place only after the current reaches I_o. With these idealisations,

$$I_o = \frac{V_o}{R_2 + 0.5R_3}\left[1 - \exp\{-(R_2 + 0.5R_3)t_1/L\}\right] \qquad (4.12)$$

Substituting the value of I_o from (4.10)

$$\frac{V_o}{R_2 + R_3} = \frac{V_o}{R_2 + 0.5R_3}\left[1 - \exp\{-(R_2 + 0.5R_3)t_1/L\}\right]$$

$$\text{or, } \exp\{-(R_2 + 0.5R_3)t_1/L\} = 1 - \frac{R_2 + 0.5\,R_3}{R_2 + R_3}$$

$$= \frac{0.5\,R_3}{R_2 + R_3}$$

$$\text{or, } \frac{R_2 + 0.5\,R_3}{L} \cdot t_1 = \ln\left(\frac{R_2 + R_3}{0.5\,R_3}\right)$$

$$\text{or, } t_1 = \frac{L}{R_2 + 0.5R_3} \ln\left(\frac{R_2 + R_3}{0.5\,R_3}\right)$$

As in ECDM the applied voltage is always greater than the critical voltage, all the components of the resistance attain their respective critical values. Hence,

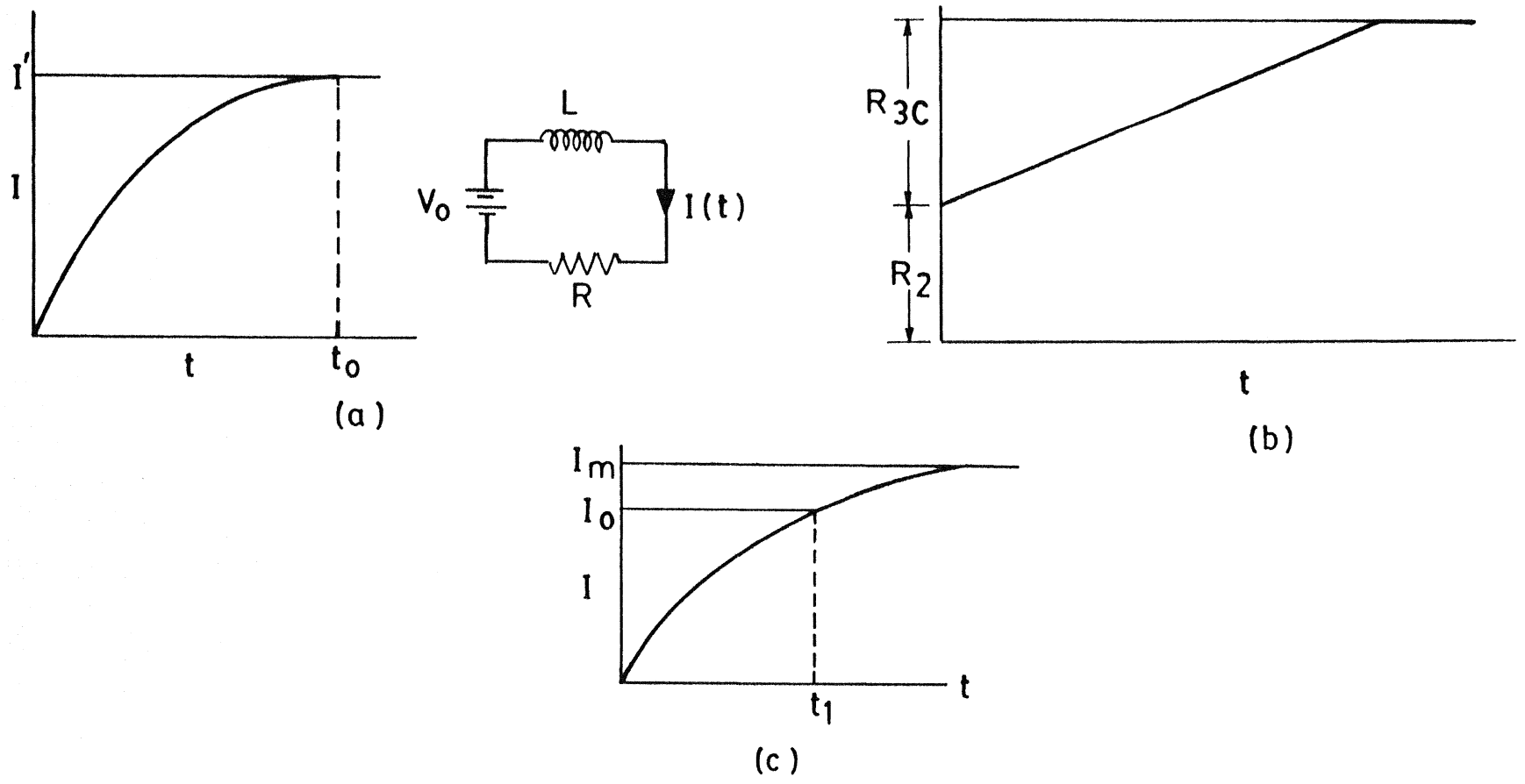

Fig. 4.8 (a) Simple L-R circuit ; (b) Resistance during the rise of current in ECD setup ; (c) Idealised condition of current in ECD circuit.

$$t_1 = \frac{L}{R_{2c} + 0.5R_{3c}} \ln\left(\frac{R_{2c} + R_{3c}}{0.5\, R_{3c}}\right)$$

$$= \frac{L}{R_{2c} + 0.5R_{3c}} \ln\left(\frac{2\, R_c}{R_{3c}}\right) \qquad (4.13)$$

as, $R_{2c} + R_{3c} = R_c$

So, the frequency of discharge,

$$\nu = \frac{1}{t_1 + t_d} \qquad (4.14)$$

where, t_d is the time of discharge.

It will be shown later [Sec.4.3.1] that the rising time of the current is in the order of 10^{-3} sec. or more, which is much greater than the discharge time, 10^{-4} sec. Therefore, the frequency can be approximately expressed, neglecting the time of discharge, as

$$\nu = \frac{1}{t_1} = \frac{R_{2c} + 0.5R_{3c}}{L \ln\left(\frac{2R_c}{R_{3c}}\right)} \qquad (4.15)$$

4.2.5 Determination of MRR in ECDM

Material removal rate in ECDM can be expressed as

$$\dot{M} = \rho.u.\nu \qquad (4.16)$$

where $\dot{M}$ is the MRR in gm/sec., ρ is the density of the workpiece material in gm/cm^3, u is the volume of the material removed per spark and ν is the spark frequency in sparks/sec. ρ for the glass

specimen used is 2.18 gm/cm^3. From (4.6) and (4.7)

$$u = 0.52 \times 10^{-5} Q^{1.5}$$

$$= 0.52 \times 10^{-5} \left[\frac{1}{2} L (I_o - I_c)^2\right]^{1.5}$$

$$= 1.84 \times 10^{-6} L^{1.5} (I_o - I_c)^{3.0} \qquad (4.17)$$

Substituting the values of u and ν from (4.17) and (4.15), respectively, in (4.16) yields

$$\dot{M} = \frac{2.18 \times 1.84 \times 10^{-6} L^{1.5} (I_o - I_c)^{3.0} (R_{2c} + 0.5 R_{3c})}{L \ln \left(\frac{2R_c}{R_{3c}}\right)}$$

$$= \frac{4.01 \times 10^{-6} L^{0.5} (I_o - I_c)^{3.0} (R_{2c} + 0.5 R_{3c})}{\ln \left(\frac{2R_c}{R_{3c}}\right)} \text{ gm/sec.}$$

$$= \frac{0.24 L^{0.5} (I_o - I_c)^{3.0} (R_{2c} + 0.5 R_{3c})}{\ln \left(\frac{2 R_c}{R_{3c}}\right)} \text{ mg/min.}$$

As, $I_o = \frac{V_o}{R_c}$ and $I_c = \frac{V_c}{R_c}$,

$$\dot{M} = \frac{0.24 L^{0.5} (V_o - V_c)^{3.0} (R_{2c} + 0.5 R_{3c})}{R_c^3 \ln \left(\frac{2R_c}{R_{3c}}\right)} \text{ mg/min} \qquad (4.18)$$

4.3 Verification of ECDM Model

Equation (4.18) indicates that the MRR is a function of inductance L. As mentioned earlier, each electrical circuit inherently possess some inductive element. Thus it is essential to determine the inherent inductance of the present ECD setup to evaluate the MRR. Let L_o be the inherent circuit inductance. If an additional inductance L_1 is introduced, the total inductance,

$$L = L_o + L_1 \qquad (4.19)$$

To evaluate L_o, MRRs with different values of L_1 were obtained experimentally for a fixed configuration and L_1 vs. MRR was plotted. Equation (4.18). Shows that MRR $\propto L^{0.5}$. The plotted parabola was extended to intersect the L_1-axis and the intercept was found to be 10×10^{-3} Henry [Fig.4.9]. As the MRR should be zero when inductance is zero, this intercept represents L_o.

Considering a typical case of 20% NaOH, 0.11 cm diameter tool and tool depth in electrolyte 0.1 cm, the critical resistance obtained are $R_{2c} = 6.7\ \Omega$ and $R_{3c} = 4.8\Omega$. Substituting these values of resistance and $L = 10 \times 10^{-3}$ Henry in (4.13)

$$t_1 = 1.72 \times 10^{-3} \text{ sec.}$$

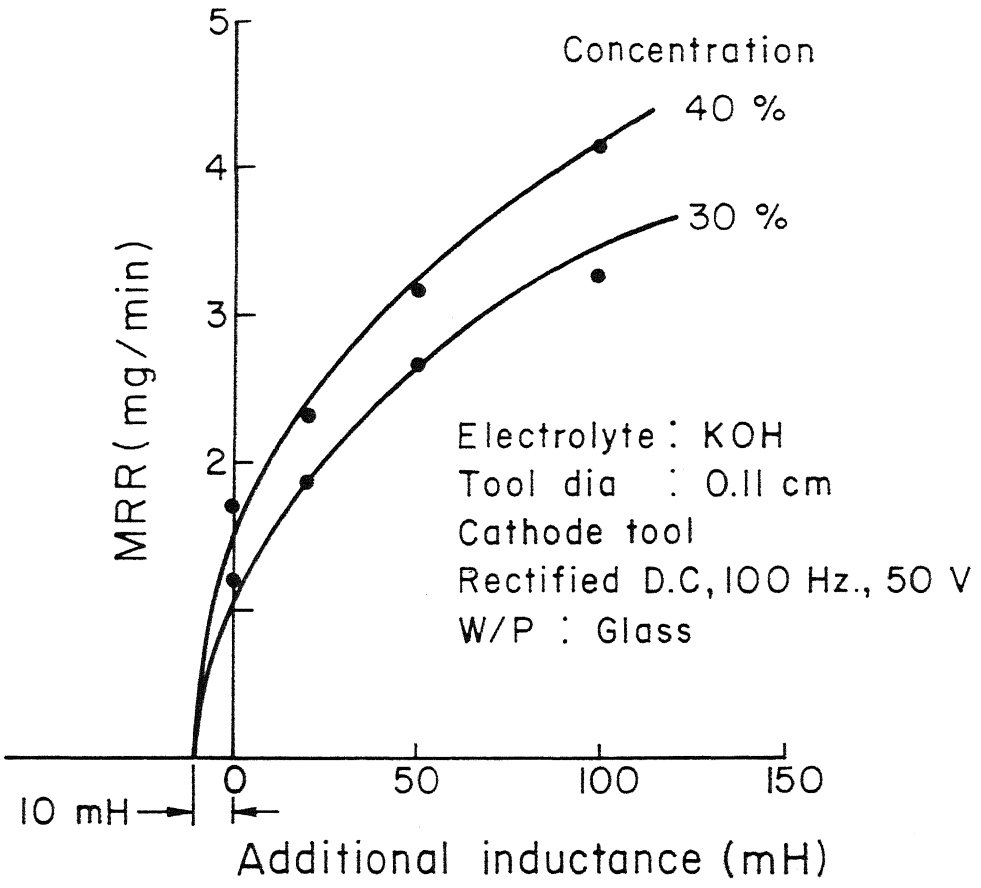

Fig 4.9 Determination of circuit inductance

which is much greater than the discharge time of 10^{-4} sec. Therefore, in calculation of the discharge frequency [Sec.4.2.4], t_d value was neglected.

The accuracy of the model developed was examined by comparing the characteristics obtained on the basis of the model with those obtained from the experiments. The model indicates that the MRR is a function of the applied voltage, inductance, the critical voltage of the configuration and the critical resistances. The last two factors are the functions of the electrolyte and its concentration. For the verification of the model some observations made under similar experimental condition reported by previous researchers are also utilised. Figure 4.10 shows the the comparison of the MRR characteristics as a function of concentration obtained experimentally by Umesh Kumar [6], with that calculated on the basis of the present model. The concentration of NaOH was varied from 10% to 60%. Figure 4.11a compares the MRR characteristics as a function of voltage, obtained by different researchers. Comparison of MRR characteristics as a function of voltage for NaCl and KOH are shown in Fig.4.11b. Figures 4.12a and 4.12b compare the MRRs obtained from the verifying experiments for different values of total inductance with those calculated on the basis of the model. the electrolytes are NaOH in Fig.4.12a and KOH in Fig.4.12b.

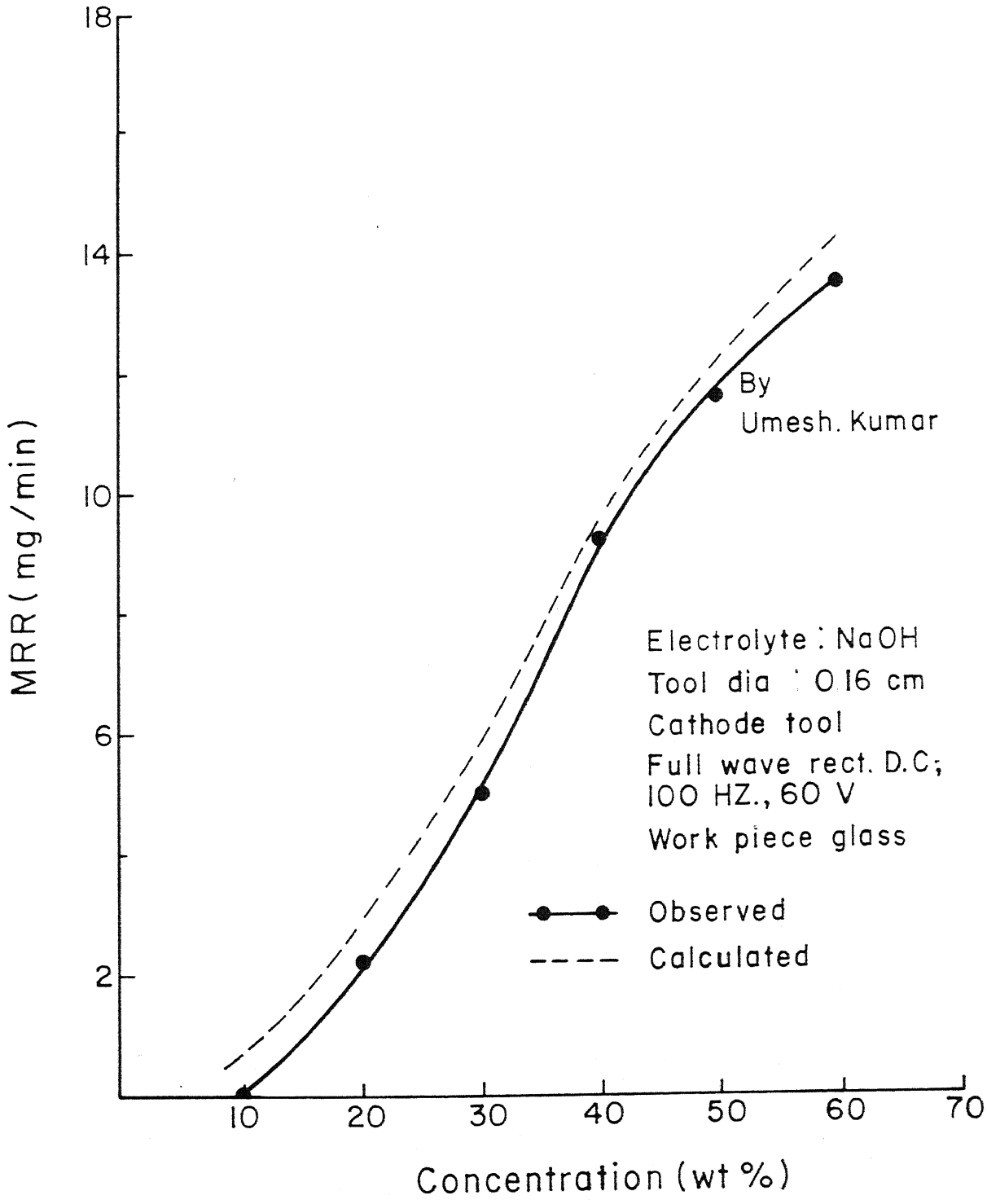

Fig 4.10 Comparison between observed and calculated MRR for varying concentration

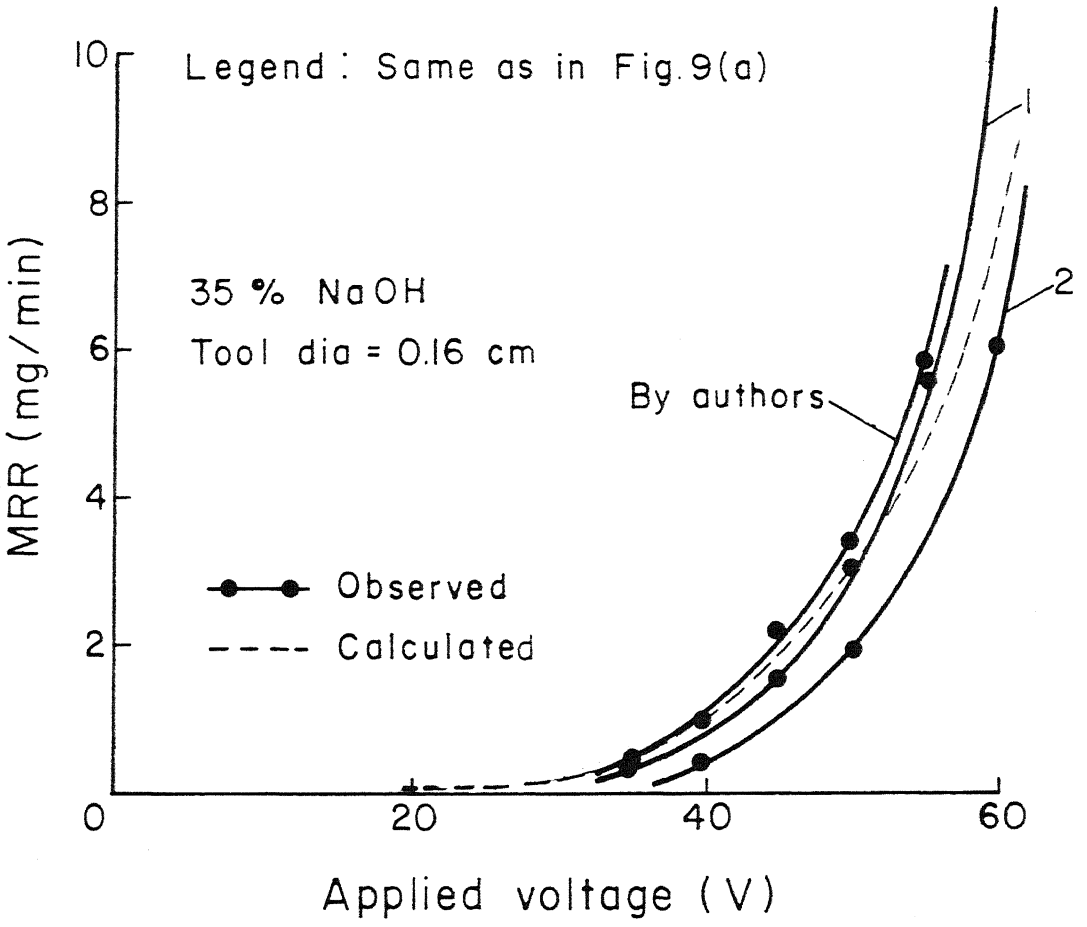

Fig 4.11 (a) Applied voltage vs MRR

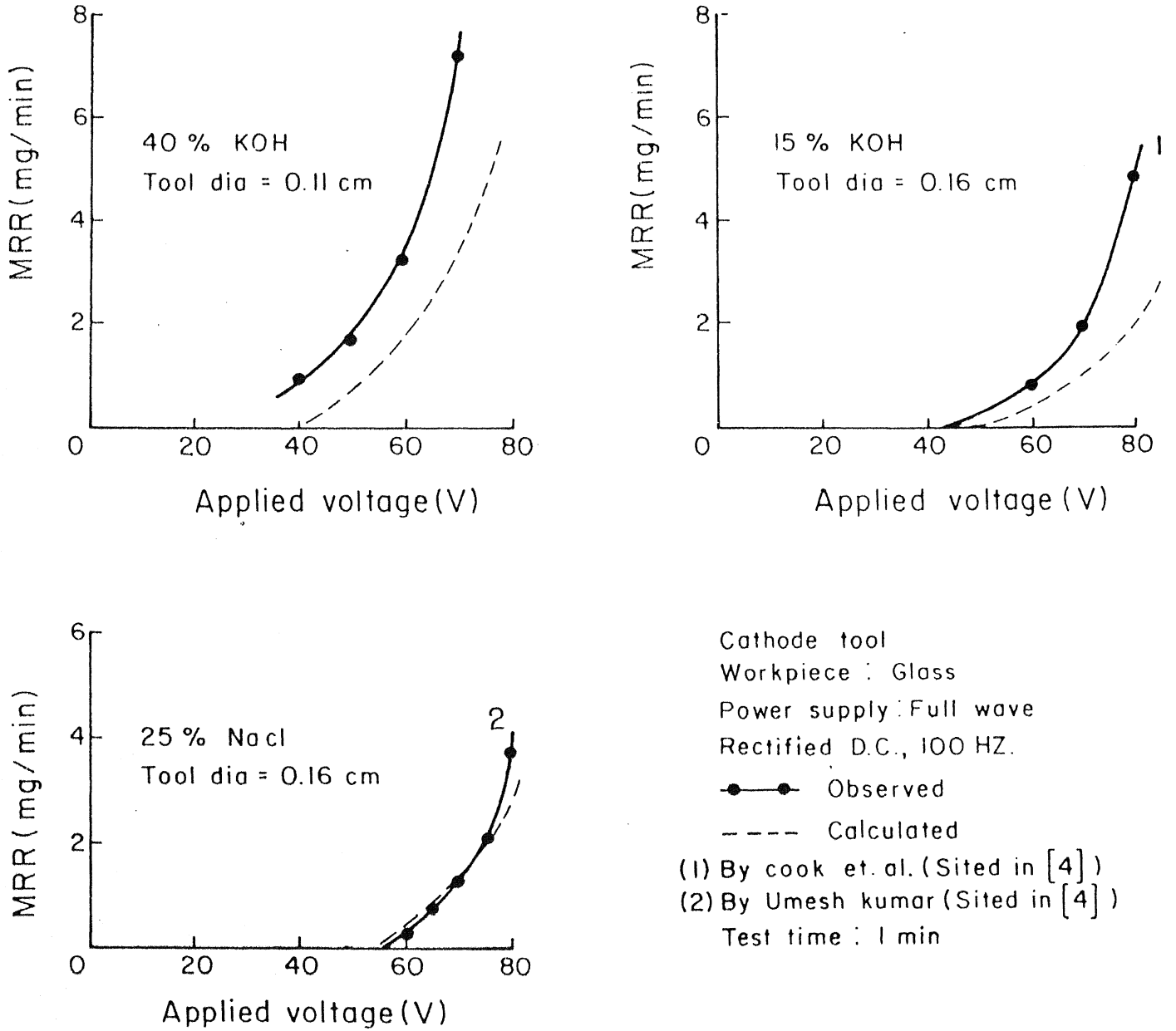

Fig 4.11 b Comparison between observed and calculated MRR for varying applied voltage

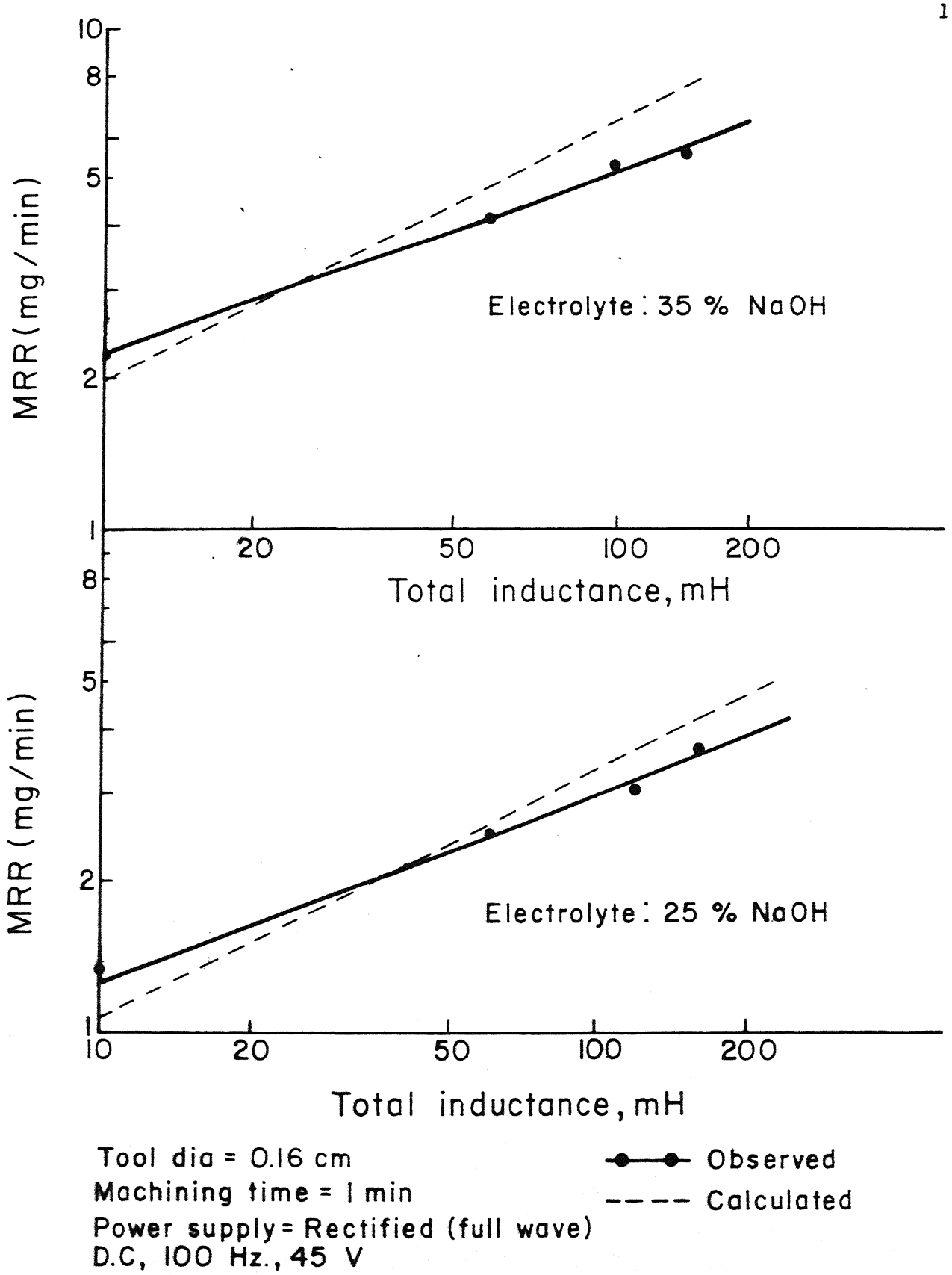

Fig. 4.12a Total inductance vs MRR (NaOH) (In log scale, Workpiece Glass).

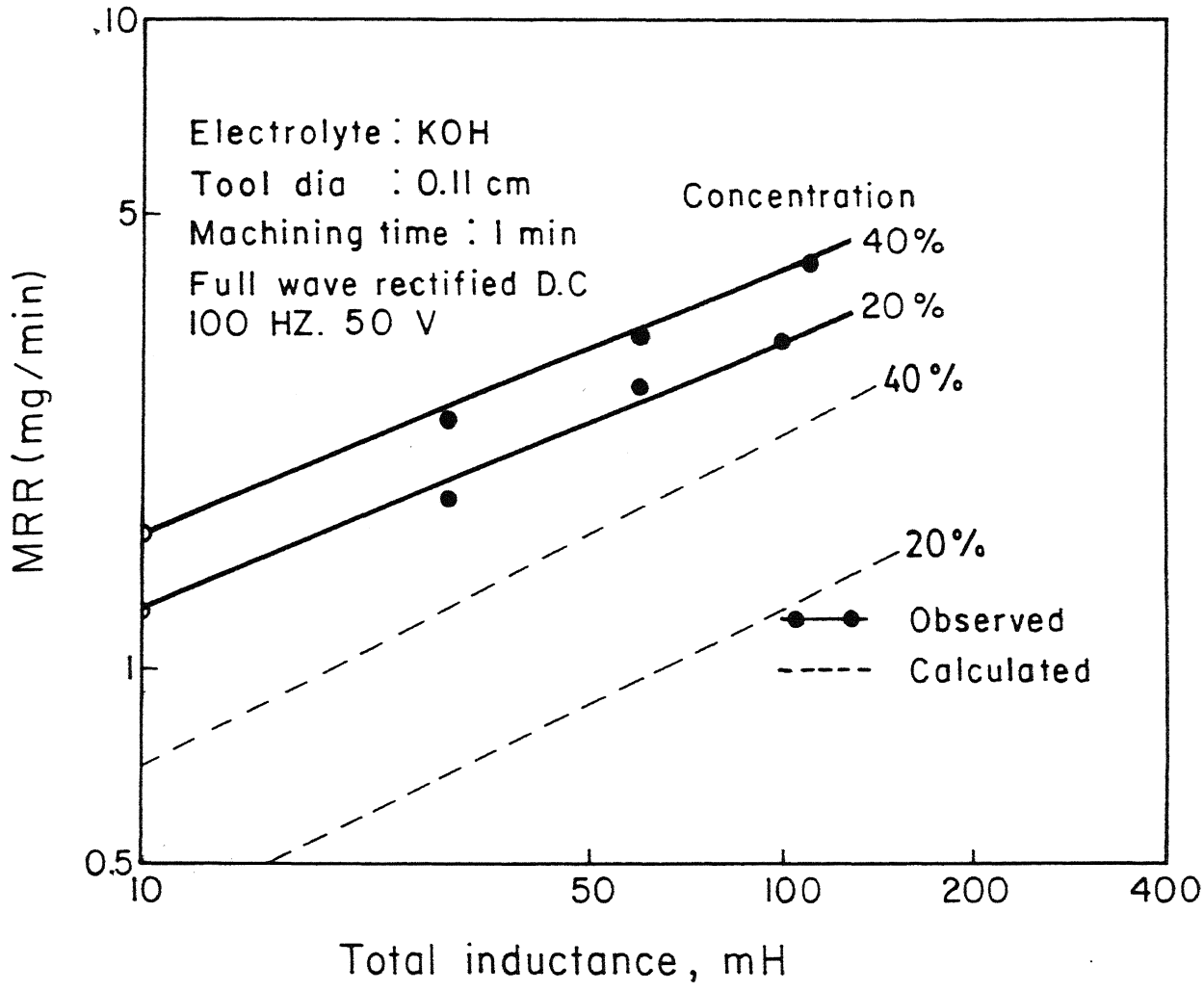

Fig. 4.12b Total inductance vs. MRR (KOH) (workpiece: glass).
(In log scale)

4.4 A Proposed Scheme for Enhancement of the Process Capability

ECDM is characteristically a low material removal rate process. The identification of the circuit inductance as an input parameter is of great importance so far as any attempt to increase the MRR is concerned. It can be seen from Figs.4.12a and 4.12b that the MRR increases by a factor of about 2.5 when an external inductance of 100mH is added to the circuit. It was also noticed that during the experiments with additional inductance the RMS value of current did not change significantly. It indicates that the power consumption was unchanged and the efficiency was improved. This can be explained in the following manner. The amount of material removal per spark depends on the spark energy in the manner shown by (4.6). If the energy per spark is increased the material removal rate per spark increases 1.5 power of inductance whereas the frequency decreases inversely. The net effect results in high MRR.

The critical voltage and resistances cannot be controlled easily during ECDM, as they are the properties of the electrolyte. As MRR $\propto (V_o - V_c)^3$, a small change in applied voltage substantially changes the MRR. But as MRR $\propto L^{0.5}$, the change of MRR with inductance is comparatively less than that with applied voltage. A finer control of MRR in ECDM can be obtained by adjusting the inductance.

CHAPTER 5

DISCUSSION AND SCOPE FOR FUTURE WORK

5.1 Introduction

The present chapter contains the discussion on the characteristics of the processes of ECD and ECDM. Some comments on the suggested models of ECD and ECDM are also included in this chapter. Furthermore the limitations found in the present work and the suggested course of future work are presented in this chapter.

5.2 Discussion on the Results Obtained from ECD Experiments

Systematic and elaborate set of investigations has been conducted in the course of the present work to understand the mechanism of ECD phenomenon. The vapour blanketing of the tool electrode has been identified as the primary reason for discharge initiation. The vapour blanketing takes place due to the generation of H_2 gas from electrochemical reaction and water vapour formation due to the interface boiling of the electrolyte. The electrolyte and its concentration are the leading factors to determine the critical voltage for discharge initiation. Alongwith these two factors the equivalent surface area of the

tool electrode determines the critical current. It is also identified that the ECD is analogous to electrical switching phenomenon. In present study the tool is used as cathode only, though the phenomenon can take place in a similar way with anodic tool. The electrode material has no significant effect on critical voltage or critical current. Interestingly, most of the potential drop takes place near the tool electrode.

The model of ECD is based on the criterion of the maximum coverage of the tool surface by the bubbles, both H_2 and vapour. The critical combined volume generation rate per unit area was found to be same for any given configuration. The comparison between the results obtained from the experiments and calculated on the basis of the suggested model are shown in Figs.3.11, 3.12 and 3.13.

In (3.17) γ being small compared to $4\delta K_3 \bar{v}_c$, it can be neglected; then

$$I_c \simeq \frac{A_e\ (4\delta K_3 M^{\lambda_a} \bar{v}_c)^{1/2}}{2\delta\ K\ M^{\lambda_a}}$$

$$= K'\ M^{-\lambda_a/2}$$

$$= K'\ M^{0.5} \qquad (5.1)$$

as $\lambda_3 = -1.0$ (from Table 3.1) and $K' = A_e \left[\frac{\bar{v}_c}{\delta K_3}\right]^{1/2}$ = constant for a particular combination of tool and electrolyte. Differentiating (5.1) w.r.t. M,

$$\frac{dI_c}{dM} = 0.5\ K' M^{-0.5} \qquad (5.2)$$

The R.H.S. of (5.2) is a positive quantity which implies that the critical current increases with the increase of mole fraction of the electrolyte, which is a function of the concentration. Equation 5.2 also indicates the variation of critical current with concentration is hyperbolic in nature. Figure 3.11 shows that the calculated characteristic of I_c with concentration slightly deviates from the predicted hyperbolic nature . This is because of thefact that the mole fraction is not an exact linear function of concentration and also because γ was neglected to determine the nature of the relationship between I_c and M.

With the same simplified relation as in (5.1) and substituting $\lambda_2 = -0.5$, (3.18) yields

$$V_c = K'' M^{0.5} \left[K_2 M^{-0.5} + K_3 M^{-1.0}\right]$$

where, $K'' = \left(\frac{\bar{V}_c}{\delta K_3}\right)^{1/2}$ = constant for an electrolyte.

$$\text{or, } V_c = K'' K_2 + K'' K_3 M^{-0.5}$$

Differentiating w.r.t. M,

$$\frac{dV_c}{dM} = - 0.5\ K''\ K_3\ M^{-1.5} \qquad (5.3)$$

which indicates that the critical voltage decreases with the increase of mole fraction, i.e., concentration. Figure 3.12 shows the calculated and experimentally obtained characteristic of V_c with respect of the concentration.

Equation 3.17 shows a linear relationship between the critical current and the equivalent area of the electrode. With the increase of the tool diameter, equivalent area of the electrode increased linearly. Therefore, the critical current increases linearly with the tool diameter, other parameters being same as shown in Fig.3.13. However, experiments show that the critical voltage increases slightly with tool diameter [Fig.3.13], whereas the model indicates it is to be independent of tool diameter. This may be due to the simplification done to idealise the phenomenon, neglecting some secondary factors.

5.3 Discussion on the Results Obtained from ECDM Experiments

In ECDM the mechanism of the material removal is found to be based on the thermal effect of the spark on the workpiece. The critical voltage increases with the flow velocity of the electrolytee. Again, stagnant electrolyte results in poor scavenging. These contradictory factors reduce ECDM to a low-efficiency process. The melting of the workpiece material by

the energy released from the spark was taken as the only reason of material removal in the model of ECDM. The inductance of the circuit emerges out to be an important parameter determining the energy of the spark. The spark energy is also a function of the current at the beginning of the spark. Some assumptions like the fraction of heat released by the spark conducted into the workpiece and the time of discharge become inevitable to quantify the model. Still, the nature of the variation of MRR under different input conditions predicted by ECDM model, is quite conforming to those obtained from the experiments.

With the change of the electrolyte concentration V_c and all the resistance components change. However, a small decrease in V_c considerably increased the MRR, as indicated by (4.18). The value of the factor $(R_{2c} + 0.5\ R_{3c})/R_c^3$ also increases with the increase of the electrolyte concentration. As, a result the MRR increases with electrolyte concentration, the applied voltage being same as shown in Fig.4.10. Other parameter being unchanged, MRR $\propto (V_o - V_c)^3$. For this reason the MRR increases rapidly with applied voltage as shown in Figs.4.11a and 4.11b. Again MRR $\propto L^{0.5}$, other parameters remaining same. Figures. 4.12a and 4.12b show the variation of MRR with different values of added inductance. The figures indicate that though the model predicts MRR $\propto L^{0.5}$, the experiments show MRR $\propto L^{0.4}$. The most probable reason for this discrepancy is the idealisation made to determine

the sparking frequency. It was noticed during the experiments with different values of additional inductance that a high value of inductance (>250mH) ultimately results in low MRR. Because, with the increase of spark energy, splashing of electrolyte results in longer time required to reestablish the contact between the electrode and electrolyte. This effect disturbs the cycle and ultimately the average cycle time increases.

It was observed that the MRR obtained experimentally using KOH as electrolyte is much higher than that predicted by the theoretical model. It is due to the chemical reaction between the glass and KOH which assist the machining. The localised temperature at the machining zone is quite high, much above the melting temperature of glass. At such a high temperature the larger size K^+ ions from the electrolyte replace Na^+ ions of the glass surface [Fig.5.1] and decrease its strength [40]. This results in higher MRR than that predicted by the model.

It is to be noted that different researchers obtained different MRR for the same input parameters. This is primarily due to the fact that glass, which was used as the workpiece material in all the experiments, is available in wide variety with different chemical compositions. The condition of experiments were quite likely to differ in terms of feed mechanism, feed force etc. The most important reason of this difference in result is,

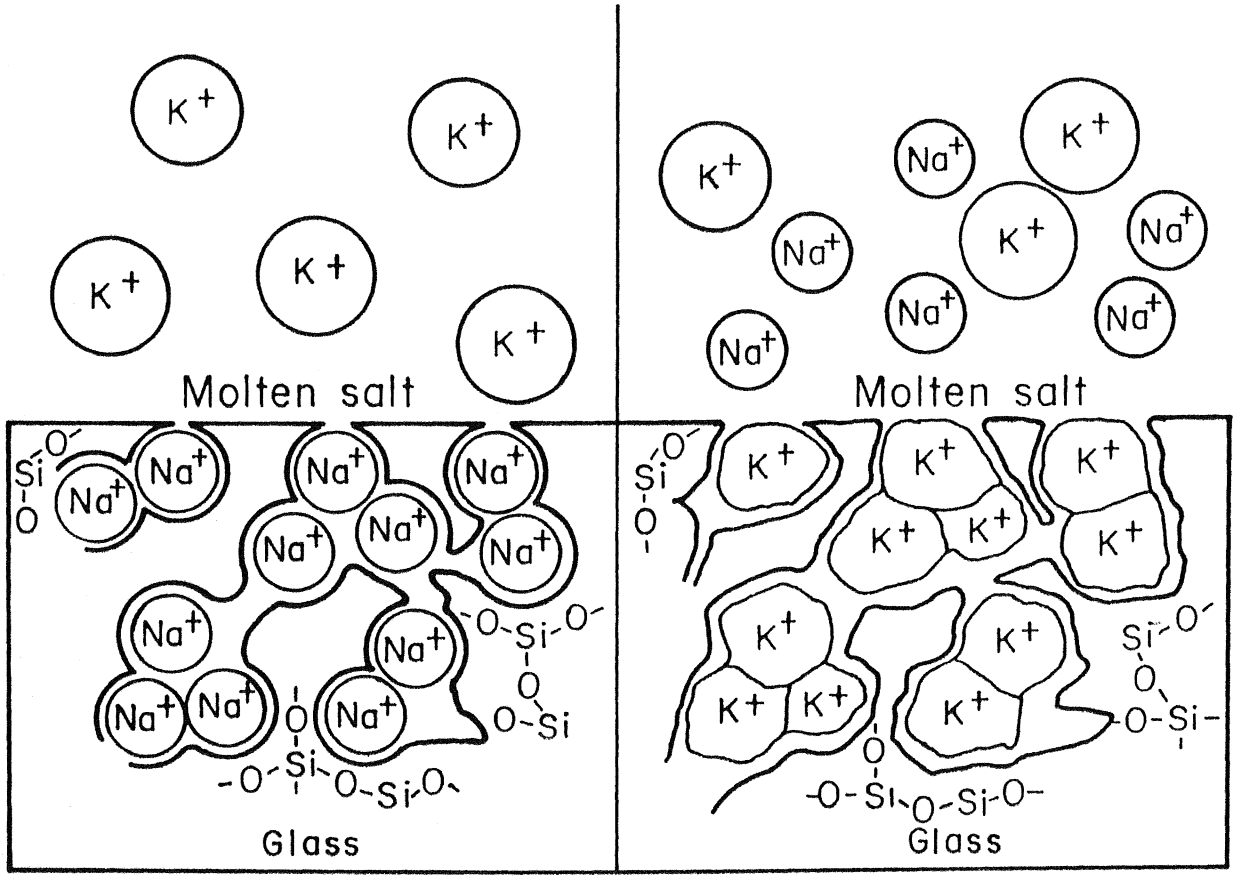

Fig.5.1 Modification of structure (schematic) by K^+ [40]

perhaps, the inductance of the circuit used which was ignored as an important parameter of ECDM in all previous researches. However, the present theoretical model and the experimental results indicate that the inductance of the circuit is a parameter having substantial influence on the MRR.

5.5 Limitations of the Present Work and Direction for Future Research.

The main objective of the present work was to identify the mechanisms of electrochemical discharge phenomenon and the material removal in electrochemical discharge machining. The tool was used as cathode only. A number of assumptions were made to verify the ECDM model. Also, the model could not be verified for workpiece materials other than glass. Considering these limitations, future work can be extended in the following directions.

(i) Verification and required modification, if any, of the model for anodic tool. Also, the validity of the model should be examined with other nonconducting materials.

(ii) The critical resistance were evaluated in a semiempirical manner. It is necessary to evaluate those theoretically in a more comprehensive manner.

(iii) The time of discharge in ECD was taken as constant. A rigorous analysis should be made for the determination of the time of discharge in ECD circuit.

(iv) The energy density of the discharge in ECDM was assumed from the data available regarding the energy density of EDM spark channel. Efforts should be made to evaluate it from investigating experiments.

(v) The present models of ECD and ECDM are much idealised and simplified. Modification of these models are possible, and also required, to develope a more realistic model.

(vi) Surface characteristic and the effect on the properties of the workpiece have not be investigated for the paucity of time. Effect of extra inductance on the surface characteristics should be investigated.

(vii) Experiments should be conducted to investigate whether any further improvement of the process is possible or not with capacitive or combination of capacitive and inductive discharge.

CHAPTER 6

CONCLUDING REMARKS

Based on the observations made during the experiments and the results of the theoretical analysis, a number of important conclusions can be drawn both for ECD phenomenon and ECDM. It will be desirable to present the conclusions in the three groups - (A) the concluding remarks on ECD phenomenon and its theoretical model, (B) the concluding remarks on the proposed model of ECDM and (C) the conclusions related to the proposed scheme of enhancing material removal capacity. The important ones are given below.

A. Concluding remark on ECD phenomenon

(i) Electrochemical discharge is based on switching phenomenon rather than the dielectric breakdown of the gas bubbles.

(ii) The bubble diameter, both H_2 and vapour, prior to departure from the electrode surface remain more or less constant and does not vary with applied voltage.

(iii) The onset of electrochemical discharge takes place when the combined generation rate of the hydrogen and vapour bubbles per unit area of the electrode surface attains a critical value.

(iv) Power required to initiate discharge can be reduced by external heating of the tool or by raising the temperature of the electrolyte.

(v) The experimentally obtained critical voltages and currents agree well with those predicted by the theoretical model of electrochemical discharge. Thus it can be considered that the model is representing the actual physical phenomenon with a reasonable degree of reliability.

B. Concluding remark on ECDM

(i) A part of the energy released by the discharge is conducted into the workpiece and melts it locally. The shock of the discharge removes the molten portion of the workpiece.

(ii) Depending on the diameter of the tool, there exists a minimum required voltage for machining. This voltage is higher than that at which the discharge initiates. The discharge initiates at the tool edge and the region of discharge gradually extends radially inward along the bottom surface of the tool with the increase of the applied voltage. The energy per spark also increase with the applied voltage. At that minimum required voltage the effect of the discharge is such that the whole surface of the workpiece under the tool can attain melting temperature due to the sparks generated.

(iii) The frequency of discharge (sparking) is random in nature as seen from the spectrum analysis.

(iv) The characteristics of material removal obtained from the experiments conducted by the author and the previous researchers and the predictions of the theoretical model are in good agreement for a wide range of parameters involved.

C. Concluding remarks of enhancing the MRR

(i) From the investigation it emerged that the inductance of the ECD circuit is an important parameter in deciding the MRR. This is helpful as an extra input parameter that can be controlled easily.

(ii) Substantial increase in MRR can be achieved (more than 200%), by introducing extra inductance in the circuit without any significant increase in the power consumption. This implies that the efficiency of the process is increased. It is suspected that this enhancement of MRR is achieved at the cost of the surface quality. Therefore, such extra inductance can be employed only for rough machining operation.

REFERENCES

1. ALLESU K. - Ph.D. Dissertation, IIT-KANPUR, (INDIA), (1988)

2. TAYLOR C.S. - Trans. Electrochemical Soc, n 47, p 301,(1925)

3. KELLOG H.H. - Jl.of Electrochemical Soc, n 97, p 133, (1950)

4. KURAFUJI H., SUDA K. - Annals of CIRP, v 16, p 415, (1968)

5. COOK N.H., FOOTE G.B., JORDAN P., KALYANI B.N. et.al - Journal for industry , p 945, (1973)

6. UMESHKUMAR N. - M.Tech. Thesis, IIT-Kanpur, (1985)

7. TSUCHIYA, INOUE, MIYAZAKI. et.al - Bull. Jap. Soc. of Prec. Engg. v 19, n 1, p 73,(1985)

8. KUBOTA M., TAMURA Y. - Bull. Jap. Soc.of Prec. Engg, v 7, n 4, p 117, (1973)

9. KUBOTA M. - Proc. Int. Conf. on Prod. Engg., Tokyo, p 51, (1974)

10. KUBOTA M. - ISEM- 5, Switzerland, p 217, (1977)

11. CRICHTON I.M., McGEOUGH J.A., MUNRO W., WHITE C. - Precision Engg., v 3, p 155, (1981)

12. DRAKE T.H., McGEOUGH J.A. - Proc. 22nd IMTDR, UMIST p 361, (1981)

13. McGEOUGH J.A., KHAYRY A.B.M., MUNRO W. - Annals of CIRP, v 32, n 1, p 113, (1983)

14. CRICHTON I.M., McGEOUGH J.A., SPENCER C.A. - Proc. of 1st Conf. of the Irish Manuf. Comm., p 109, (1984)

15. KHAYRY A.B.M., McGEOUGH J.A. - Proc. of 25th IMTDR, London, p 321, (1985)

16. deSILVA A., McGEOUGH J.A. - Proc. Inst. of Mech. Engg., v 200, n B4, p 237, (1986)

17. EL-HOFY H., McGEOUGH J.A. - Trans ASME, Jl. of Engg. for Inds., n 110, p 119, (1988)

18. NI X.W., McGEOUGH J.A. - Winter Annual Meeting of ASME (PED - v 34), p 63, (1988)

19. TANDON. S - M.Tech. Thesis, IIT-KANPUR (1987)

20. SREENIVAS RAO - M.Tech. Thesis, IIT-KANPUR (1988)

21. HOLM R. - "Electric Contacts, Theory and Application", Spriger Verlag, NY,p 52 (4th Edn, 1981).

22. PASCHEN F. - mentioned in "Electric contact - Theory and application (4th Edn 1981)" - p 276. (1967).

23. JANSSEN L.J.J., HOOGLAND J.G. - Electrochim Acta, v 15, p 1013, (1970)

24. STANISZEWSKI B.E. - Tech. Report 16, DSR 7673, office of Nav. Res. cont. NONR - 1841(39), MIT-Heat Trans Lab, (Aug. 1959)

25. ROHSENOW & GRIFFITH - Chem. Engg. Programme Symp. Series, v 52, n 18, p 47 (1956)

26. ZUBER - Doctoral Dissertation, University of California LosAngeles (1959)

27. VENCJEL J. - Electrochim. Acta, v 15, p 1909, (1970)

28. IVEY J.H. - Int. Jl. of Heat & Mass Tranf, n 10, p 1023, (1976)

29. VAN STRALEN S.J.D., COLE R. - Boiling Phenomenon (vol 1), Hemispherical Publishing Corporation, p 211, (1979)

30. VAN STRALEN S.J.D., COLE R. - Boiling Phenomenon (vol 1), Hemispherical Publishing Corporation, p 259, (1979)

31. WILSON S.D.R , HULME A - Proc. of Royal Soc. of London, v A387, p 133, (1983)

32. YOSHITSUGU, MUKOYAMA - Bull of JSME, Processing Engineers, v 2, n 6, (1967)

33. KONIG W., WERTHEIM R., ZVIRIN Y., TOREN M. - CIRP Annals, v 24, n 1, p 95, (1975).

34. CARSLAW H.S., JAEGAR J.C. - "Conduction of Heat in Solids", Oxford at the Clarendon Press (2nd Edn, 1959).

35. MYERS G.E. - "Analytical Methods in Conduction Heat Transfer" McGraw Hill, p 491, (1971).

36. PERRY R.H., CHILTON C.H. - "Chemical Engineering Handbook", McGraw Hill, p 23-60, (5th Edn).

37. RIDDLESTONE J. - Proc. Inst. Elect. Engr, n C102, p 29, (1955).

38. HOLM R. - "Electrical Contacts, Theory and Application", p 338, (4th Edn, 1981).

39. HOLM R. - "Electrical Contacts, Theory and Application", p 278 (4th Edn, 1981).

40. LAWRENCE H.V.V. - "Materials for Engineers", Addison - Wesley Publishing Comp. Inc, Amsterdam, p 525, 364, (Edn. 1982).

APPENDIX A

CALCULATION OF R_{2C} AND R_{3C}

The following tables show the data obtained from the pilot experiments with NaOH of different concentration. Smooth D.C. with tool diameter 0.11cm at depths 0.1cm and 0.2cm were used in these experiments.

TABLE A1 (Tool depth = 0.1 cm)

Concentration wt%	V_c (volts)	I_c (Amp)	R_c (Ω)	R_{2c} (Ω)	R_{3c} (Ω)
40	17	2.2	7.7	4.9	2.8
30	18	1.9	9.5	6.0	3.5
20	20	1.7	11.8	7.0	4.8
10	26	1.55	16.8	9.0	7.8
5	35	1.25	28.0	11.8	16.2

TABLE A2 (Tool depth = 0.2 cm)

Concentration wt%	V_c (volts)	I_c (Amp)	R_c (Ω)	R_{2c} (Ω)	R_{3c} (Ω)
40	17	2.8	6.1	3.9	2.2
30	18	2.5	7.2	4.4	2.8
20	20	2.3	8.7	4.8	3.9
10	26	2.0	13.0	6.6	6.4
5	35	1.7	20.6	10.7	10.1

The plots of R_{2c} and R_{3c} with different concentration of electrolyte are shown in Fig. A1. Fig.A2 shows the same set of curves when the critical resistances are plotted against the mole fraction of NaOH in log scale.

The curves were found to follow the relations

$$R_{2c} = \frac{1}{A_e}\left[0.15M^{-0.5}\right]$$

$$R_{3c} = \frac{1}{A_e}\left[0.03M^{-1.0}\right]$$

where, A_e = Equivalent area = 0.076 cm^2 for 0.1cm depth

= 0.110 cm^2 for 0.2cm depth

In a similar manner relation between mole fraction and critical resistance for other electrolytes were obtained.

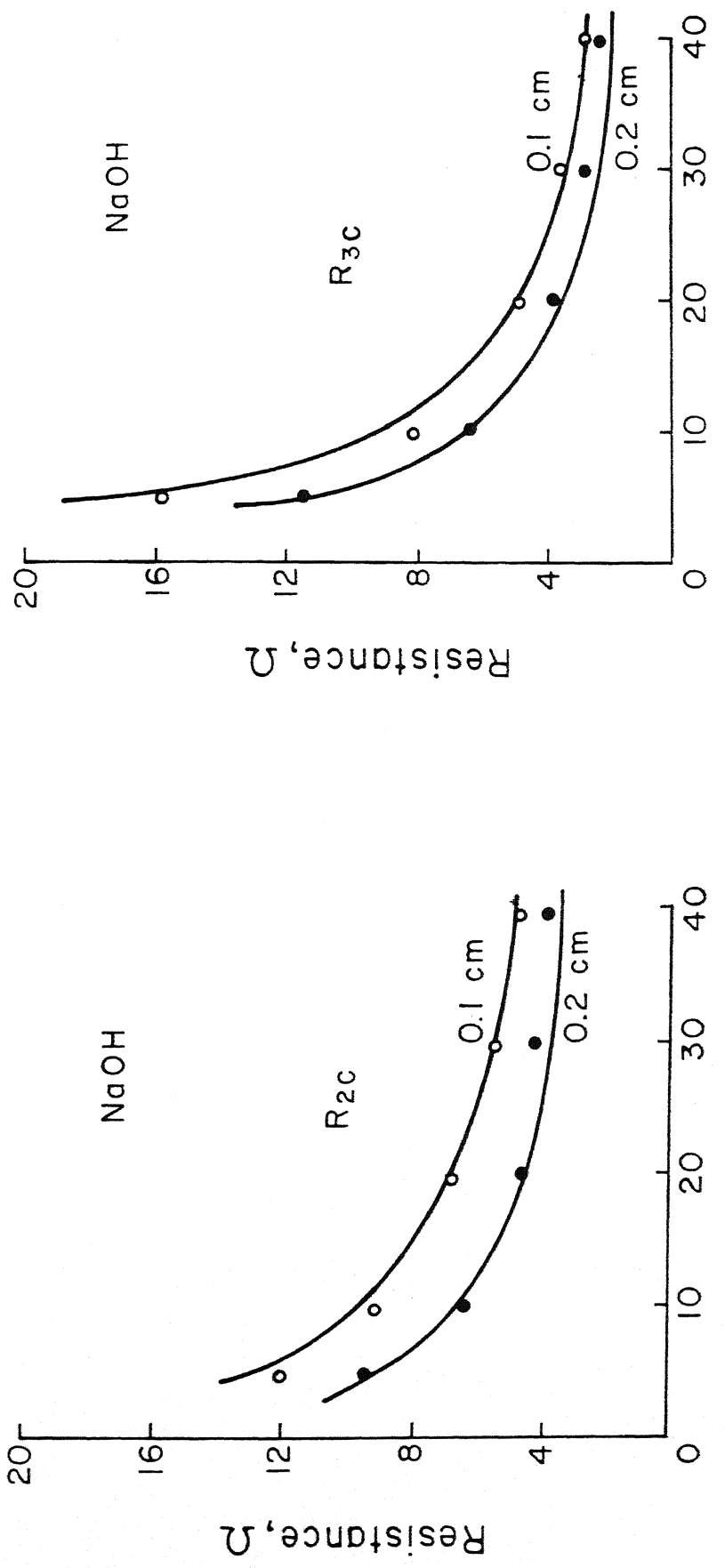

Fig. A1 Variation of R_{2c} and R_{3c} with electrolyte concentration (Electrolyte : NaOH).

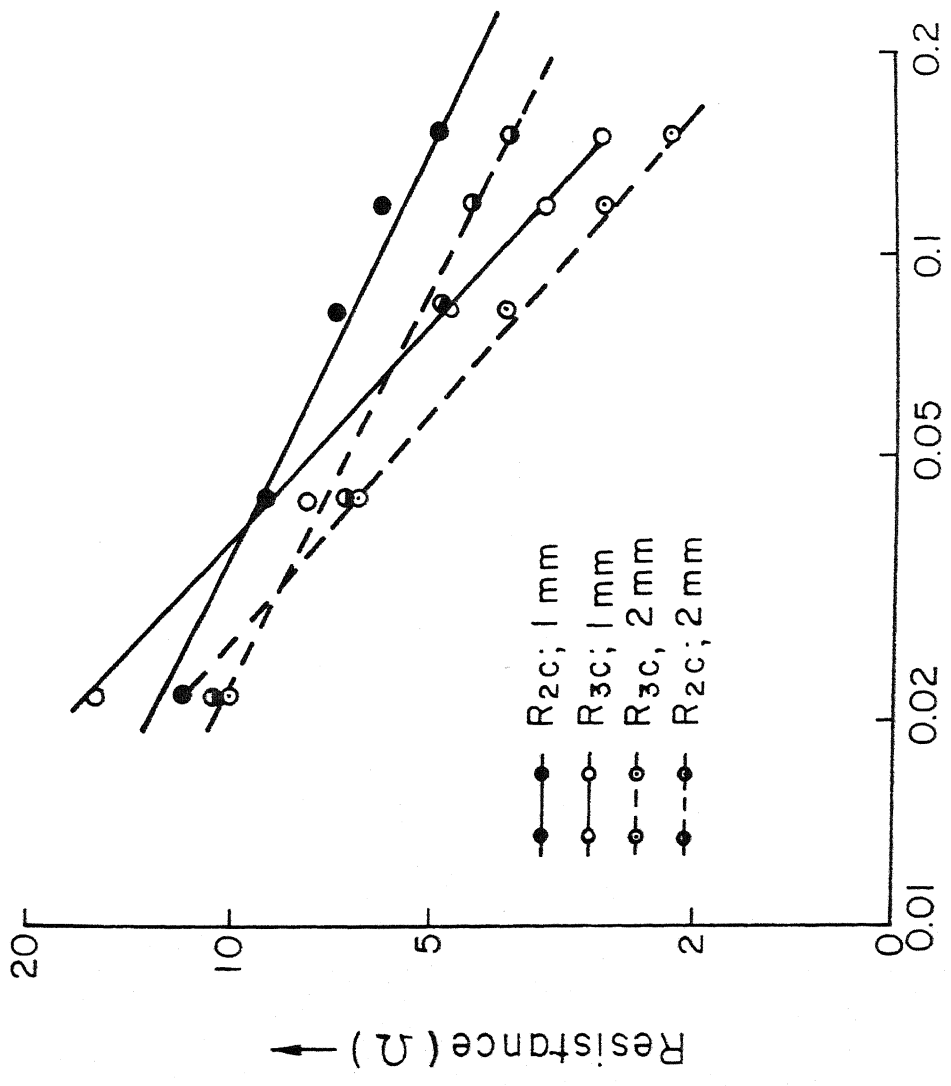

Fig. A2 Variation of critical resistances with mole fraction. (Electrolyte: NaOH). (In log scale)

APPENDIX B

DETERMINATION OF $\bar{v}_c$ AND δ

A few quadratic equations of $\bar{v}_c$ and δ were formed for different electrolyte and at different conditions with the corresponding values of I_c and R_{3c}. It is illustrated with the following table of observation. Tool diameter in all cases is 0.11 cm and γ = 0.16 cm^3/Amp-sec as calculated in Sec. 3.3.1.

Expt No	Electrolyte and concentration	Tool depth (cm)	Observed			
			critical current	critical voltage	R_{2c} (Ω)	R_{3c} (Ω)
1	10% KOH	0.1	0.9	33	12.5	24.2
2	20% KOH	0.1	1.15	24	8.0	12.9
3	10% KOH	0.2	1.2	33	9.2	18.3
4	20% KOH	0.2	1.7	24	6.5	7.6
5	5% NaCl	0.1	0.7	52	26.1	48.2
6	20% NaCl	0.1	1.3	29	11.6	10.7
7	5% NaCl	0.2	0.8	52	21.0	44.0
8	20% NaCl	0.2	1.6	29	9.6	8.5

Equation (3.13) gives

$$\gamma I_c + \delta I_c^2 R_{3c} - \dot{v}_c = 0 \; ; \; \gamma = 0.16 \text{ cm}^3/\text{Ampsec}$$

From Expt. (1): $0.144 + 19.60\,\delta - \dot{v}_c = 0$

(2): $0.184 + 17.06\,\delta - \dot{v}_c = 0$

which yield $\delta = 0.016$; $\dot{v}_c = 0.453$;

Dividing $\dot{v}_c$ by corresponding A_e, $\bar{\dot{v}}_c = 5.96$

From expt. (3): $0.192 + 26.35\delta - \dot{v}_c = 0$

(4): $0.272 + 21.96\delta - \dot{v}_c = 0$

which yields $\delta = 0.018$; $\dot{v}_c = 0.672$; or, $\bar{\dot{v}}_c = 6.11$

Similarly the pairs of equations obtained from experiments (5)&(6) and (7)&(8) yield

$$\delta = 0.017; \; \bar{\dot{v}}_c = 6.78$$

and $\delta = 0.020$; $\bar{\dot{v}}_c = 6.28$, respectively.

Hence, the avarage value of those quantities which were taken into account are

$$\delta = 0.018 \text{ cm}^3/\text{watt-sec and } \bar{\dot{v}}_c = 6.28 \text{ cm/sec}$$